**UNIVERSITY OF CRETE**

**DEPARTMENT OF CHEMISTRY**

**POSTGRADUATE GENERAL PROGRAM OF CHEMISTRY**
**IN BIOCHEMISTRY SECTION**


**MASTER THESIS**

# Study of lymphoma cell lines before and after Nutlin-3a induced wild type (wt) p53-activation by Raman spectroscopy

**Katsara Klytaimnistra**

**Master thesis supervisor: Prof. D. Ghanotakis**

**HERAKLION 2019**

**ΠΑΝΕΠΙΣΤΗΜΙΟ ΚΡΗΤΗΣ**

**ΤΜΗΜΑ ΧΗΜΕΙΑΣ**

**ΓΕΝΙΚΟ ΜΕΤΑΠΤΥΧΙΑΚΟ ΠΡΟΓΡΑΜΜΑ ΧΗΜΕΙΑΣ ΣΤΗ ΚΑΤΕΥΘΥΝΣΗ ΒΙΟΧΗΜΕΙΑΣ**

**ΜΕΤΑΠΤΥΧΙΑΚΟ ΔΙΠΛΩΜΑ ΕΙΔΙΚΕΥΣΗΣ**

# Μελέτη λεμφωματικών κυτταρικών σειρών με φασματοσκοπία Raman πριν και μετά την επαγόμενη από την Νατλίνη-3α ενεργοποίηση του αγρίου τύπου πρωτεΐνης p53

**Κατσαρά Κλυταιμνήστρα**

**Υπεύθυνος Καθηγητής: Δ. Γανωτάκης**

**ΗΡΑΚΛΕΙΟ 2019**

**UNIVERSITY OF CRETE**

**DEPARTMENT OF CHEMISTRY**

**POSTGRADUATE GENERAL PROGRAM OF CHEMISTRY**
**IN BIOCHEMISTRY SECTION**


**MASTER THESIS**

# Study of lymphoma cell lines before and after Nutlin-3a induced wild type (wt) p53-activation by Raman spectroscopy

**Katsara Klytaimnistra**

**Supervisor: Prof. M. Aivaliotis**
**Co-supervisors: Dr. V. Papadakis**
**Dr. K. Psatha**

**Academic Supervisor Department of Chemistry: Prof. D. Ghanotakis**

**HERAKLION 2019**

**Αφιέρωση**

Στους παππούδες μου και στο Σεμπάστιαν

**Εξεταστική επιτροπή**

**Επιβλέπων καθηγητής: Γανωτάκης Δημήτρης**

**Καθηγητής**

**Μέλος: Αϊβαλιώτης Μιχάλης**

**Αναπληρωτής Καθηγητής**

**Μέλος: Τσιώτης Γεώργιος**

**Καθηγητής**

# Ευχαριστίες

Για την εκπόνηση της μεταπτυχιακής μου εργασίας αρχικά θα ήθελα να ευχαριστήσω τον κο **Μιχάλη Αϊβαλιώτη** που με δέχτηκε στο εργαστήριό του και μου έδωσε την ευκαιρία να ασχοληθώ με την συγκεκριμένη εργασία και επίσης να τον ευχαριστήσω για την εκπαίδευσή μου στον χώρο της έρευνας.

Έπειτα θα ήθελα να ευχαριστήσω την κα **Κωνσταντίνα Ψαθά** για τις κυτταρικές καλλιέργειες, την υποστήριξη και τη συνεργασία της, τις Άννα Καρκαβίτσα και Κατερίνα Καλαντίδου για την συνεισφορά τους στις κυτταρικές καλλιέργειες αλλά και τον κο **Ηλία Δράκο** που μας παρείχε τις κυτταρικές σειρές. Θα ήθελα να ευχαριστήσω όλα τα υπόλοιπα μέλη του εργαστηρίου που διαμόρφωσαν ένα πολύ ευχάριστο και φιλικό κλίμα κατά τη διάρκεια της μεταπτυχιακής μου εργασίας.

Ένα θερμό ευχαριστώ στο συνεργάτη μας κο **Βασίλη Παπαδάκη** για την εκμάθησή μου στη φασματοσκοπία Raman, τις μετρήσεις, την υπομονή και την βοήθειά του.

Θα ήθελα ακόμα να ευχαριστήσω το Τμήμα Χημείας του Πανεπιστημίου Κρήτης που με δέχτηκε στο μεταπτυχιακό του πρόγραμμα, την Επιτροπή Μεταπτυχιακών φοιτητών και φυσικά τον κο **Γανωτάκη Δημήτρη** που αποτέλεσε τον επόπτη καθηγητή μου εκπροσωπώντας το Τμήμα Χημείας. Παράλληλα θα ήθελα να ευχαριστήσω το Ινστιτούτο Τεχνολογίας και Έρευνας του Ηρακλείου Κρήτης και το Ινστιτούτο Μοριακής Βιολογίας και Βιοτεχνολογίας για τις παροχές, τη φιλοξενία και τη φιλική υποδοχή του.

Τέλος το μεγαλύτερο ευχαριστώ ανήκει στους γονείς και στον σύντροφό μου για την αμέριστη υποστήριξη, κατανόηση και αγάπη που μου έδωσαν αυτά τα 2 χρόνια συνέχισης των σπουδών μου, όπως και στους φίλους μου που πάντα είναι εκεί για να με ενθαρρύνουν σε ό,τι κάνω.

# Βιογραφικό Σημείωμα

**ΠΡΟΣΩΠΙΚΑ ΣΤΟΙΧΕΙΑ**

Ονοματεπώνυμο: Κλυταιμνήστρα Κατσαρά

Ημερομηνία γέννησης: 22/03/1994

Τόπος γέννησης: Ρόδος

Οικογενειακή κατάσταση: Άγαμη

Διεύθυνση κύριας κατοικίας: Βαλλέστρας 33, Ηράκλειο Κρήτης, Τ.Κ. 71202

Αριθμός σταθερού τηλεφώνου: 2814006670, Κινητό: 6938754772

Διεύθυνση ηλ/κού ταχ/μείου: clytokatsara@gmail.com

**ΣΠΟΥΔΕΣ – ΕΚΠΑΙΔΕΥΣΗ**

**Ανωτάτη εκπαίδευση**:

Τρεχόντως στο Μεταπτυχιακό Γενικό Πρόγραμμα του Τμήματος Χημείας του Παν/μιου Κρήτης στον τομέα της Βιοχημείας, Φεβρουάριος 2017

Παν/μιο Κρήτης – Πτυχίο Επιστήμης και Τεχνολογίας Υλικών, 2012 – 2016, Βαθμός Πτυχίου 7,74 – Λίαν Καλώς

Πτυχίο Πιάνου από τη Σχολή Πιάνου «Μουσικοί Ορίζοντες», του Κώστα Γαϊτάνου, αναγνωρισμένο από το Κράτος, Αθήνα, Ιούνιος 2016

Μέση Εκπαίδευση: Ροδίων Παιδεία Λύκειο Ρόδου, 2009 – 2012, Βαθμός Απολυτηρίου– 18,5 - Άριστα

**ΔΙΑΚΡΙΣΕΙΣ – ΒΡΑΒΕΙΑ**

**Εκπαίδευση:**

Οικονομική υποτροφία για συμμετοχή στο 69$^{ο}$ Συνέδριο Ελληνικής Εταιρείας Βιοχημείας & Μοριακής Βιολογίας με παρουσίαση poster: “Study of lymphoma cell lines after Nutlin-3a induced wild type (wt) p53-activation by Raman spectroscopy”.Παρουσίαση 25/11/2018.

Αριστείο Προόδου Β’ Λυκείου ( ΥΠΕΘ ) με βαθμό 19 και 2/10

Βραβείο Προόδου Α’ Λυκείου ( ΥΠΕΘ ) με βαθμό 19 και 4/10

Βαθμολογημένη εξέταση στον χορό «Κλασσικό μπαλέτο»: ROYAL ACADEMY OF DANCE (2000-2006) INTERMEDIATE (GRADE 5). Διάκριση

**ΞΕΝΕΣ ΓΛΩΣΣΕΣ**

Αγγλικη: Certificate In English – Toeic (Test Of English For International Communication)- Lower (17/12/2016)

Αγγλικη: Certificate In English- Cambridge Esol Entry Level 3 (B1) (05/2008)

Γαλλικη : Diplome D'etudes En Langue Francaise Delf A2 (Ministere Education Nationale) (10/07/2009)

**ΓΝΩΣΕΙΣ ΠΛΗΡΟΦΟΡΙΚΗΣ**

Επαρκείς γνώσεις Origin, ChemBioDraw

Πτυχίο χρήσης H/Y Global Intermediate C Informatics Certificate by "GLOBAL CERT" 1/6/2018

Πτυχίο χρήσης H/Y Vellum Global Educational Services ,International Diploma in IT Skills Proficiency (Microsoft PowerPoint)

**ΕΡΓΑΣΤΗΡΙΑΚΗ ΕΜΠΕΙΡΙΑ**

Τρεχόντως στο Ινστιτούτο Μοριακής Βιολογίας και Βιοτεχνολογίας (IMBB) και Ίδρυμα Τεχνολογίας και Έρευνας (ITE), στην ομάδα του Μιχάλη Αϊβαλιώτη .

Βοηθός σε προπτυχιακά εργαστήρια Βιοχημείας 2/2018-5/2018

Βοηθός σε προπτυχιακά εργαστήρια Αναλυτικής Χημείας 9/2017-12/2017

Εργαστήριο Βιοϋλικών της καθηγήτριας Μητράκη Άννας ως προπτυχιακή φοιτήτρια για την διεξαγωγή της πτυχιακής εργασίας «Μελέτη αυτό-οργάνωσης πορφυρινών συζευγμένων με το πεπτίδιο της διφαινυλαλανίνης», 2015-2016

Εργαστήριο Βιοανόργανης Χημείας του καθηγητή Αθανάσιου Κουτσολέλου ως προπτυχιακή φοιτήτρια για την διεξαγωγή της πτυχιακής εργασίας «Μελέτη αυτό-οργάνωσης πορφυρινών συζευγμένων με το πεπτίδιο της διφαινυλαλανίνης», 2016

**ΕΡΓΑΣΙΕΣ/ΠΑΡΟΥΣΙΑΣΕΙΣ**

Παρουσίαση poster: "Study of lymphoma cell lines after Nutlin-3a induced wild type (wt) p53-activation by Raman spectroscopy, στο στο 69ο Συνέδριο Ελληνικής Εταιρείας Βιοχημείας & Μοριακής Βιολογίας. Προυσίαση 23/11/2018

Μεταπτυχιακή εργασία: "Reaction Mechanism of Prostaglandins from arachidonic acid". Παρουσίαση: 01/2018

Μεταπτυχιακή Εργασία: «NMR σε Φάρμακα και Φυσικά προϊόντα», στο μάθημα NMR (Φασματοσκοπία Μαγνητικού Πυρηνικού Συντονισμού). Παρουσίαση: 01/2017

Μεταπτυχιακή Εργασία: «Ατμοσφαιρική Ρύπανση και ανθρώπινη Υγεία», στο μάθημα Χημεία και Φυσική της Ατμόσφαιρας-Κλιματικές Αλλαγές. Παρουσίαση: 01/2017

Μεταπτυχιακή Εργασία: «Μέθοδοι κατευθυνόμενης/στοχευμένης εξέλιξης πρωτεϊνών και Αναλύσεις εξελικτικών στρατηγικών που οδηγούν στην αντίσταση σε αντιβιοτικά», στο μάθημα Δομής και λειτουργίας Πρωτεϊνών. Παρουσίαση: 06/2017

Μεταπτυχιακή Εργασία**:** «Επιδράσεις Ναρκωτικών σε συγκεκριμένους Νευροδιαβιβαστές», στο μάθημα Μεμβρανικών Βιολογικών Συστημάτων-Εφαρμογές στη Φαρμακευτική Χημεία. Παρουσίαση: 05/2017

Μεταπτυχιακή Εργασία: «Τα Μανιτάρια ως Αντιοξειδωτικά», στο μάθημα της Περιβαλλοντικής Μικροβιολογίας. Παρουσίαση: 05/2017

Πτυχιακή Εργασία: «Μελέτη αυτό-οργάνωσης πορφυρινών συζευγμένων με το πεπτίδιο της διφαινυλαλανίνης». Παρουσίαση: 10/2016

Προπτυχιακή Εργασία: «Εφαρμογές Πορφυρινών στην φωτοδυναμική θεραπεία και η αυτοοργάνωσή τους με πεπτίδια: αντιμικροβιακό σύστημα;» στο μάθημα Ενζυμικής Βιοτεχνολογίας. Παρουσίαση: 05/2016

Προπτυχιακή Εργασία: "Direct Visualization of Walking Motions of Photocontrolled Nanomachine on the DNA Nanostructure" στο μάθημα Βιοοργανικών Νανοδομών. Παρουσίαση: 12/2015

Προπτυχιακή Εργασία: «Cyberknife» στο μάθημα Βιοϊατρικής Μηχανικής. Παρουσίαση: 05/2015

Προπτυχιακή Παρουσίαση στο πλαίσιο της Βιοϊατρικής Μηχανικής : Kevlar, 05/2015

Προπτυχιακή Εργασία: «Υγροί Πολυμερικοί Κρύσταλλοι» στο μάθημα Φυσικής Πολυμερών. Παρουσίαση: 05/2015

Παρουσίαση στο πλαίσιο των Αγγλικών ΙΙ: Polymers, Optical Fibers, 2013

**ΣΕΜΙΝΑΡΙΑ**

**Εκπαιδευτικά:**

Πιστοποιητικό παρακολούθησης στο 69ο Συνέδριο Ελληνικής Εταιρείας Βιοχημείας & Μοριακής Βιολογίας, Ξενοδοχείο Imperial, Λάρισα, από 23/11/2018-25/11/2018

Πιστοποιητικό παρακολούθησης στο 20$^{o}$ Congress of Chemistry for Graduate Students, by the Department of Chemistry, Πανεπιστήμιο Κρήτης, 25/06/2018-27/06/2018

Πιστοποιητικό παρακολούθησης στο 19$^{o}$ Congress of Chemistry for Graduate Students, by the Department of Chemistry, Πανεπιστήμιο Κρήτης, 2/05/2017-4/05/2017

Διαδικτυακό σεμινάριο «Προετοιμασία αρωμάτων και αιθέριων ελαίων, βότανα, φαρμακευτικά αρωματικά φυτά», πιστοποιημένο από «ΕΟΠΠΕΠ» ,διάρκεια 18 ώρες, 11/2016-01/2017

**ΑΛΛΕΣ ΔΕΞΙΟΤΗΤΕΣ-ΣΥΜΜΕΤΟΧΕΣ**

Δίπλωμα οδήγησης, Κατηγορία Β, 09/2017

Παρουσιάσεις χορών Λάτιν, 2012-2016

Κλασσικό μπαλέτο (ROYAL ACADEMY OF DANCE AND VAGANOVA), 2000-2013

16ος πανελλήνιος μαθητικός διαγωνισμός ποίησης "Spiritual May" "The Cultural Spring of Thessaloniki", 08/05/2011

Σεμινάρια σύγχρονου χορού, Πιστοποιητικό παρακολούθησης, 2010

Μαθητικές επιστημονικές συγκεντρώσεις, 2006-2009

Σεμινάρια αστροφυσικής, πιστοποιητικό παρακολούθησης, 2008

Παραδοσιακοί Ελληνικοί χοροί, 2004-2006

Παρουσιάσεις χορωδίας, 2006-2009

# Curriculum Vitae (CV)

## PERSONAL DETAILS


Full name: Klytaimnistra Katsara

Date of birth: 22/03/1994

Place of birth: Rhodos - Greece

Marital status: Unmarried

Residence address: Vallestras 33, Heraklion Crete, zip code 71202

Land-line no: 2814006670, Mobile: 6938754772

Email address: clytokatsara@gmail.com


## STUDIES-EDUCATION

**University Education**:

Currently in the Postgraduate General Program of the Department of Chemistry /Biochemistry Section, University of Crete, February 2017

University of Crete – Degree in Materials Science and Technology, 2012 – 2016, GPA 7,74 – "Very Good"

Music Diploma in Piano by the Conservatory "Music Horizons" of Kostas Gaetanos, State Accredited, Athens, 2016

Secondary Education: Rodion Pedia High School in Rhodos, 2009 – 2012, Graduation Degree: 18,5 - Excellent

## DISTINCTIONS - AWARDS

**Education:**

Financial Grand for participation in 69$^{th}$ Panhellenic Conference of the Hellenic Society of Biochemistry and Molecular Biology with Poster presentation**:** "Study of lymphoma cell lines after Nutlin-3a induced wild type (wt) p53-activation by Raman spectroscopy". Presentation: 25/11/2018

High School 2$^{nd}$ year Distinction Academic Award (Ministry of Education), grade 19 and 2/10

High School 1$^{st}$ year Academic Award (Ministry of Education), grade 19 and 4/10

Other: Graded examination in dance CLASSICAL BALLET: ROYAL ACADEMY OF DANCE (2000-2006) INTERMEDIATE (GRADE 5)

**FOREIGN LANGUAGES**

English: Certificate In English – Toeic (Test Of English For International Communication) - Lower (17/12/2016)

English: Certificate In English- Cambridge Esol Entry Level 3 (B1) (05/2008)

French : Diplome D'etudes En Langue Francaise Delf A2 (Ministere Education Nationale) (10/07/2009)

**COMPETENCY IN INFORMATICS**

Adequate knowledge on Origin, ChemBioDraw

Global Intermediate C Informatics Certificate by "GLOBAL CERT" 1/6/2018

Vellum Global Educational Services, International Diploma in IT Skills Proficiency (Microsoft PowerPoint)

**LABORATORY EXPERIENCE**

Currently in Institute of Molecular Biology and Biotechnology (IMBB) Foundation for Research and Technology - Hellas (FORTH), in Michalis Aivaliotis group.

Assistant in Biochemical undergraduate labs 2/2018-5/2018.

Assistant in Analytical Chemistry undergraduate labs 9/2017-12/2017.

Biomaterial Laboratory under prof Mitraki Anna, as an undergraduate student, to conduct my Thesis with subject "A study of self-organization of porphyrins, linked with the diphenylalanine peptide".

Inorganic Chemistry Laboratory under prof Athanasios Koutsolelos, as an undergraduate student, to conduct my Thesis with subject "a study of self-organization of porphyrins, linked with the diphenylalanine peptide".

**PROJECTS/PRESENTATIONS**

Poster presentation**:** "Study of lymphoma cell lines after Nutlin-3a induced wild type (wt) p53-activation by Raman spectroscopy", 69$^{th}$ Panhellenic Conference of the Hellenic Society of Biochemistry and Molecular Biology. Presentation: 23/11/2018

Postgraduate Presentation: "Reaction Mechanism of Prostaglandins from arachidonic acid". Presentation: 01/2018

Postgraduate Project: "NMR on drugs and natural products" for the course in NMR (Nuclear Magnetic Resonance Spectroscopy). Presentation: 01/2017

Postgraduate Project: “Atmospheric pollution and human health” for the course in Atmospheric Chemistry and Physics-Climate Change. Presentation: 01/2017

Postgraduate Project: “Methods of guided/targeted progression of proteins and analysis on progressive strategies that lead to resistance in antibiotics”, for the course in Structure and Operation of Proteins. Presentation: 06/2017

Postgraduate Project: “Effects of narcotics on specific neurotransmitters”, for the course in Membranic Biological Systems – Applications in Pharmaceutical Chemistry. Presentation: 05/2017

Postgraduate Project: “Mushrooms as antioxidants”, for the course in Environmental Microbiology. Presentation: 05/2017

Thesis: “A study of self-organization of porphyrins, linked with the diphenylalanine peptide”. Presentation: 10/2016

Graduate Project: “Applications of porphyrins in the photodynamic therapy and their self-organization into peptides: antibacterial system?”, for the course in Enzyme Biotechnology. Presentation: 05/2016

Graduate Project: “Direct Visualization of Walking Motions of Photocontrolled Nanomachine on the DNA Nanostructure” for the course in Bioorganic Nanostructures. Presentation: 12/2015

Graduate Project: “Cyberknife”, for the course in Biomedical Engineering. Presentation: 05/2015

Graduate Presentation in the framework of Biomedical Engineering: Kevlar, 05/2015

Graduate Project: “Liquid Polymer Crystals”, for the course in Polymer Physics. Presentation: 05/2015

Presentation in the framework of English II: “Polymers, Optical Fibers”, 2013

**SEMINARS**

**Educational:**

Certificate of attendance in the 69$^{th}$ Panhellenic Conference of the Hellenic Society of Biochemistry and Molecular Biology, Hotel Imperial, Larisa, από 23/11/2018-25/11/2018

Certificate of attendance in the 20$^{th}$ Congress of Chemistry for Graduate Students, by the Department of Chemistry, University of Crete, 25/06/2018-27/06/2018

Certificate of attendance in the 19$^{th}$ Congress of Chemistry for Graduate Students, by the Department of Chemistry, University of Crete, 2/05/2017-4/05/2017

Web Seminar “PREPARATION OF PERFUMES and SPIRITUAL OILS, HERBS, PHARMACEUTICAL AROMATIC PLANTS”, accredited by «ΕΟΠΠΕΠ», duration 18 hours, 11/2016-01/2017.

**OTHER SKILLS/PARTICIPATIONS**

Driver’s License, Category B, 09/2017

Latin dance presentations, 2012-2016

Classical Ballet (ROYAL ACADEMY OF DANCE AND VAGANOVA), 2000-2013

16th PanHellenic Student Poetry Competition "Spiritual May" "The Cultural Spring of Thessaloniki", 08/05/2011

Modern dancing seminars , Certificate of attendance, 2010

Student scientific meetings, 2006-2009

Seminars in Astrophysics, Certificate of attendance, 2008

Traditional Greek dances 2004-2006

Choral music presentations 2006-2009

## Περίληψη

Το ογκοκατασταλτικό γονίδιο *p53* είναι συχνά μεταλλαγμένο σε πολλούς ανθρώπινους καρκίνους. Παρόλα αυτά, η πλειοψηφία των αιματολογικών κακοηθειών φέρουν την αγρίου τύπου πρωτεΐνη TP53 (wt-TP53), η οποία όμως είναι απενεργοποιημένη. Η πρωτεΐνη MDM2 (HDM2 στους ανθρώπους) προσδένεται στη wt TP53, ρυθμίζοντας αρνητικά τη μεταφραστική δραστηριότητα και σταθερότητα της wt TP53. Η Νατλίνη-3α (N3a) παρεμποδίζει την αλληλεπίδραση μεταξύ της TP53 και της MDM2, με αποτέλεσμα να σταθεροποιεί και να ενεργοποιεί μη-γενοτοξικά το μονοπάτι της wt-TP53 στα λεμφωματικά κύτταρα, προκαλώντας αναστολή του κυτταρικού κύκλου, και τελικά απόπτωση στις περισσότερες των περιπτώσεων.

Η ανάλυση και απεικόνιση σημάτων με φασματοσκοπία Raman επιτρέπει την ανίχνευση των δονήσεων των χημικών δεσμών, την αναγνώριση των τεσσάρων δομικών λίθων των βιομορίων (αμινοξέα, λιπίδια, νουκλεϊκά οξέα, σάκχαρα) και τέλος την ανάλυση του μοριακού προφίλ των δειγμάτων, χωρίς την ανάγκη ετικετών σήμανσης ή επιλεκτικών ανιχνευτών στα βιομόρια, και κυρίως με μη-επεμβατικό τρόπο.

Η έρευνά μας είχε δύο κυρίαρχους στόχους:

α) Την ανάλυση και σύγκριση τριών διαφορετικών Hodgkin και μη-Hodgkin λεμφωματικών σειρών, πριν και μετά την χορήγηση N3a, η οποία επάγει την επανενεργοποίηση της wt-TP53, με τεχνικές της φασματοσκοπίας Raman.

β) Την ανίχνευση και παρατήρηση της N3a στα λεμφωματικά κύτταρα, ώστε να ακολουθήσουμε την ενδοκυτταρική της πορεία και να εντοπίσουμε χωρικά την ενδοκυτταρική της δράση. Επιπλέον, η ανάλυσή μας επέτρεψε να εντοπίσουμε πιθανές δυσκολίες εισαγωγής της N3a στο κύτταρο.

Έπειτα από τη δοκιμή και βελτιστοποίηση διαφορετικών πειραματικών προσεγγίσεων, κυρίως στο κομμάτι της προετοιμασίας του δείγματος και στην ανάλυσή του, αναπτύξαμε μία πειραματική μεθοδολογία με ικανοποιητικά αποτελέσματα. Συνοπτικά, κυτταρικό εναιώρημα από τους διαφορετικούς τύπους λεμφώματος, σε συγκεκριμένη φάση της ανάπτυξής τους πριν και μετά την επίδραση με N3a, τοποθετήθηκε απευθείας επάνω σε αντικειμενοφόρο πλάκα μικροσκοπίου από $CaF_2$, για απεικόνιση με Raman σε διαφορετικές θερμοκρασίες και συνθήκες εστίασης. Οι παρατηρήσεις των κυττάρων πραγματοποιήθηκαν με έναν καταδυτικό φακό Olympus 60x, ο οποίος είχε άμεση επαφή με το δείγμα.

Με τη φασματοσκοπία Raman καταφέραμε να εντοπίσουμε διακριτά σήματα-«αποτύπωμα», τα οποία μπορούσαν να διαφοροποιήσουν μεταξύ τους τα δύο κυτταρικά μοντέλα που χρησιμοποιήσαμε, λαμβάνοντας σήματα από τρεις ενδοκυτταρικές περιοχές (πυρήνας, μεμβράνη, κυτταρόπλασμα) και μία εξωκυτταρική, σε διαφορετικές θερμοκρασίες. Παρόλα αυτά, η σύγκριση των δύο κυτταρικών μοντέλων στηρίχθηκε σε σήματα Raman κυττάρων που λάβαμε από την περιοχή του πυρήνα, καθώς οι αντίστοιχες μετρήσεις είχαν μεγαλύτερη επαναληψιμότητα σε σχέση με αυτές του κυτταροπλάσματος και των μεμβρανών. Με την

PCA ανάλυση καταφέραμε να επιβεβαιώσουμε τη διαφοροποίηση των δύο κυτταρικών μοντέλων. Επιπλέον, με τη φασματοσκοπία και ανάλυση Raman κατορθώσαμε να προσδιορίσουμε κορυφές ταυτοποίησης της N3a στα 480-481 $cm^{-1}$ και 2436-2438 $cm^{-1}$, οι οποίες δεν ανιχνεύονται σε άλλα βιολογικά μόρια. Αυτές χρησιμοποιήθηκαν για να παρακολουθήσουμε την πορεία και για τον εντοπισμό της N3a ενδοκυτταρικά και εξωκυτταρικά. Τα αποτελέσματα μας έδειξαν ότι σε μη ζωντανά κύτταρα η N3a βρίσκεται εντός και εκτός των κυττάρων σε αντίθεση με τα ζωντανά κύτταρα όπου η N3a δεν εντοπίστηκε εντός αλλά μόνο εκτός των κυττάρων. Η φασματοσκοπία Raman αποτελεί μια πιθανή πολλά υποσχόμενη, γρήγορη και μη επεμβατική στρατηγική, για έγκαιρη, ακριβή διάγνωση, κατηγοριοποίηση και αξιολόγηση της αποτελεσματικότητας των φαρμάκων.

## Λέξεις κλειδιά

Νατλίνη-3α, TP53, MDM2, μη-Hodgkin λέμφωμα, Hodgkin λέμφωμα, καρκίνος, Φασματοσκοπία Raman, απεικόνιση, σήμα, PCA

## Abstract

The p53 tumor suppressor gene is commonly mutated in many human cancers. However, the majority of hematological malignancies express wild type (wt) *p53*, which is somehow inactivated. MDM2 (HDM2 in humans) binds to wt TP53, negatively modulating its transcriptional activity and stability. Nutlin-3a (N3a) inhibits the p53-MDM2 interaction, resulting in stabilization and non-genotoxic reactivation of the wt TP53 signaling pathway in lymphoma cells, followed by cell cycle arrest, and in most of the cases apoptosis.

Raman spectroscopy allows the detection of chemical bonds vibration, the recognition of the four building blocks of biomolecules: amino acids, lipids, nucleic acids, carbohydrates and finally the analysis of the molecular profile of specimens without the need for labels or selective probes, and most importantly in a non-invasive manner.

Our research had two main objectives:

a) The analysis and comparison of three different lymphoma Hodgkin and non-Hodgkin model cell lines, before and after N3a-induced (wt) TP53-activation, through Raman spectroscopy.

b) The detection and observation of N3a into lymphoma cells, in order to follow its course and determine its localization and site of action within the cell. Moreover, this analysis revealed possible difficulties regarding the entry of N3a in the cell.

After testing and optimization of different experimental procedures, mainly concerning sample preparation and analysis, we developed an experimental procedure yielding satisfactory results. Briefly, cell suspension from different lymphoma cell types, at the appropriate cell growth stage, before and after N3a treatment, was placed directly on $CaF_2$ microscope slide, for Raman imaging in different temperatures and focal conditions. Cell observations were made with an Olympus 60x water immersion lens in direct contact with the sample.

With Raman spectroscopy we managed to detect distinct “signature” signals, which can differentiate the two cell models used, by receiving signals from three intracellular areas (nucleus, membrane, cytoplasm) and one extracellular, at different temperatures. However, the comparison of the two cell models was based on Raman signals from the nucleus area, because the corresponding spectrums presented higher repeatability, compared to those received from the cytoplasm and the membrane. Using PCA we managed to confirm the differentiation of the two cell models. Furthermore, with Raman spectroscopy and analysis we managed to determine the signature peaks of N3a that do not correspond to biological compounds. Those were used for the observation and detection of N3a intracellularly and extracellularly. Based on our results, in N3a-effected (possibly apoptotic) cells, N3a is present inside and outside of the cell, in contrast to live cells where N3a is not detected inside, but only outside of the cell. In conclusion, our study supports Raman spectroscopy as a potential

promising, fast and non-invasive strategy, for the early, accurate diagnosis, categorization and assessment of putative drug efficacy against lymphoma and other human diseases.

## Keywords

Nutlin-3a, TP53, MDM2, non-Hodgkin lymphoma, Hodgkin lymphoma, cancer, Raman spectroscopy, imaging, signal, PCA

# Contents

## Abbreviations

Nutlin-3a: N3a

Wild type: wt

non-Hodgkin lymphoma: NHL

Hodgkin lymphoma: HL

Mouse double minute 2: MDM2

Wavenumber: wn

Principal component analysis: PCA

Polylysine: PDL

Phosphate buffer saline: PBS

Wagging: wag

Vibration: v

Deformation: def

Asymmetric: asym, as

Symmetric: sym

Stretching: str

Initial protocol: PR1

Modified protocol: PR2

New protocol: PR3

Biological Replicate: BR

# Chapter 1: Introduction and Theoretical back ground

## 1.1 Introduction

Cancer, especially lymphomas, is a sudden and seriously threatening disease for humans. In most cases, early diagnosis increases the probability of a full recovery, reducing mortality rates. Raman spectroscopy is a potential strategy in the investigation of the underlying lymphomagenetic mechanisms for early diagnosis [1].

Nutlins are a promising new class of anti-cancer drugs paving the way for improving the future of cancer treatment. Nutlins are presently in early clinical trials for treating blood cancers. They gained worldwide attention due to their ability to prevent cancer growth and activate TP53 to trigger programmed cell death (apoptosis) in blood cancer cells [2].

We attempted to determine whether or not Hodgkin (HL) and non-Hodgkin Lymphoma (NHL) cell lines could be differentiated and compared using Raman spectroscopy. Furthermore, we attempted to determine if it is possible to observe N3a's effect inside treated lymphoma cells using Raman spectroscopy.

## 1.2 Lymphoma

### 1.2.1 What is lymphoma?

Thomas Hodgkin, in 1832, first recognized human lymphomas. Lymphomas are types of blood cancer. Being lymph node cancers, they emanate from lymphocyte cells of nodes. Cancer cells display a metabolic reprogramming that includes increased glycolysis and increased dependence on glycolysis for ATP production. This is one of the reasons why cancer cells, as well as lymphomas grow uncontrollably [3].

A lymph node is an ovoid organ of the lymphatic system, which is part of the vascular system and an important part of the immune system, including a network of lymphatic vessels that transfer a clear fluid, called lymph, directly towards the heart. The main cells that are affected are B, T and Natural killers (NK) lymphocytes. Therefore, based on their morphology and origin, they are divided into HL and NHL.

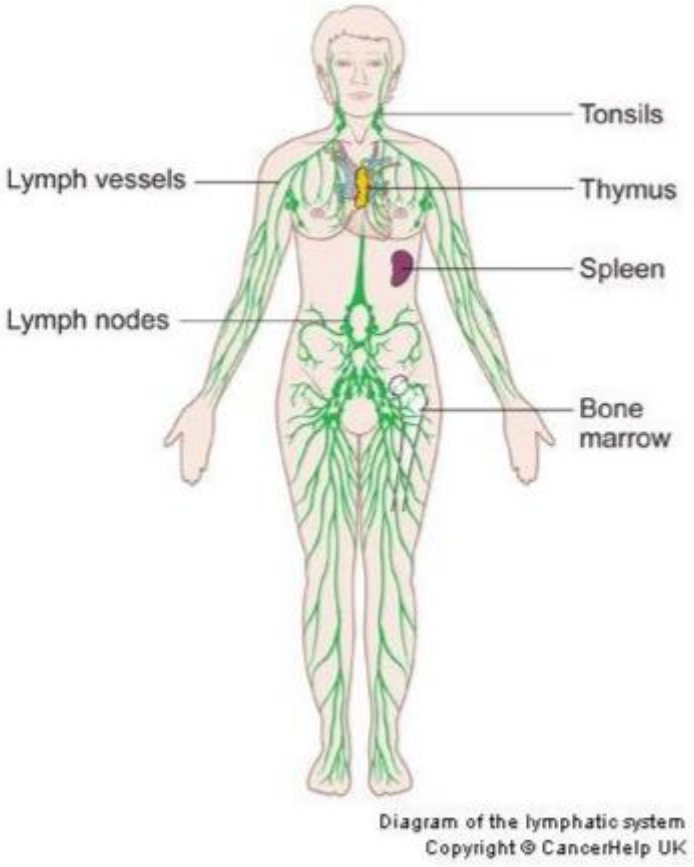


**Figure 1.2.1.** The lymphatic system and associated organs in the Human body [4].

Approximately 90% of aggressive lymphoma cases are derived from B-cells. NHL cells are derived either from B or T/NK cells and appear to be more common than HL. The most common subtype of NHL is the Diffuse Large B-cell lymphoma (DLBCL or DLBL). 6% of NHL cases are a subtype of B-cell lymphoma called Mantle cell lymphoma (MCL). MCL appear within the mantle zone of a lymphatic nodule that surrounds normal germinal center follicles. There are two classifications of HL, Nodular Lymphocyte Predominance HL and Classical HL. Reed Sternberg cells, derived from B cells, are often present in the lymph nodes of individuals with Classical HL and thus their existence is necessary for the diagnosis of the disease. "Popcorn cells" are present in Nodular Lymphocyte Predominance HL, which are embedded in nodules consisting of B cells and mainly reactive T cells.

The risk of developing NHL increases with age and is more common in males than in females. In 2010, from patients diagnosed with NHL, 37% of males and 36% of females died (Cancer Research incident and mortality UK report).

However, HL is a rarer cancer phenomenon, where only 17% of the diagnosed patients die. Early diagnosis and treatment of HL increases the probability of a full recovery, in contrast to NHL [4, 5].

Finally, NHL is linked with a number of risk factors such as smoking or family history, but the cause of most lymphomas is still not known. Nevertheless, 30-50% of HL cases are caused by infection with the Epstein-Barr virus [6].

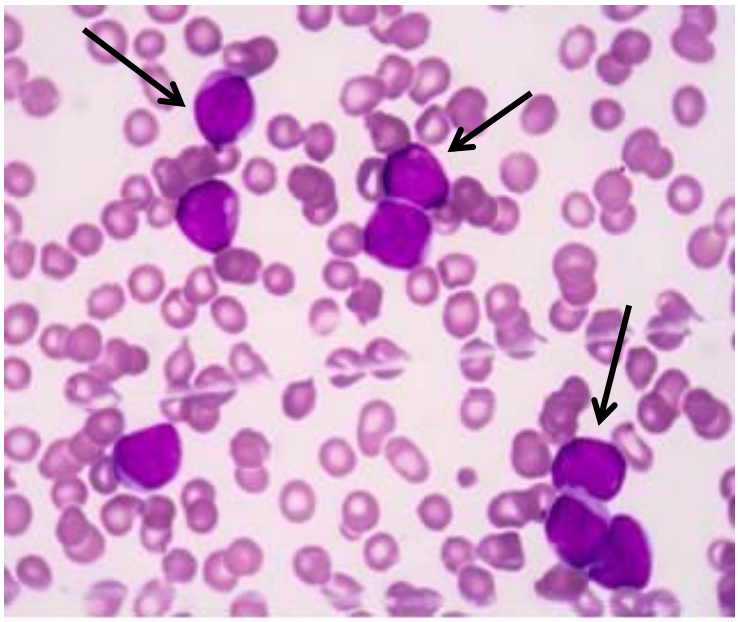

**Figure 1.2.2.** Non-Hodgkin Lymphoma [7].

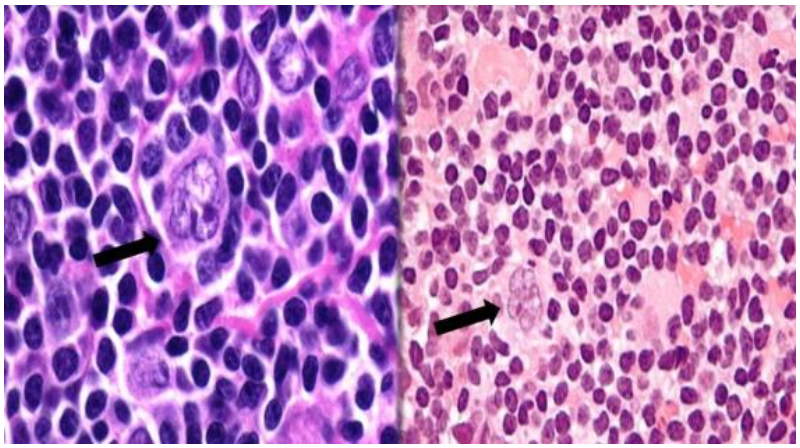

**Figure 1.2.3.** Lymphocyte predominant Hodgkin Lymphoma [8].

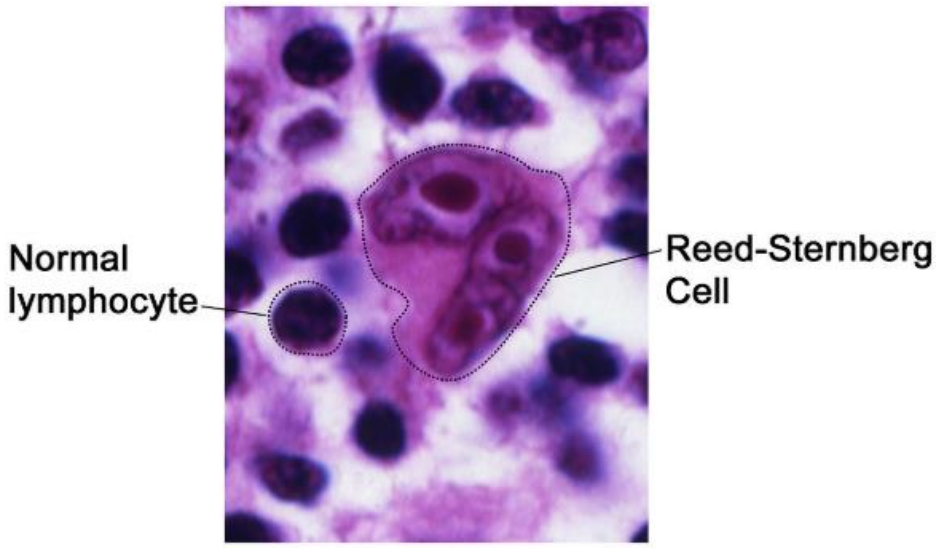


**Figure 1.2.4.** Classical Hodgkin Lymphoma [9].

## 1.3 *p53* signaling pathway related to cellular stress

The p53 signaling pathway is associated with cellular stress responses; TP53 can initiate DNA repair, cell-cycle arrest, senescence and most importantly, apoptosis. These responses are very important for tumor suppression and cancer, as well as lymphoma therapies.

TP53 is acting as a transcription factor that regulates genes, which can induce either cell cycle arrest (at the G1/S regulation point) or apoptosis. For this reason TP53 tumor suppressor is very important for the regulation of cell cycle progression. **In response to stress,** before the cell becomes cancerous, wt-TP53 protein rapidly **accumulates in the nucleus** and then it functions as a transcription factor which binds to DNA and induces expression of cell growth arrest genes or DNA repairing genes [10, 11]. Wt-TP53 is a labile protein, comprising of folded and unstructured regions that function in a synergistic manner. Wild type refers to the phenotype of the typical form of a species as it occurs in nature[12] .

## 1.4 MDM2 in relation to p53

In a normal cell, p53 is inactivated by its negative regulator MDM2 (mouse double minute 2), which contains an N-terminal p53 interaction structural domain. p53 can activate MDM2 expression, which leads to the regulation and repression of p53. Interestingly, many human neoplasias, including lymphomas bear an MDM2 gene that is frequently found to be amplified or overexpressed.

Regarding the MDM2-p53 interaction, firstly, MDM2 binds p53 at its transactivation domain and blocks its ability to activate transcription. Secondly, MDM2 is an E3 ubiquitin-protein ligase which monoubiquitinates p53 (and itself) leading it for degradation by the proteasome.

Finally, MDM2 is involved in the nuclear export of p53 and MDM2 itself is induced by p53, therefore the two molecules form an auto regulatory loop [10, 11].

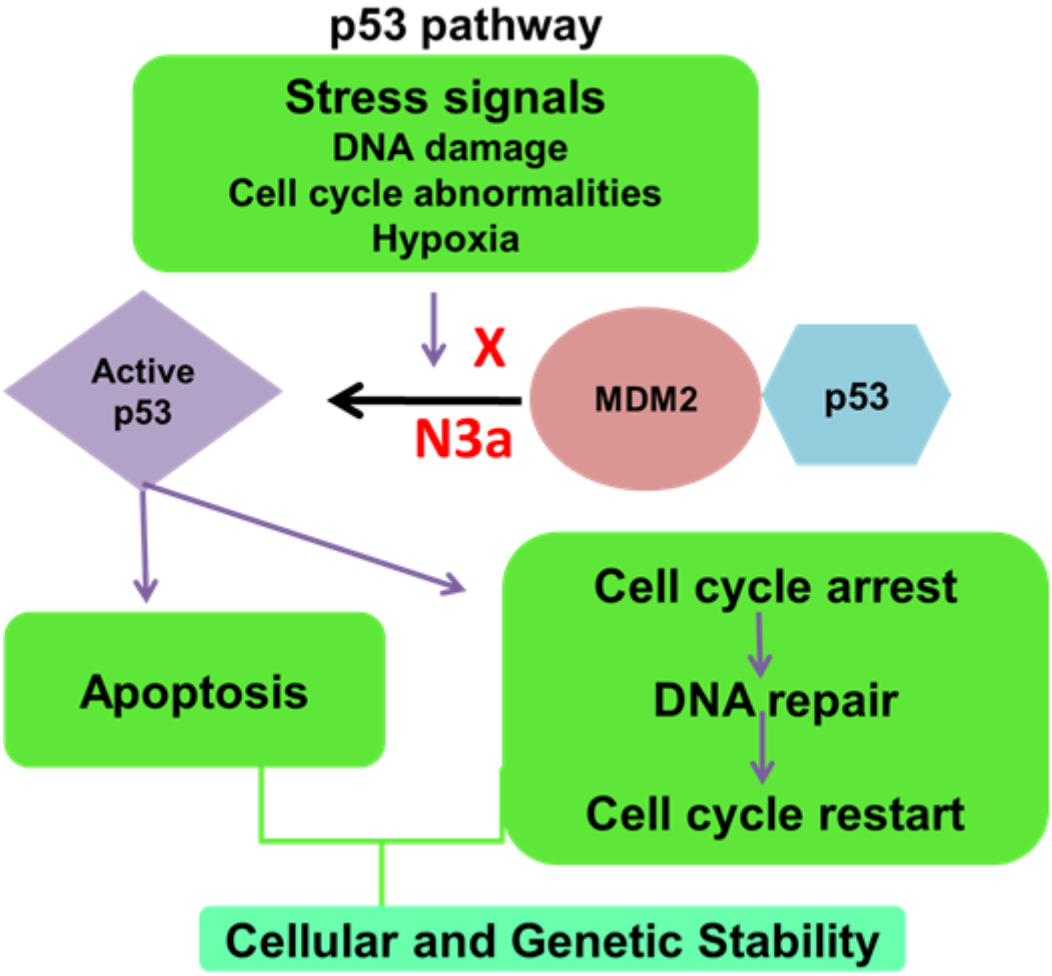


**Figure 1.4.1.** p53 pathway.

The activation of the p53 pathway through inhibition of MDM2 has been proposed as a promising approach for the treatment of cancer, as well as for lymphoma therapy [10, 11].

MDM2-p53 interactions have been studied by X-ray crystallography and NMR spectroscopy. The α-helix of p53 binds into a relatively deep cleft in the amino terminus of the MDM2 protein. The three critical amino acid residues within the transactivation domain (TAD) of p53 are Phe19, Trp23, and Leu26. These residues of p53 interact with three hydrophobic cavities in the MDM2 molecule, called Phe19, Trp23, and Leu26 pockets [11].

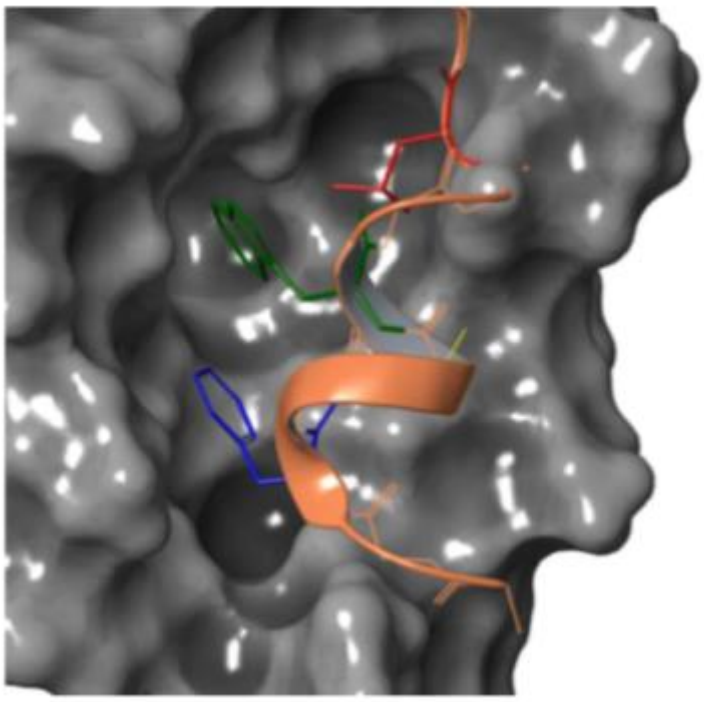

**Figure 1.4.2.** An α-helix of p53 in the hydrophobic cavity of MDM2. Three critical amino acids of the p53-MDM2 interaction are denoted with different colors: Phe19 (blue), Trp23 (green), Leu26 (red) belong to p53 [11].

## 1.5 Nutlin-3a (N3a)

**Nutlin-3a (N3a): (2-piperazinone, 4-[[(4S,5R)-4,5-bis(4-chlorophenyl)-4,5-dihydro-2-[4 methoxy-2-(1-methylethoxy)phenyl]-1H-imidazol-1-yl]carbonyl]-) [13]**

Nutlin-3, as an organic molecule, is a racemic mixture of N3a (active enantiomer) and nutlin-3b (inactive enantiomer). The binding affinity of N3a to MDM2 is 150-fold higher than nutlin-3b [14].

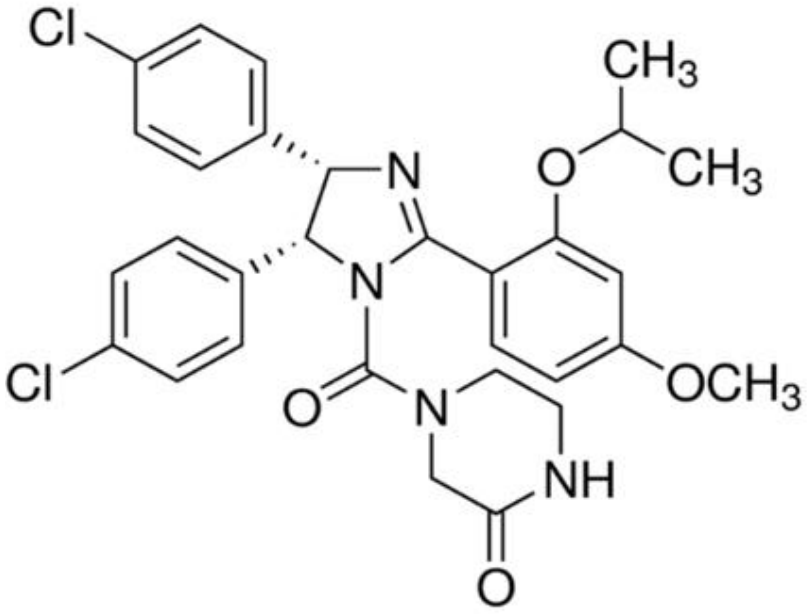


**Figure 1.5.1.** N3a's molecule from Sigma-Aldrich.

### 1.5.1 N3a in relation to MDM2

As mentioned above, α-helix of p53 binds into a relatively deep cleft in the amino terminus of the MDM2 protein. Researchers designed a molecule which can mimic this interaction, N3a, a cis-imidazoline analog used as a cancer drug [11]. This small organic molecule is an MDM2 competitive inhibitor, which mimics three hydrophobic residues on p53, required for MDM2 binding. While N3a binds to the p53-binding pocket of MDM2, it disrupts the interaction between p53 and MDM2. As a result, p53 ubiquitination and proteasomal degradation is inhibited, p53 protein and its transcriptional activity are stabilized (transactivation of p53 target genes) and finally tumor suppression is activated in various cancer tissues including lymphoma. Based on recent research, malignant lymphoma cells are more sensitive to N3a than normal lymphocytes, so N3a is a forerunner of new cancer therapeutics that have reached clinical trials. It has to be pointed out that Nutlin does not interfere with MDM2's ability to monoubiquitinate p53, and also it does not bind to p53 or induce post-translational modifications [2, 10].

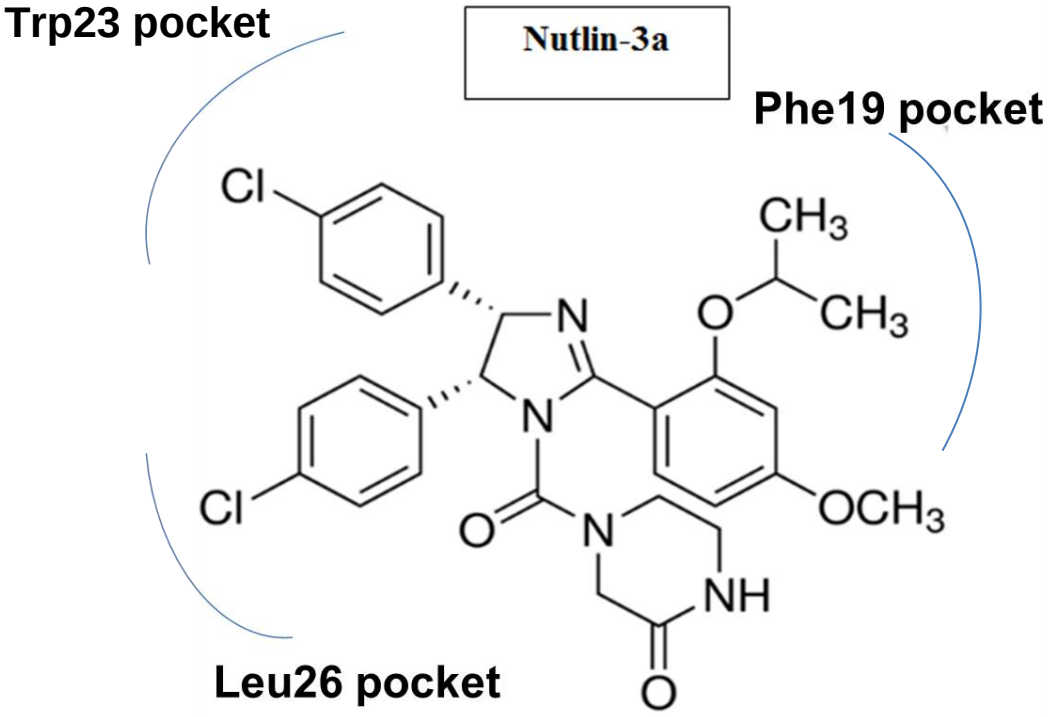


**Figure 1.5.2.** MDM2 inhibitors. Canonical binding to three hydrophobic pockets (Phe19, Trp23, Leu26) is shown for N3a [11].

## 1.5.2 N3a's interactions

Nutlin-3 has extensive hydrogen bonding/electrostatic interactions with MDM2 while also mimicking three hydrophobic residues on p53 required for MDM2 binding. Specifically in the MDM2–p53 model, there are three hydrogen bonding interactions between MDM2 and p53, where the energy of the sum from the three hydrogen bonds is -12.90 kcal/mol; while in the MDM2–Nutlin-3 model there are **four** hydrogen bond interactions between MDM2 and Nutlin-3, where the energy of the sum from the three hydrogen bonds is -18.12 kcal/mol. From this fact we can conclude that the **MDM2–Nutlin-3 complex is relatively more stable than the MDM2– p53 complex**, so Nutlin-3 can easily block the p53 binding pocket of MDM2 and disrupt the MDM2– p53 interaction for the activation of the p53 pathway, leading to tumor cell apoptosis [10].

The H169 of Nutlin-3 is hydrogen bonded with the side chain oxygen atom O76 of Glutamine72. The N133–H–O76 bond angle is 148.24°, and the bond energy is -4.21 kcal/mol. O175 of Nutlin-3 is hydrogen bonded with the side chain hydrogen H65. The calculated H–O bond distance is 1.77 A˚, C58–H65–O175 bond angle is 135.7°, and the bond energy is –6.63 kcal/mol. O125 of Nutlin-3 is hydrogen bonded with the side chain hydrogen atom H81 of Glutamine72. The calculated H–O bond distance is 2.48 A˚, H145 of the C73–H81–O125 bond angle is 131.43°, and the bond energy is –3.65 kcal/mol. H145 of the chlorophenyl moiety of Nutlin3 is hydrogen bonded with the backbone oxygen atom O91 of Valine93. The calculated H–O bond distance is 2.39 A˚, the C109–H145–O91 bond angle is 150.13°, and the bond energy is –3.63 kcal/mol. The interaction energy among MDM2 residues and Nutlin-3 is calculated as –18.12 kcal/mol (fig 1.5.3) [10].

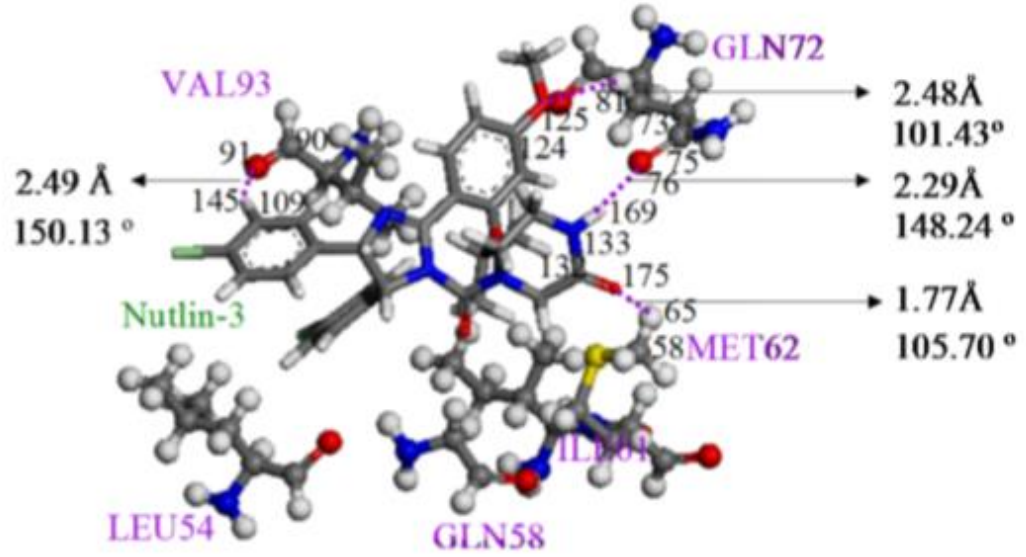


**Figure 1.5.3.** Interaction of Nutlin-3 with surrounding MDM2 residues. Hydrogen bonding is represented by dashed line [10].

### 1.5.3 Nutlin in the cell

### Nutlin causes p53 translocation to mitochondria

Nutlins, especially Nutlin-3 has a significant role in wt p53 human tumor cells, inducing apoptosis through the activation of p53's transcriptional program. In response to stress, aside from wt p53 nuclear stabilization, Nutlin causes cytoplasmic monoubiquitinated p53 accumulation and translocation to mitochondria without any interference in MDM2's ability to monoubiquitinate wt p53. It is worth stating that this translocation occurs as early as 1 hr after adding Nutlin and continues to increase over time. For these reasons it is suggested that mitochondrial p53 pathway and apoptotic p53 response to Nutlin have interdependent relations [15].

### Nutlin's concentration

Recent preclinical studies reported that Nutlin is an effective antitumor drug for important types of cancers carrying wt p53. Some of the cancer types besides Hodgkin lymphoma [16] are HCT116, RKO (colon carcinoma) and, SJSA-1 (osteosarcoma) tumor cell lines, which were exposed to Nutlin. According to MTT colorimetry assay the loss of "viability" measures indicates either cell cycle arrest or cell death. When the drug concentration increases, the viability is being suppressed; this means that more cells are led to apoptosis [17].

## N3a tissue concentrations in mouse organs

Cis N3a (98% purity) was given orally and injected intravenously; tissue concentrations of N3a were determined in plasma, liver, spleen, intestine, muscle, lung, adipose, bone marrow, adrenal gland, brain, retina, and vitreous fluid. In addition, N3a was adhered nonlinear to murine plasma proteins at approximately 2 h after the drug deposition. Concluding, when N3a is administered once or twice daily at high dosages, all the simulations suggested high bioavailability, rapid attainment of steady state, and little accumulation [14].

## Cellular influx and efflux of Nutlin modeling

A **computational stochastic model** was created for the response of tumor cells with wt p53 gene to Nutlin. Based on this model three physical compartments were distinguished between: the nucleus, the cytoplasm and the extra-cellular space, **where Nutlin was present**. Simultaneously this model showed evidence that **Nutlin can be a substrate for ABC transporters like p-glycoprotein**, which suggests the possibility of a nonlinear efflux rate. However, there is substantial **binding of Nutlin to plasma proteins;** Nutlin's concentration in the cytoplasm is only a small fraction of the total Nutlin [17]. Finally, in a mouse pharmacokinetic modeling model for N3a, researchers confirmed that N3a is a substrate for the ATP binding cassette transporter P-glycoprotein (P-gp), but at higher concentrations it can also inhibit P-gp efflux activity [13].

## ABC transporters

Transporters are membrane proteins that are decisive for controlling the influx and efflux of ions, glucose, bile acids, vitamins, hormones, lipids, fatty acids, toxins, and drugs across cell membranes. ABC transporters are a family of active transporters relying on adenosine triphosphate (ATP) hydrolysis to pump substrates in (influx) and out (efflux) of the cell membranes. In eukaryotes, ABC transporters function only as efflux transporters, although in prokaryotes ABC transporters function as both uptake and efflux transporters. ABC transporters do not metabolize drugs themselves, but they affect metabolic clearance remarkably through interplay with drug metabolism enzymes [14].

ABC transporters utilize the energy of ATP hydrolysis to pump anti-cancer agents out of the cell, thus reducing the intracellular drug concentration (fig 1.5.4) [14].

ABC transporters, such as P-glycoprotein (P-gp), MRP2, and BCRP are located mostly on the apical membrane of enterocytes, where they can pump their substrates back to the intestinal lumen, thus limiting the absorption of some orally administered drugs. These canicular membrane transporters excrete their substrates directly into bile. P-gp, MRP2, and MRP4 are expressed at the proximal tubular basolateral membrane facilitating the excretion of compounds into the urine. It was found that P-gp is responsible for excretion of digoxin and

some hydrophobic cationic drugs, while MRP2 and MRP4 are for anionic drugs or metabolites. Also there are different ABC transporters such us MRP1, MRP3, MRP4 and MRP6 which in most cases extrude some drug metabolites or intact drugs back to the blood, and present them to bile or renal excretion. Finally, some ABC transporters are also located at both the apical and basolateral membrane of the renal epithelial cells (fig 1.5.5) [14].

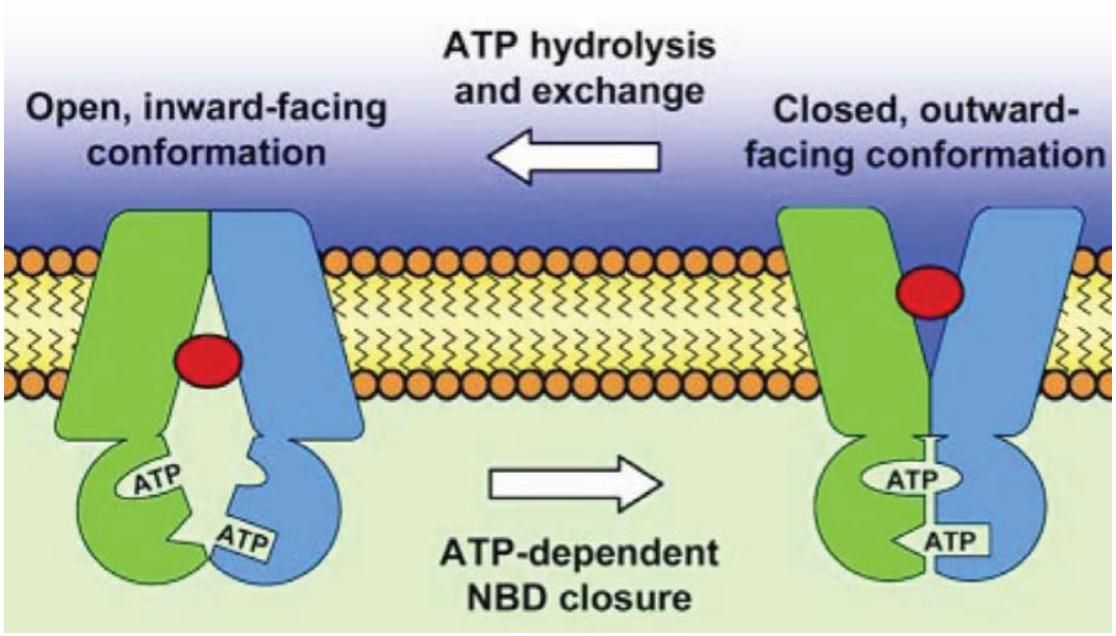


**Figure 1.5.4.** Mechanism of action of a typical ABC transporter [14].

| Name | Polarity | Locations |
|---|---|---|
| P-gp | Apical | Kidney, adrenal gland, liver, pancreas, intestine, lung, BBB, placenta, prostate, skin, heart, skeletal muscle, ovary, testis, retina |
| MDR3 | Apical | Liver |
| BCRP | Apical | Placenta, mammary gland, BBB, liver, intestine, kidney, lung |
| MRP1 | Apical (placenta, BBB) Basolateral (others) | Kidney, lung, testis, skeletal muscle, heart, placenta, liver, intestine, brain |
| MRP2 | Apical | Liver, kidney, intestine, placenta |
| MRP3 | Basolateral | Adrenal gland, intestine, pancreas, intestine, gallbladder, placenta, liver, kidney |
| MRP4 | Apical (kidney, BBB) Basolateral (prostate, choroid plexus) | Prostate, kidney, liver, brain, pancreas |
| MRP5 | Apical (BBB) Basolateral (others) | Heart, brain, neurons |
| MRP6 | Basolateral | Liver, kidney, skin, lung, heart, intestine, pancreas, stomach |
| BSEP | Apical | Liver |

**Figure 1.5.5.** Important ABC transporters [14].

## ABC transporters and N3a

For the treatment of cancer, a major impediment is drug-resistance, where ABC transporters have an important role**.** Recently, researchers noticed that **Nutlin-3 can interfere with the function of the ABC transporters P-pg and MRP1 by functionally inhibiting the action of drug efflux proteins.** This inhibition occurs independently of cellular p53 status. As a result, **cells are sensitive to treatment with cytotoxic agents that are substrates of these efflux proteins.** Furthermore, N3a reverses resistance to the BCRP substrate mitoxantrone by inhibiting BCRP efflux (inhibition of ATPase activity of BCRP), but it is not a BCRP substrate, thereby the intracellular accumulation of mitoxantrone is strongly increased in the malignant cells. The examined cell lines were Saos-2-BCRP, however preclinical studies suggested that N3a inhibited the function of three major efflux transporters BCRP, P-gp, and MRP1 in a variety of pediatric malignancies, including neuroblastoma, retinoblastoma, leukemia, and rhabdomyosarcoma [14].

## N3a in relation to the oncoprotein Notch and to reactive oxygen species

## Notch oncoprotein

So far, we have analyzed the relation between N3a and p53 pathway in correlation to MDM2 E3 ubiquitin ligase. The present class of Nutlin drugs targets the N-terminal allosteric peptide binding pocket in MDM2 without inhibiting the MDM2 ubiquitin ligase function, however they can activate or inhibit MDM2 protein-protein interactions. This situation in a cell culture can result in **Nutlin-3 stabilizing p53 protein or Notch proteins**, preventing the activation of the p53 pathway [18]. Notch proteins are oncogenic proteins, which function as transmembrane receptors that regulate differentiation in all types of tissues and organisms. In particular, Notch receptors and their ligands are responsible for communication between cells in a developing tissue. **The stabilization of the oncoprotein Notch by N3a, might be one reason why tumors in patients do not regress after drug treatment despite the biomarker wt p53 pathway being "activated"** [19]**.**

## Reactive oxygen species

Dihydrolipoamide dehydrogenase is a mitochondrial protein, the E3 component of the three proteins that assemble the pyruvate dehydrogenase complex. Dihydrolipoamide dehydrogenase and dihydrolipoamide acetyltransferase forms protein-protein interaction foci in growing cells. Nutlin-3 treatment dissociates the pyruvate dehydrogenase holoenzyme complex, thereby the number of these protein-protein interaction foci is being reduced. Thus the mitochondrial proteome changes, it causes mitochondrial dysfunction which leads to **overproduction of reactive oxygen species** (ROS) [18].

After Nutlin-3 treatment, the majority of MDM2 is in the nucleus and the majority of dihydrolipoamide dehydrogenase is in the cytoplasm (fig 1.5.6) [18].

**It has been reported that Nutlin-3 causes p53 translocation to the mitochondria**. As depicted in fig 1.5.7., Nutlin-3 treatment increases p53 protein levels where afterwards a quantity of p53 protein is translocated to the mitochondria of cancer cells. There, mitochondrial **p53 induces the generation of ROS**, which, in turn, activates the JNK-death pathway, which in turn mediates $HO^{-1}$ transcription and apoptosis [20].

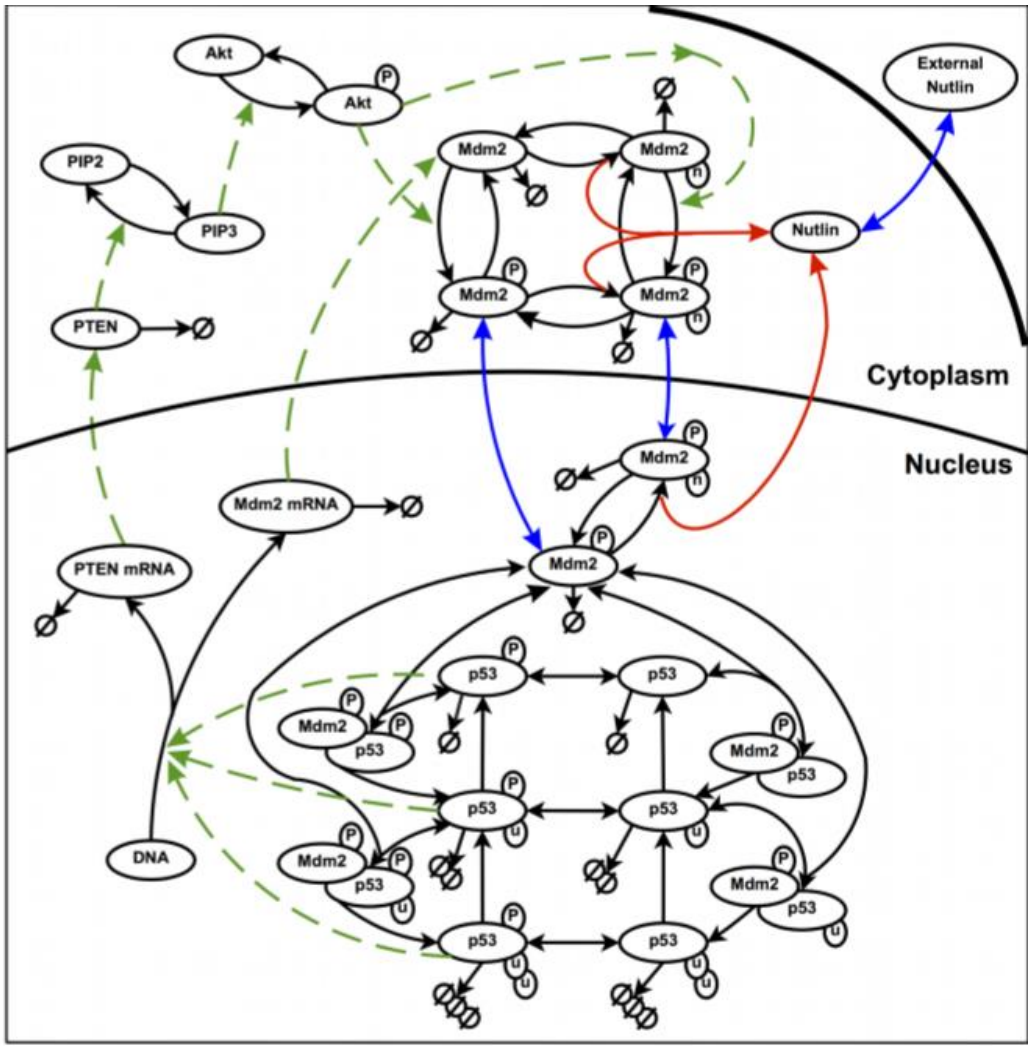


**Figure 1.5.6.** Nutlin-3 is related to the elevated induction of MDM2 in the nucleus. Pictorial view of the p53-MDM2 interactions in the presence of Nutlin. Black solid arrows: chemical reactions; red solid arrows: chemical reactions involving Nutlin; green dashed arrows: induction of activities; blue solid arrows: translocations. P, phosphate group; u, ubiquitin; n, Nutlin; the symbol w denotes degradation [17].

Ultimately the non-genotoxic activation of p53 by Nutlin-3, induces apoptosis by the mitochondrial translocation of p53 in cancer cells, including **leukemia and lymphoma cells** [20].

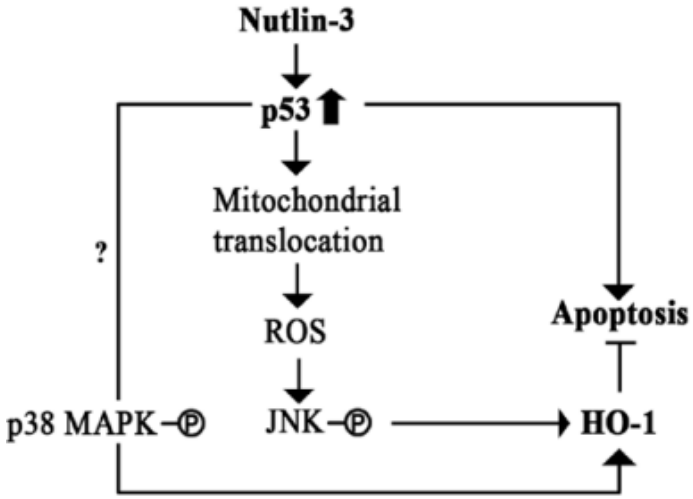


**Figure 1.5.7.** Schematic diagram of nutlin-3-induced $HO^{-1}$ expression [20].

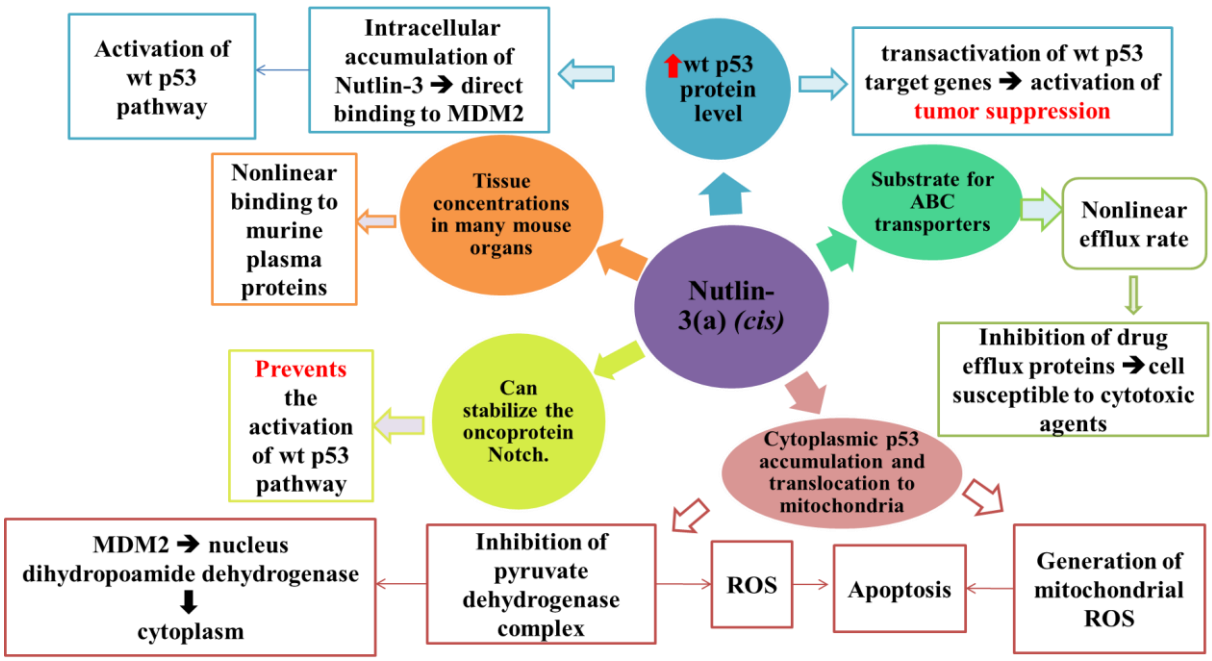


**Figure 1.5.8.** Summary table: most common effects of Nutlin-3.

## 1.6 Raman spectroscopy

### 1.6.1 Introduction to Raman

Raman spectroscopy is a spectroscopic technique sensitive to **changes in the polarizability of vibrating molecules**, investigating the **molecular vibrations,** providing fingerprint-like information about the molecular structure of the analyzed samples. This technique is promising for **cell characterization and analysis**, allowing the **detection of several chemical bonds**, therefore the recognition of amino acids, lipids, nucleic acids, carbohydrates and also structural variations such as protein folding. It can be used in a range of applications from *in vivo* or *in vitro* diagnostics to basic science laboratory testing because it is rapid, non-destructive and label-free, with no requirement for taggings, selective probes or any other sample preparations [21, 22]. It is important to note that the range of measurements fluctuates from micron measurements in single cells to macroscopic regions of tissues, and is uninfluenced by water Raman bands [22].

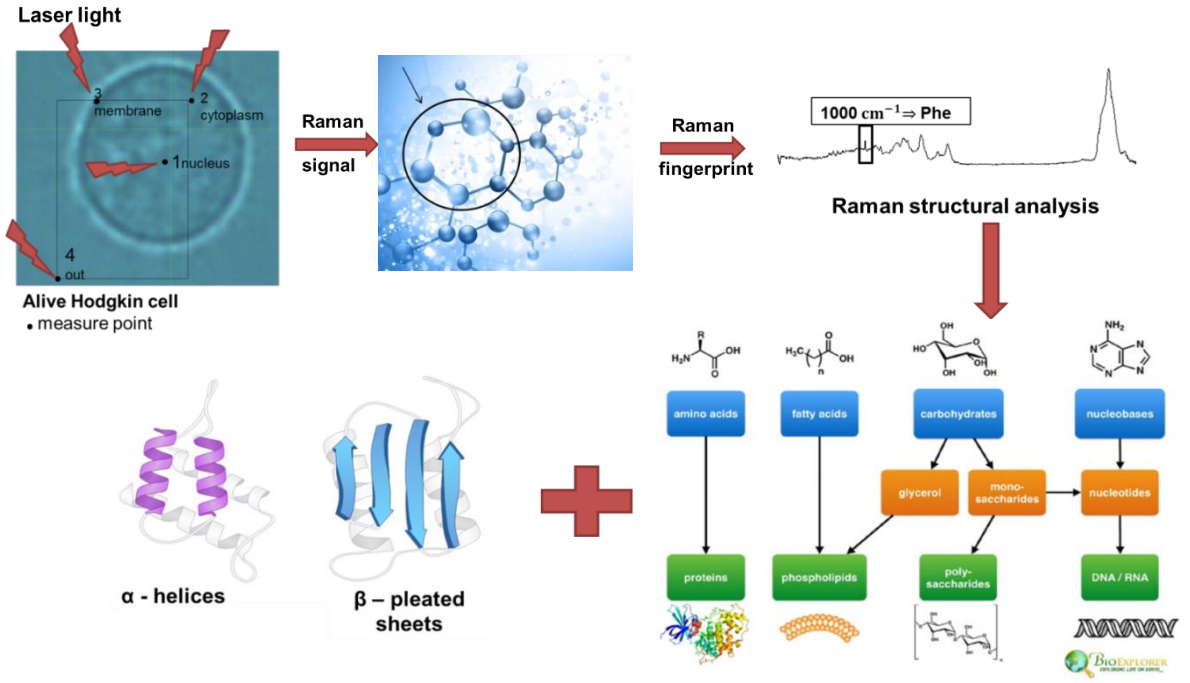


**Figure 1.6.1.** Raman analysis procedure. The Raman signal corresponds to the scattering of light (described in Chapter 1.6.2) and the Raman fingerprint is the representation of said scattering, in a Raman spectrum. [23].

.

If we know the frequency of the incident light, by measuring the frequency of the Raman inelastic scattered light, we can calculate the vibrational energy difference which is called Raman shift, expressed in wavenumbers ($cm^{-1}$), in a Raman spectrum plot. Since complex molecules have several specific vibrational energy modes, Raman spectral features can be used as identification markers of particular substances [24].

### 1.6.2 Operating principles

Raman spectroscopy uses **monochromatic light**, often in the near-IR (NIR), visible or UV range. **Photons of light** (from a laser source) are focused on the sample through the microscope objective at a defined magnification. Immediately after, there is an interaction between the photons and the chemical bonds, where **electrons** are excited to virtual energy levels. The **biological molecules** return to the original energy level by emitting a photon of light (elastic or Rayleigh scattering, where the frequency of the scattered light is the same as that of the incident light), **they can either be raised to** higher energy levels (Stokes scattering, where the frequency of the scattered light will be lower than that of the incident light) **or** they can undergo an energy shift and return to lower energy levels (anti-Stokes scattering, where the frequency of the scattered light will be higher than that of the incident light), known as **Raman scattering** [25, 26].

**Raman scattering** was discovered in 1928 by the Indian Physicist Sir C. V. Raman (1888 - 1970). It refers to **inelastic scattering** of a photon (**1 in $10^8$ photons are inelastically scattered)** from molecules which are excited to higher vibrational energy levels, where we can observe a partial frequency and phase change of the passing radiation. This scattering is quite different **from the usual elastic scattering**, it is about **10 million times weaker** and usually observed in directions perpendicular to the incident beam of light. This phenomenon is caused due to the fact that some of the molecules of the material absorb or provide energy to the incident photons; after scattering they will have a lower or higher frequency. In detail, **the scattered photon exchanges energy with molecular bond oscillations and crystal lattice oscillations of the molecule, and usually gives energy to the fundamental state of the molecule (Stokes phenomenon); it is also observed to receive energy from excited eigenstate (anti-Stokes phenomenon) which transits to lower wavelength than the original one** [27]. When electrons are excited to higher vibrational energy levels and return to the ground energy level, by emitting a photon of light at a longer wavelength**,** fluorescence can be occurred.

All the interactions between the molecules of the sample material in combination with other bound molecular components compose the Raman spectrum of a complex biological sample, which consists of amino acids, lipids, nucleic acids, and other individual chemical signatures [22].

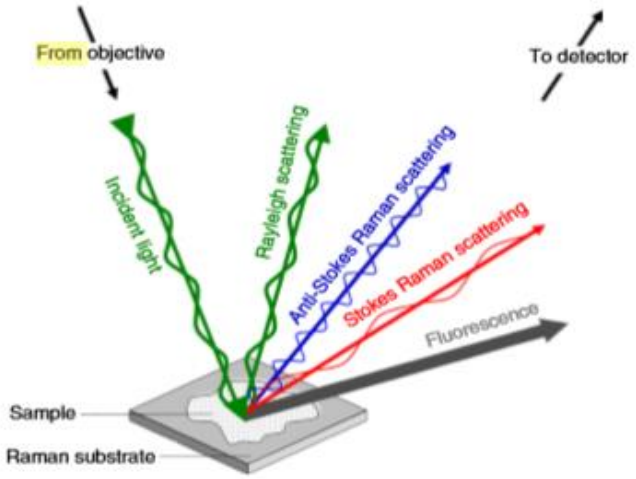


**Figure 1.6.2.** Schematic identifying light scattering after laser exposure on a sample surface [25].

### 1.6.3 Raman stretches and bonds

As it was analyzed before, in Raman spectroscopy the laser light interacts with **molecular vibrations**, therefore the energy of the laser photons is shifted up or down (e.g. Raman shift). This shift in energy provides useful information about the vibrational modes in the system of molecules, identifying the types of bonds which are present in the compound. Molecules have three types of motion: translational, rotational and vibrational. Translational motion is the relocation of the molecules. Rotational motion includes the entire molecule rotating or the internal parts of the molecule rotating with respect to one another. Finally, the motion that interests us, the vibrational motion is the movement of the bonds between atoms within a molecule and is caused by thermal energy, which is present in the surroundings. There are many possible different types of molecular vibrations, such as symmetric and asymmetric stretching, scissoring, rocking, wagging and twisting. When an atom is displaced from its equilibrium position in a molecule and subject to a restoring force, we can say that it makes stretches, wags or twists [28].

### Raman spectrum

A Raman spectrum is unique to a material, and consists of a range of features, each associated with a vibrational mode. Every type of bond (e.g. C-H, C-C, C=C) has unique vibrational modes, which lead to specific interactions with laser light which produces different Raman shifts (see Table 1.6.1.). This information is used for the identification of molecules and chemical bonding studies [28].

**Table 1.6.1.** Approximate Raman shifts ($\mathbf{cm^{-1}}$) for several common functional groups [28].

| Functional group | Region |
|---|---|
| C−C | ~600-1300 $cm^{-1}$ |
| C=C | ~1600 $cm^{-1}$ |
| C≡C | ~2100-2300 $cm^{-1}$ |
| C−H | ~2700-3100 $cm^{-1}$ |

The symmetry of a molecule is necessary for obtaining Raman spectra as symmetric stretches have greater intensity. Functional groups such as –C-X (X=F, Cl, Br or I), –C–$NO_2$, –C–S–, –S–S–, –C=C–, –C=S–, –N=N–, –S–H–, –CN, etc., have more polarizability changes, so they give strong Raman signals [26, 28].

The Raman spectrum of lipids is mainly due to vibrations in the hydrocarbon chains. However, vibrations in the head group region can generate specific lipid fingerprints. Protein spectral marker bands can be divided into two main groups: the bands related to the side chains and the main chain bands (amide bands) related to the protein backbone [22].

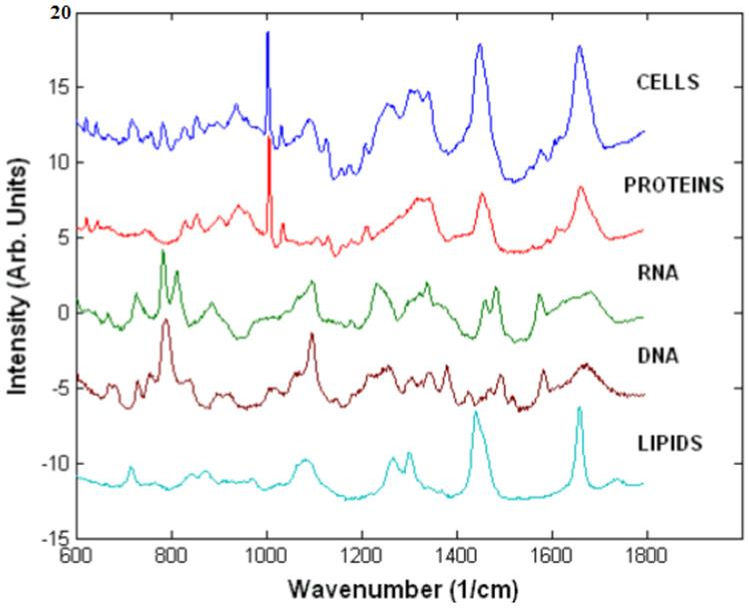


**Figure 1.6.3.** Raman spectra of human cells and constituents [4].

**Table 1.6.2.** A table with important biological peaks [29, 30].

| **Raman Shift ($cm^{-1}$)** | **Assignment** |
|---|---|
| 621 | Phe in $H_20/D_20$ |
| 643/642 | Tyr in $H_20/D_20$ |
| 699 | Amide V in $H_20$ |
| 722 | Met, Tyr, Δ (C-C-C) in $H_20/D_20$ |
| 758/754 | Trp, Ala in $H_20/D_20$ |
| 825 | Tyr Fermi doublet in $H_20/D_20$ |
| 831 | Tyr ➔ O-P-O asym str. |
| 850 | Tyr Fermi doublet in $H_20/D_20$ |
| 877 | Trp, in $H_20$ |
| 897/887 | Lys, Arg, Ala in $H_20/D_20$ |
| 910 | Amide III', side chains in $D_20$ |
| 927 | Amide III' (β-strand) in $D_20$ |
| 934 | σ(Cα-Cβ) (α-helix) in $H_20$ |
| 950 | Amide III' (a-helix) in $D_20$ |
| 957 | Val, Leu, $\delta(CH_3)$ in $H_20$ |
| 963 | Amide III' (coil) |
| 992 | Amide III' extended conformation in $D_20$ |
| 1003-1004 | Phe in $H_20/D_20$ |
| 1012 | Trp in $H_20$ |
| 1032 | Phe in $H_20/D_20$ |
| 1060 | Lys, Arg ,Ala, σ(C-C,C-O) in $H_20$ |
| 1081 | Lys, v(C-N), in $H_20$ |
| 1094 | DNA ➔ O-P-O-, protein ➔ C-N |
| 1101 | Pro, Ala, σ(Ca-N), σ(C-C), in $H_20$ |
| 1127 | Trp, σ(C-C), σ(C-N), in $H_20$ |
| 1156 | $\Delta(CH_3)$, in $H_20$ |
| 1174 | Tyr, Phe, Trp in $H_20/D_20$ |
| 1206 | Tyr, Phe, Trp in $H_20/D_20$ |
| 1210 | Tyr and phe v mode |
| 1230-1240 | Amide III (β-strand), in $H_20$ |
| 1226-1243 | Amide II ➔ β-Poly-L-alanine (β-strand) |
| 1231 | Amide II ➔ P22 tailspike (β-Strand) |
| 1235 | Amide II ➔ P22 coat subunit (β-Strand/turns) |
| 1236 | Amide II ➔ β-Poly-L-glutamate (β-strand) |
| 1240 | Amide II ➔ β-Poly-L-lysine (β-strand) |
| 1243-1248 | Amide II ➔ α-Poly-L-Lysine (pH=4) |
| 1245 | Amide II ➔ cI repressor (1-102) (α-Helix) (Turns) |
| 1245-1255 | Amide III (coils, turns)in $H_20$ |
| 1257 | Protein: Amide III-α |
| 1264-1272 | Amide III (α-helix)in $H_20$ |
| 1264/1260 | Tyr in $H_20/D_20$ |
| 1265-1348 | Amide II ➔ α-Poly-L-alanine (α-Helix) |
| 1249 | Amide II ➔ α-Poly-L-glutamate (pH=11) |

| | |
|---|---|
| 1249 | P22 tailspike (Turns) |
| 1270-1300 | Amide II ➔ fd coat subunit (α-Helix) |
| 1270-1300 | Amide II ➔ Pf1 coat subunit (α-Helix) |
| 1273 | Amide II ➔ P22 coat subunit (α-Helix) |
| 1290 | Amide II ➔ α-Poly-L-glutamate (α-Helix) |
| 1286-1297 | Amide II ➔ cI repressor (1-102) (α-Helix) |
| 1295-1311 | Amide II ➔ α-Poly-L-Lysine (α-Helix) |
| 1300 | Amide III" (α-helix) in $H_20$ |
| 1318 | $\Delta(CH_2)$, in $H_20/D_20$ |
| 1338 | A,G, protein: C-H def. |
| 1340 | Trp (Fermi douplet), δ(C-H), in $H_20$ |
| 1358 | Trp (Fermi douplet), δ(C-H), in $H_20$ |
| 1406/1404 | $\sigma(CO_2)$ in $H_2O$/ $D_2O$ |
| 1450 | $\delta(CH_2)$, $\delta(CH_3)$ in $H_2O$/ $D_2O$ |
| 1458 | Amide II' in $D_2O$ (α-helix) |
| 1470-- | Amide II' (extended conformation) in $D_2O$ |
| 1552 | Trp in $H_2O/D_2O$ |
| 1578 | A,G |
| 1605/1608 | Phe, Tyr in $H_2O/D_2O$ |
| 1618/1614 | Tyr, Trp in $H_2O/D_2O$ |
| 1645-1654/1633-1640 | AmideI/I' (α-helix) in $H_2O/D_2O$ |
| 1645 | Amide I ➔ α-Poly-L-Lysine (α-Helix) |
| 1650 | Amide I ➔ fd coat subunit (α-Helix) |
| 1650 | Amide I ➔ Pf1 coat subunit (α-Helix) |
| 1650 | Amide I ➔ cI repressor (1-102) (α-Helix) |
| 1652 | Amide I ➔ α-Poly-L-glutamate (α-Helix) |
| 1653 | Amide I ➔ P22 coat subunit (α-Helix) |
| 1655 | Amide I ➔ P22 coat subunit (β-Strand/turns) |
| 1655 | Amide I ➔ α-Poly-L-alanine (α-Helix) |
| 1656 | Amide I ➔ α-Poly-L-glutamate (pH=11) |
| 1658 | Protein: Amide I-α |
| 1665-1674/1655 | AmideI/I' (α-helix) (β-strand)in $H_2O/D_2O$ |
| 1660-1665 | Amide I (coil) in $H_2O$ |
| 1665 | Amide I ➔ α-Poly-L-Lysine (pH=4) |
| 1668 | Amide I ➔ P22 tailspike (β-Strand) |
| 1669 | Amide I ➔ β-Poly-L-alanine (β-strand) |
| 1670 | Amide I ➔ β-Poly-L-lysine (β-strand) |
| 1672 | Amide I ➔ β-Poly-L-glutamate (β-strand) |
| 1675 | Amide I ➔ cI repressor (1-102) (α-Helix) (Turns) |
| 1684/1669 | Amide I/I' (extended conformation) in $H_2O/D_2O$ |

### 1.6.4 Instrument Components

## Light scattering after laser exposure on a sample surface

Initially, laser photons are emitted from the **excitation source** and pass through the **Rayleigh filters** towards the **focusing mirror** and finally towards the **sample material**. The scattered photons return back to the **focusing mirror**, the **Rayleigh filters, the monochromators**, **another focusing mirror** and finally the **detector [25]**.

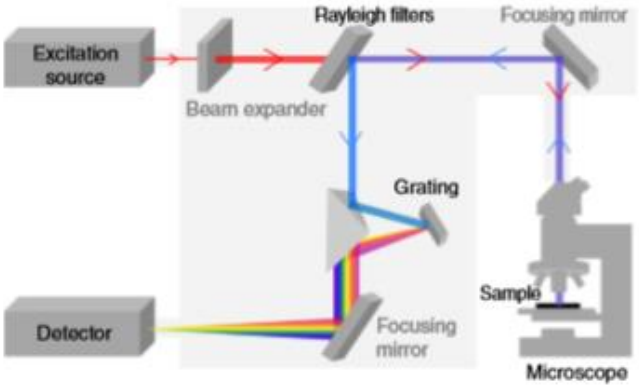


**Figure 1.6.4.** Generalized overview of instrumentation options within a typical spontaneous Raman spectroscopic microscope system [25].

## Laser system

The **total laser intensity** (power/area) which illuminates the sample material is a determining factor for high-quality Raman measurements from biological samples. The **laser system** is determined by the type of laser source, the desired wavelength and spot size. **Diode lasers** are increasingly common, especially for biological investigations, which are based on solid or semiconductor technology. **Laser power** is also important as we want to minimize photodamage leading to phototoxicity. It would be reasonable to reduce exposure times wherever possible and to conduct controls to determine the toxic effects of the in use laser wavelength. Additionally, **spectral resolution** depends on the line width of the laser and is greater at higher excitation wavelengths, provided that the Raman optical configuration remains constant. A higher spectral resolution can be achieved by increasing the number of smaller-sized pixels within the detector and reducing levels of cross talk between pixels. **The spatial resolution** is defined by the diffraction limit of laser light, therefore on the laser wavelength (λ) in use, as well as on the numerical aperture of the objective. It also depends on the spot size of the illuminating beam, based on the optics and the wavelength of the laser. Finally, **sensitivity** is also based on the excitation wavelength and **specialized filters** are used for the selection of specific wavelengths from the sample [25].

## Filters and monochromators

The informative signal is overpowered by Rayleigh scattering which is more intense than Raman scattering, so it must be optically filtered. Depending on the dispersion, nondispersive Raman spectrometers use **Fourier transformation (FT)** and dispersion Raman spectrometers use specialized **Rayleigh filters** such us **holographic notch and edge filters (dielectric edge, Metal oxide edge)** or **multistage monochromators.** Rayleigh filters must be specific to the laser wavelength. Edge filters only transmit light wavelengths above that of the laser in use**. Metal oxide edge** filters have noticeably longer lifetimes than notch filters. **Single monochromators** which include a diffraction grating to disperse the Raman scattered light are universally used in conjunction with **Rayleigh filters** [25].

## 2D Detectors

The production of true Raman images from relatively flat samples can be carried out with specialized filters, as described above, and with **2D Detectors.** Due to the fact that Raman scattering has weak intensity and particularly high noise, the detector needs to be extremely sensitive. Nowadays, 2D Detectors have **Charge-coupled devices (CCDs)** integrated in Raman systems; they display high quantum efficiencies and low signal-to-noise ratios (SNRs) across the laser line, compared to early alternative detectors. CCDs are multichannel arrays consisting of thousands of pixels, which can collect directly proportional charge to the Raman scattering intensity from scattered photons. The detector **recognizes and translates** the charge from each pixel, the information then reaches the readout electronics [25].

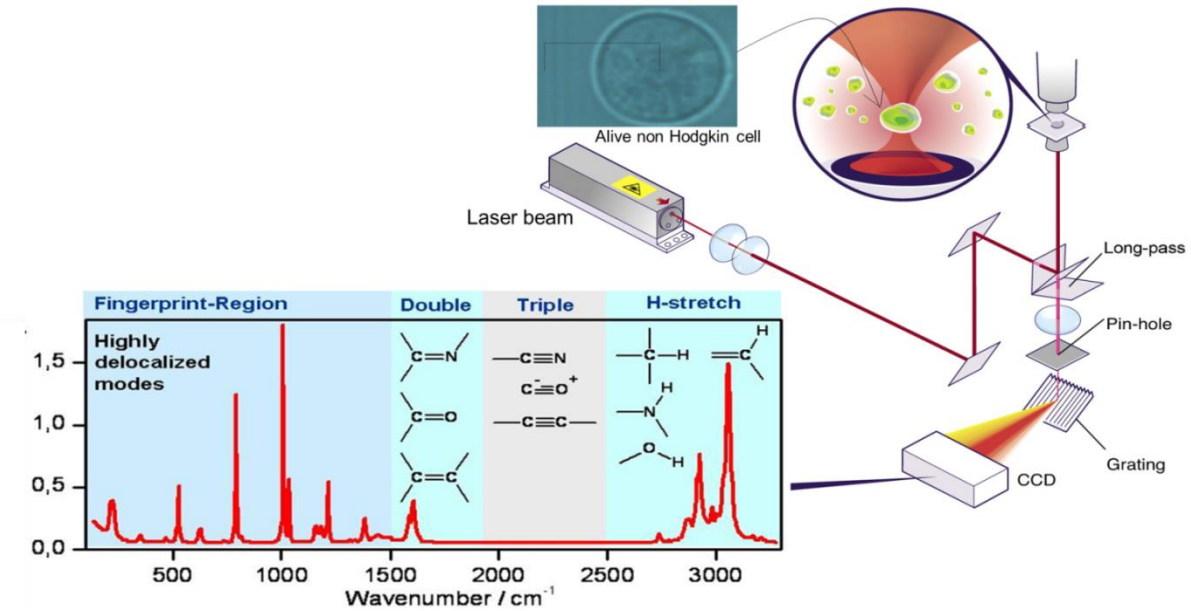


**Figure 1.6.5.** Raman measurement representation [31, 32].

## Microscope slides

Microscope slides made of glass have strong background fluorescence at most wavelengths except 532 nm. **Metal-coated glass slides** (aluminum/gold-coated glass) eliminate the glass signal. **Calcium fluoride ($CaF_2$),** quartz or fused silica slides are commonly used as Raman microscope slides because they have minimal background fluorescence but they are expensive [25].

## Calibration

Calibration is a necessity before each Raman measurement. Primarily, the user has to confirm the position of the laser spot which has to correspond with the visual and spectrometer sampling point. Also, depending on the instrument manufacturer, there are manual and/or automatic calibration options. Secondly pixels must be converted to wavelength by measuring the light emissions of a calibration lamp and after that the wavelength has to be converted to wavenumber units by forming its inverse. Finally, the laser wavelength must be corrected, using reference materials with defined Raman signatures, such as silicon (sharp peak at 520.5 $cm^{-1}$) [25].

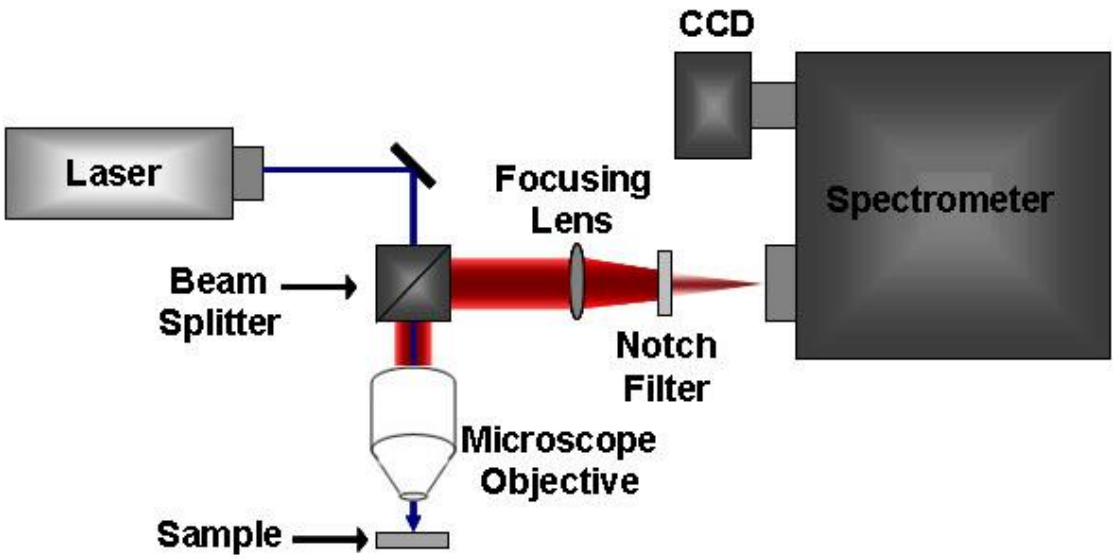


**Figure 1.6.6.** Raman spectroscopy experimental setup [33].

### 1.6.5 Confocal Raman spectroscopy

The first confocal scanning microscope was invented in 1955 by Marvin Minsky in order to avoid thin-slicing of brain tissues. In confocal Raman microscopy, laser light from the probe-head is focused on the sample through the microscope objective. Furthermore, the back scattered Raman signal is refocused onto a pinhole aperture that acts as a spatial filter. The filtered Raman signal then returns to the spectrometer where it is dispersed on a CCD (charge coupled device) camera to produce a spectrum.

Confocal Raman spectroscopy allows two or three dimensional imaging (possible scale 0.5–1.0 μm), and also combines Raman spectroscopy with confocal microscope optics. The wavelength of the excitation laser determines the resolution and the volume measured is small enough to prevent the fluorescence interference. This Resolution enhancement is achieved through a particular lens and laser beam arrangement focused on one point, where the diameter of the beam is reduced. Thus, **the energy is increased, while laser intensity is doubled**. For cell imaging, **Trans and Epi-illumination is combined** as **absorption and reflection of laser photons happens at the same time from the same lens**. As a result the internal observation of proteins and other molecules is more efficient and the Raman signals are slightly better.

However, measurement time can be extensive since many points must be measured and integrated to create an image. Due to the increased laser intensity, the energy targeted at the focused point is higher, so thermal damage of the specimen is possible. To avoid this, it is beneficial to reduce the measurement time. **The combination of confocal Raman microspectroscopy and confocal scanning laser microscopy (CSLM) is a novel non-invasive promising method to obtain information about the molecular composition of tissues** [25, 26].

### 1.6.6 Raman spectroscopy applications

Raman spectroscopy as vibrational spectroscopy has versatility in the sampling methods and produces the vibrational spectrum of the analyzed sample, allowing its interpretation and identification in various fields of science. The range of Raman spectroscopy applications is wide; Raman measurements can be used to analyze diverse substances applying to ancient archaeology, advanced nanotechnology, biotechnology, mineralogy, environmental monitoring, food and beverages, forensic science, medical and clinical chemistry, diagnostics, pharmaceutical, material science, surface analysis, etc. Some of the materials that have been analyzed successfully by Raman spectroscopy are fibers, explosives, drugs, paints, inorganic fillers and lipsticks [26].

### Bioanalysis

Live cells can interact with toxic agents or drugs which can be related to diseases, cell death and differentiation. Each interaction can produce changes in Raman spectra which can be observed by the displacement of peaks or intensity fluctuations.

Raman spectra of biological macromolecules arise from the molecular vibration of either the backbone chains or the side chains. The wavenumbers of the Raman bands lie in a region

between 200 and 3000 $cm^{-1}$. The conformation of secondary structure can be determined by analyzing Amide I and Amide III vibrations of polypeptides and protein backbone chains. Similarly, in polynucleotides and nucleic acids the wavenumbers of phosphate diester stretch of phosphate furanose chain varies between 814 $cm^{-1}$ for A conformation and 790 $cm^{-1}$ for B conformation. Finally, the examination and identification of unenhanced bio-membrane monolayer spectra can be attributed to Raman spectroscopy [26].

## Diagnostics

Raman spectroscopy in endoscopic imaging and quantization of biochemical constituents, during clinical studies, can offer various advantages, analyzing a variety of biomedical materials for disease diagnosis. This can be accomplished by histochemical analysis of biological tissues (gynecological, breast, colon, bladder, brain and cancer tissues), tissue proteins, lenses, corneas, blood constituents, biological stones, hard tissues, etc. Since benign and malignant tumors have different spectra, Raman techniques can be used as an alternative for cancer detection [26].

### 1.6.7 Raman in lymphoma cell lines

Before we get started on our research on Raman spectroscopy in lymphoma cell lines with/without N3a treatment, it would be beneficial to mention some examples of previous researches on Raman spectroscopy in different lymphoma cell lines.

## Human Burkitt's lymphoma cells treated with paclitaxel

In 2011, researchers used Raman spectroscopy to study the human Burkitt's lymphoma cells (CA46) in vitro, treated with the drug paclitaxel, in different doses. The Raman measurements showed that paclitaxel hardly had any interference signals; small deviations grew as the concentration of the drug was increasing, which indicated that there was something abnormal in the structure and content of the biochemical molecules inside the tumor cells. The signal differences were associated to changes in protein structures and decreased cellular DNA concentration, as the concentration of paclitaxel increased [29].

| Peak positions ($cm^{-1}$) | Major assignment |
|---|---|
| 831 | O–P–O asym. str., Tyr |
| 1003/1004 | Symmetric ring breathing mode of Phe |
| 1094 | DNA: $O–P–O^{-}$ p: C–N |
| 1210 | Tyr and phe ν mode |
| 1257 | p: Amide III-α |
| 1338 | A, G, p: C–H def. |
| 1578 | A, G |
| 1658 | p: Amide I-α |

*Notes*: str. – stretching; def. – deformation vibration; sym. – symmetric; asym. – asymmetric; A, G – ring breathing modes of the DNA/RNA bases; p – protein; Tyr – tyrosine and Phe – phenylalanine.

**Figure 1.6.7.** The most important Raman peaks of human Burkitt's lymphoma cells. Peak positions and assignments of Raman spectra [29].

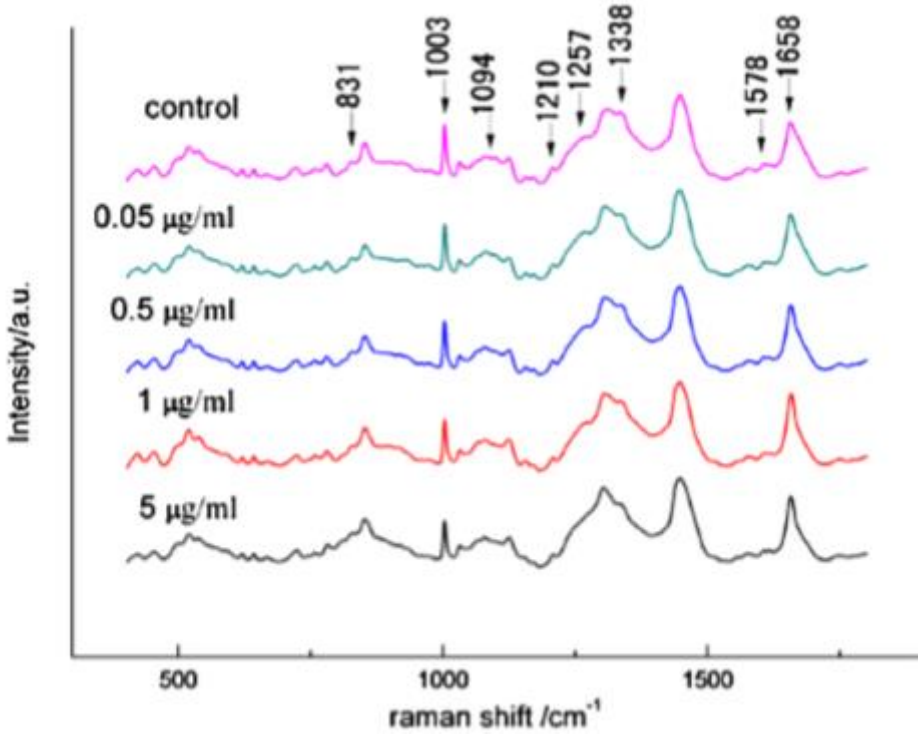


**Figure 1.6.8.** Raman spectra for the control CA46 cells and the treated CA46 cells after interacting with paclitaxel of different concentrations for 24 h [29].

## Human Jurkat lymphoma cells treated with the drug Bleocin™

Sometimes, double stranded DNA breaks [DSBs] and the subsequent repair can lead to mutations that can cause cell damage and disease. Raman spectroscopy can measure DSBs from purified DNA samples. For the detection of DNA damage, human Jurkat lymphocytes were cultured in the presence of the chemotherapy drug Bleocin™. DNA from the Bleocin™ treated cells demonstrated enhanced Raman absorption at 880, 1044, 1084, and 1458 $cm^{-1}$ versus untreated cells [34].

## BCBL-1, BC-1, and BJAB (B lymphoma) cells

As it was mentioned before, many of HL cases are caused by Epstein-Barr virus infection. Additionally, there are some other viruses that also cause many lymphoma-like diseases. Herpesvirus-8 (KSHV/HHV-8) causes tumors, and it is associated with several diseases, such as Kaposi's sarcoma, multicentric Castleman disease, and **primary effusion lymphoma.**
Scientists used Raman tweezers spectroscopy to study BJAB (Burkitts lymphoma) and infected BCBL-1, BC-1(KSHV) single cells. Raman tweezers includes a confocal microscope, combining the use of laser (optical) tweezers and Raman spectroscopy (LTRS). Optical tweezers is a technique that uses the same laser beam to analyze the optical spectrum of the cell but without physically touching it.
The Raman spectrum of infected lymphoma cells under physiological conditions was recorded at 22°C, where their Raman band intensities were significantly altered in the nucleus. In particular, at 1004, 1093, and 1664 $cm^{-1}$, which represent the side-chain bond (predominantly phenylalanine) of proteins, backbone of nucleic acids, and amide I main-chain of proteins, respectively, KSHV infected cells had greater Raman intensities compared to uninfected cells (BJAB) [35].

| Bands ($cm^{-1}$) | Assigned component |
|---|---|
| 1663 | Amide I |
| 1612 | Trp/Tyr/Phe |
| 1581 | Nucleic acids (A, G) |
| 1452 | Lipid/P (—CH; def) |
| 1343 | Nucleic acids (A, G; def) |
| 1320 | Nucleic acids (A) |
| 1254 | Amide III |
| 1128 | C—N |
| 1096 | DNA:BK |
| 1032 | Phe |
| 1004 | Phe |
| 934 | DNA:BK |
| 852 | Tyr |
| 782 | Nucleic acids (C, T) |
| 728 | Adenine |

*Abbreviation*: P: protein, BK: the backbone of DNA, def: the deformed vibration of the C—H bond due to the local micro-environmental change.

**Figure 1.6.9.** Raman bands for human B cells and their assignments [35].

## Non-Hodgkin lymphoma B-cells compared to normal B-cells

In January 2018, scientists wanted to distinguish non-Hodgkin lymphoma B-cells from normal B-cells using Raman spectroscopy to demonstrate the unique fingerprint of each cell line. B-NHL Burkitt's lymphoma cell lines (Ramos and CA46) were cultured and normal B-cells were isolated from peripheral blood. A Micro-Raman RXN system was used for the Raman measurements, cells were placed directly on aluminum reflective slides cleaned with methanol before and after the measurements. Each measurement was collected for 60 seconds with 10mW laser power. Finally, the molecular fingerprint Raman spectral region of B-cell lymphoma ranged from 600 to 1800 $cm^{-1}$ providing the biological information of the cells' constituents. Raman spectroscopy analysis provided fingerprints for DNA/protein concentrations and saccharide bonds which however were difficult to be distinguished. For this reason, additional analysis, like Asymmetric least squares (AsLS) and principal component analysis (PCA) were performed to detect the differences between the cell types. In conclusion, the Raman spectroscopy fingerprints of normal B-cells and B-NHL cells had similar peaks and phenotypes, which could be assigned to cellular constituents (DNA/RNA, amino acids, lipids, carbohydrates) [1].

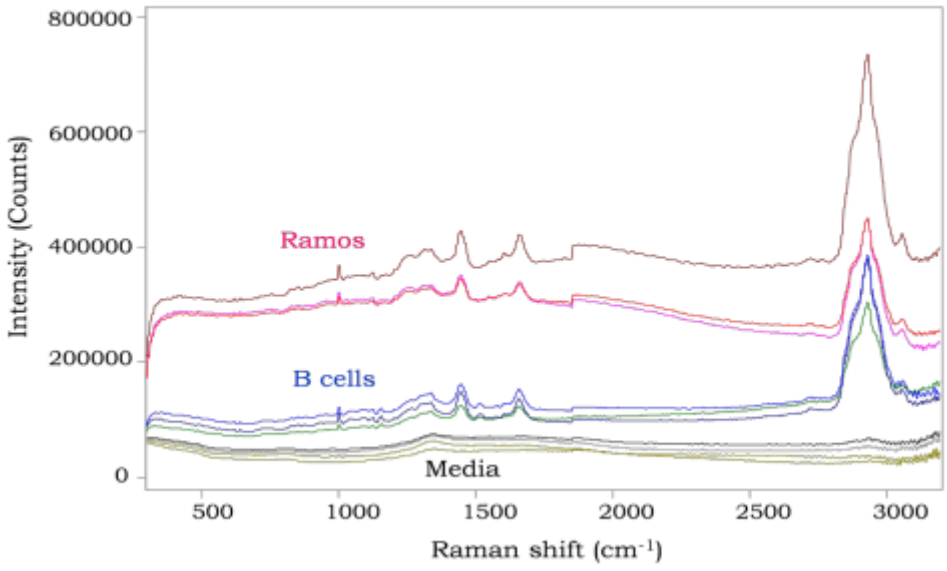


**Figure 1.6.10.** Representative Raman spectra (RS) fingerprints of cells and media. RS fingerprints of Ramos cells, normal B-cells and cell culture media [1].

## 1.7 PCA analysis

Principal component analysis (PCA) is a **statistical technique of linear regression** for reducing the dimensionality of large datasets which are often difficult to interpret, increasing interpretability but at the same time minimizing information loss. The regression estimates are used to explain the relationship between one dependent variable and one or more independent ones (coordinate system).

$$y = c+bx$$

In that equation, y is the estimated dependent variable score, b is the regression coefficient, x is the score on the independent variable and c is the constant.

It concerns the creation of new uncorrelated variables, (linear functions of those in the original dataset) principal components, which solve an eigenvalue/eigenvector problem and then successfully maximize variance. The quantity of principal components is equal to the quantity of the initial variables, and presents the same statistical information. Principal components represent the axes which virtually don't have any physical definition but lead to spatial linear imaging, introducing information related to our data.

When we carry out a PCA analysis our aim is to find the principal components which indicate the greatest differentiation among them, so that data can be separated in clusters of spots, where each spot represents one individual graph in our occasion [36].

# Chapter 2: Experimental Procedure

The lymphoma cell lines used in this project were:

- **MDA-V/HL:** Classical HL (cHL) derived from B-cells (an Epstein Barr virus (EBV) + cHL)
- **JMP-1/MCL:** NHL, Mantle cell (MCL), derived from B-cells
- **SUP-M2:** NHL, Anaplastic large cell lymphoma (ALCL), derived from T-cells (an ALK + ALCL)

## 2.1 Lymphoma cell cultures

The average time lymphoma cells needed culturing, for experiments to begin, was from 15 days up to 1 month (depending on the cell line). Cells were placed in 6 (or 12) well-plates with a final volume of 5(or 2) ml in each well, with or without N3a treatment [37]. The concentration of N3a used in the -/+ N3a-effect experiments was 5μM, according to previous unpublished work performed by our group (Aivaliotis group). After lymphoma cell cultures were maintained appropriate cell growth stage (log phase), we performed the following cell preparation procedure for Raman spectroscopy, as described below.

## 2.2 Sample preparation for Raman measurements

### 2.2.1 Initial 2-3 days protocol (PR1) cell preparation for Raman

The initial 2-3 days protocol is followed 2-3 days prior to the Raman measurements of the cells. Throughout the whole duration of the procedure, we maintained sterile conditions at all times, working in a cell culture hood. Lymphoma cells were maintained in regular plating medium, incubated at 37° C in 5% $CO_2$/95% humidified air, and routinely seeded at a cell density of ~ 0.75 x $10^6$ viable cells/ml.

**Materials:** $CaF_2$ coverslips in paper-container, poly-D-lysine (PDL) stock solution (1mg/ml in double delisted water), sterile 35 mm plastic petri culture dishes, sterile PBS, fixative, cell-cultures, silicone ring, $CaF_2$ microscope slide, blunt-nosed thumb forceps, hook-like-edged needle, well plates, RPMI 1640 (phenol free)

**PDL**: Polylysine (PDL) is a Cationic polymer with a pH of 7 and a positively charged hydrophilic amine group. Polymerization leads to formation of α or ε polylysine; ε polylysine acts as a binding bridge on the surface of the cells and also has the ability to adhere on the coverslip. Specifically, Polylysine enhances electrostatic interactions between negatively-charged ions of the cell membrane and positively-charged surface ions of the attachment factors on the culture surface (in our case, coverslip). When absorbed to the culture surface, it increases the number of positively-charged sites, available for the cell binding. As a reference ε polylysine is electrostatically adsorbed on the surface of bacteria by stripping off the outer

membrane and finally entering the bacterial cell causing damage. Also it is used as a food preservative [38, 39, 40].

**PBS**: Phosphate buffer saline is a buffer solution commonly used in biological research. It is a water-based salt solution containing disodium hydrogen phosphate, sodium chloride and in some formulations, potassium chloride and potassium dihydrogen phosphate. The buffer helps to maintain a constant pH. It is non-toxic to most cells and it is used for substance dilution and cell container rinsing [41].

**RPMI 1640**: RPMI 1640 is a form of medium used in cell cultures and tissue cultures for growing a variety of mammalian cell lines such us human lymphocytes [42]. This medium is high in phosphate and is formulated for use in a 5% carbon dioxide atmosphere. RPMI 1640 has traditionally been used for the serum-free growth of human lymphoid cells.

RPMI 1640 Medium is unique compared to other media because it contains the reducing agent glutathione and high concentrations of vitamins, furthermore RPMI 1640 Medium contains biotin, vitamin B12, and PABA, which are not found in Eagle's Minimal Essential Medium or Dulbecco's Modified Eagle Medium. In addition, inositol and choline are present in very high concentrations; however no proteins, lipids, or growth factors are present in the medium. Therefore, RPMI 1640 Medium requires supplementation, commonly with 10% Fetal Bovine Serum (FBS). Finally, RPMI 1640 Medium uses a sodium bicarbonate buffer system (2.0 g/L), and consequently requires a 5–10% $CO_2$ environment to maintain physiological pH [42].

## Procedure:

- **Preparation of coverslips in culture hood (1st day)**

We first sterilize the $CaF_2$ (coverslip) covering with 500μl EtOH in a petri dish for 5min. Secondly, we leave the petri dish with the coverslip inside into the incubator or in the hood to air-dry for about 30 min. Next, we coat the coverslip with 500μl PDL to form a thin film, avoiding any formation of bubbles in the center of the coverslip and we leave it in the incubator for at least 1 h. Afterwards, we aspirate the excess PDL from the petri dish and we store it at 4°C for later use. Then we make 2 repeated thorough washes with sterile PBS. Finally, we let the coated coverslip completely air dry in the incubator for about 6 h.

- **Live cells (2nd day)**

On the second day we place our lymphoma cells (a small quantity of the cell culture) in the petri dish containing the coverslip by gently shaking a few times in a clock-wise or anti clock-wise movement and then we leave them to bind to the coverslip for a minimum of 12h. This particular waiting time allows the cells to develop the appropriate electrostatic interactions, caused by the PDL, between the cell membranes and the coverslip.

- **Raman measurement day (3rd day)**

On the third day we first remove the medium from the petri dish and immediately afterwards we make 2 repeated thorough washes with sterile PBS to remove any traces of the medium

and any unattached cells from the petri dish. We then place a silicone ring on the microscope slide and we fill it with PBS (or a medium with no Phenols and Hepes), aspirating the excess liquid from the microscope slide. Subsequently, using the forceps and the needle to handle the coverslip we place it on top of the silicon ring in such a manner that the cells face towards the inner side and are in contact with the PBS. Finally, we gently tap the coverslip to ensure a secure adherence to the microscope slide. After that the samples are ready to be analyzed with Raman spectroscopy.

**Fixation method**

The disadvantages of live cell imaging are the reason why sometimes we use fixatives for Raman observation of lymphoma cells. Cell fixation is a chemical process by which the internal biochemical constituents and external structures of the cell are preserved.

For the fixation of the cells, after the 2$^{nd}$ day the medium was removed from the petri dish and 2 repeated thorough washes were made with sterile PBS, we then placed 500μl 10% $CH_2O$ (fixative) on the coverslip in the petri dish, letting it incubate for 10 min before removing the $CH_2O$ from the petri dish. Afterwards we made 3 repeated thorough washes with sterile PBS to remove the fixative and finally we continued the protocol of the 3$^{rd}$ day with the positioning of silicon ring on the microscope slide.

**Advantages and disadvantages**

There are some advantages and some disadvantages in the fixation method. When we use a fixative, cells lose their mobility, stabilizing the cells and causing enzyme inactivation during the observation, they also become permeable to large molecules and future sample observation is possible. Nevertheless, there are some disadvantages that are harmful for Raman observations. With fixation cells are dead, so all the cell's dynamic biological processes cease to exist, consequently there will be significant spectral differences compared to live cells. Another disadvantage is the internal water loss which induces structure collapse and the delocalization of biomolecules. Finally, fixatives penetrate cells and react with proteins, lipids and DNA, hence lipids and DNA may be damaged and protein conformation may be altered. As a result, Raman peaks will be shifted and intensity fluctuations will be present [43, 44].

**Formaldehyde fixative**

Fixation methods can be classified by their chemical nature: aldehydes, alcohols, oxidizing agents and metallic fixatives, or by their action: cross-linking, dehydration, heat effects, or acid effects. Aldehyde-based fixatives like formaldehyde, paraformaldehyde and glutaraldehyde, act as cross-linking agents that react with proteins and nucleic acids in the cell.

### 2.2.2 Modified protocol (PR2) based on the PR1 for Raman spectroscopy

## Modifications in cell preparation protocol for Raman spectroscopy

- PBS washes were made with gentler handling and after every wash, we observed the coverslip under a microscope, to verify the cells' presence. After 2 washes with PBS (3rd day), we observed higher cell mobility.
- We didn't use any silicone rings, instead we placed the coverslip face down on the microscope slide, on top of the round holes of a small, thin polyimide tape (kapton) of 25 μm thickness; on top of the coverslip, and a small quantity of PBS was placed. As a result of that, without the use of any silicon ring, we didn't have any difficulty detecting the cells using the lens. We regulated a constant cell temperature using the "PE120-XY Linkam Scientific" stage. By maintaining a low temperature, cells receive lower energy amounts from their environment, so they lose their mobility; this is another reason that we don't require any fixatives, so none were used.

### 2.2.3 New cell preparation protocol (PR3) for Raman spectroscopy

Due to the increased cells' mobility, the use of a coverslip proved to be unnecessary; instead, we decided to place the **cells directly on the microscope slide**. As it was ascertained from other researchers (Shiramizu et al., J Biol Med Sci 2018, 2:1) who used this method, this is the optimal way for cell Raman imaging. For this reason, the preparation of cell suspension was completely different and far more simple [1].

## Preparation of cell suspension (Raman measurement day)

To begin with, cells with a viability of approximately 90% were mixed in an eppendorf tube with RPMI (step 1) and centrifuged at 1200rpm (=266g) for 5min (Centrifugation Thermo Scientific SL 16R centrifuge) (step 2). Next, we removed the supernatant (step 3) and we added PBS in a new eppendorf tube, to reach a concentration of 100,000 cells/ml (step 4-resuspension). Afterwards, we repeated some of the steps according to the following sequence: 2➔3➔4➔2➔3. Finally, we added **RPMI phenol-free** (RPMI 1640 without dye to avoid fluorescence, which creates interference in Raman spectrum) and we were ready for Raman measurements. Using this method, the starting concentration of the cell culture was 500,000 cells/ml and the final concentration was 100,000 cells/ml.

## Raman measurements

For the Raman measurements of our lymphoma cells, 20 μl of cell suspension was placed directly on a $CaF_2$ microscope slide, previously cleaned and stored in Et-OH. An Olympus 60x water immersion lens was used for the measurements, which was in direct contact with the sample, and created a thin layer of approximately 200um of thickness. The theoretical laser beam diameter was approximately 1um, with an axial size about 1um. There was no visible evaporation of the RPMI after the measurements were completed, indicating that Raman signal intensities should remain constant. Images were acquired before and after the measurement to detect any possible movements of the cell, or jitter of the microscope stage,

or defocusing due to thermal changes caused by laser absorption from the sample. It is worth noting that the Rayleigh scattering was removed and the light passing through the lens is the Raman scattering.

# Chapter 3: Results

## 3.1 Sample preparation method development

Recent Raman studies have reported that aldehyde fixation methods appear significantly better than organic solvents and other fixation methods, with less severe loss of biochemical information but also show an altered cell biochemical content as all fixatives [43, 44].
An extensive research on the fixatives in Raman spectroscopy has been carried out, although we are not going to look further into them since we did not use fixatives extensively in our experiments except only once.

During Raman measurements, in one of our experimental cases, where the PR1 was followed, for unknown reasons, JMP-1/MCL lymphoma cells were detached from the coverslip, so they resulted on the microscope slide and Raman observation was impossible. Some probable causes might be that JMP-1/MCL cells formed weak bonds with PDL or they did not at all, ergo PBS washes removed all the cells from the coverslip or were strong enough to break the bonds between PDL and JMP-1/MCL cells. Another reason may be the high temperatures which increased cell mobility, so cells were detached and resulted on the microscope slide.

This unexpected situation was the reason why we decided to modify our PR1 for Raman spectroscopy (PR2), as well as the fact that Formaldehyde fixative had very close Raman shifts to N3a (fig 3.1.1) which was not acceptable for our experiments with N3a.

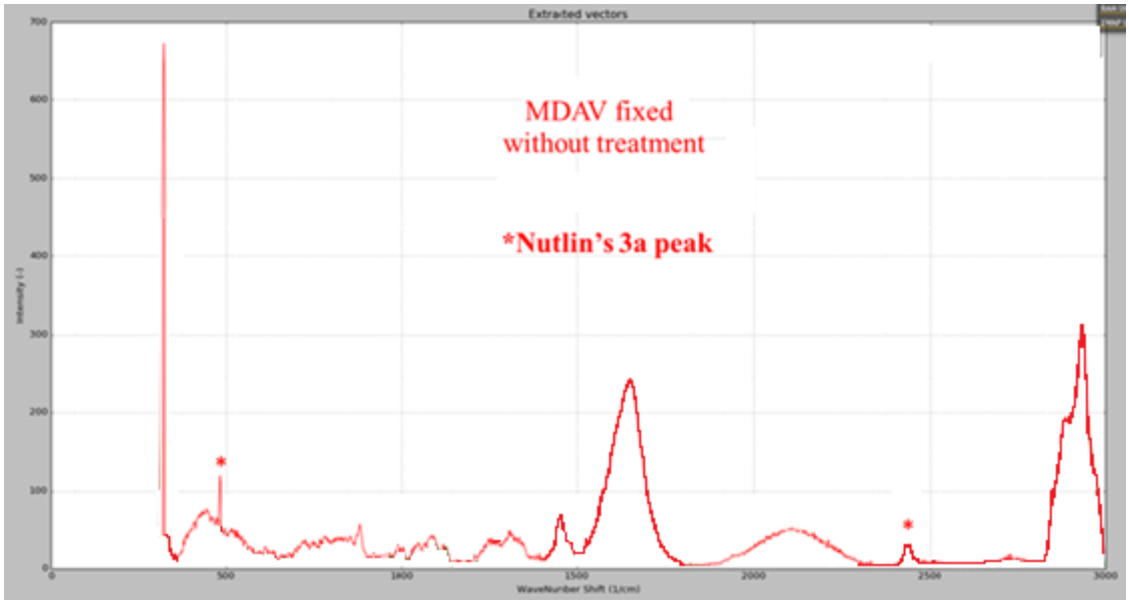


**Figure 3.1.1**. Raman plot of formaldehyde fixation effect on MDA-V/HL cells without N3a treatment. The Raman N3a's strong peaks at **480 cm$^{-1}$** and **2436 cm$^{-1}$** of the fixated cell are also present during formaldehyde fixation.

## Advantages of PR3 for Raman spectroscopy”

The PR1 protocol alterations made leading to PR2 protocol (Chapter 2.2.2) were not adequate, so we proceeded to more alterations leading to PR3 protocol (Chapter 2.2.3).

Following the PR3 for Raman spectroscopy we observed a lot of advantages compared to the previous method. To begin with, preparation time was considerably reduced due to the absence of the coverslip and the silicone rings. Subsequently, cells were clearly defined under the lens, so their detection and localization was easier. Furthermore, during the measurements, the sample was covered entirely by the lens, therefore no visible evaporation of the RPMI was observed after the measurements as well as Raman signal intensity losses, due to no intermediate interfaces. This advantage helps Raman signal intensities remain constant. Finally, **live cell analysis gives more accurate and clear results in regards to the “fingerprint” of the cells**. As a result of this we were able to detect stronger and more distinct peaks in lower exposure times, which in turn allowed us to increase the laser intensity to maximum.

We measured JMP-1/MCL and SUP-M2/ALCL (NHL) and MDA-V/HL (cHL) cell lines with Raman spectroscopy with/without N3a treatment. In order to follow N3a’s course and determine its localization within the cell, we measured N3a in solution to find its unique Raman peaks. We could not find any available Raman spectrum of N3a in literature.

## 3.2 Raman measurements of NHL cell lines without N3a treatment

The JMP-1/MCL and SUP-M2/ALCL cells were measured with Raman spectroscopy in different conditions, to compare them without N3a treatment.

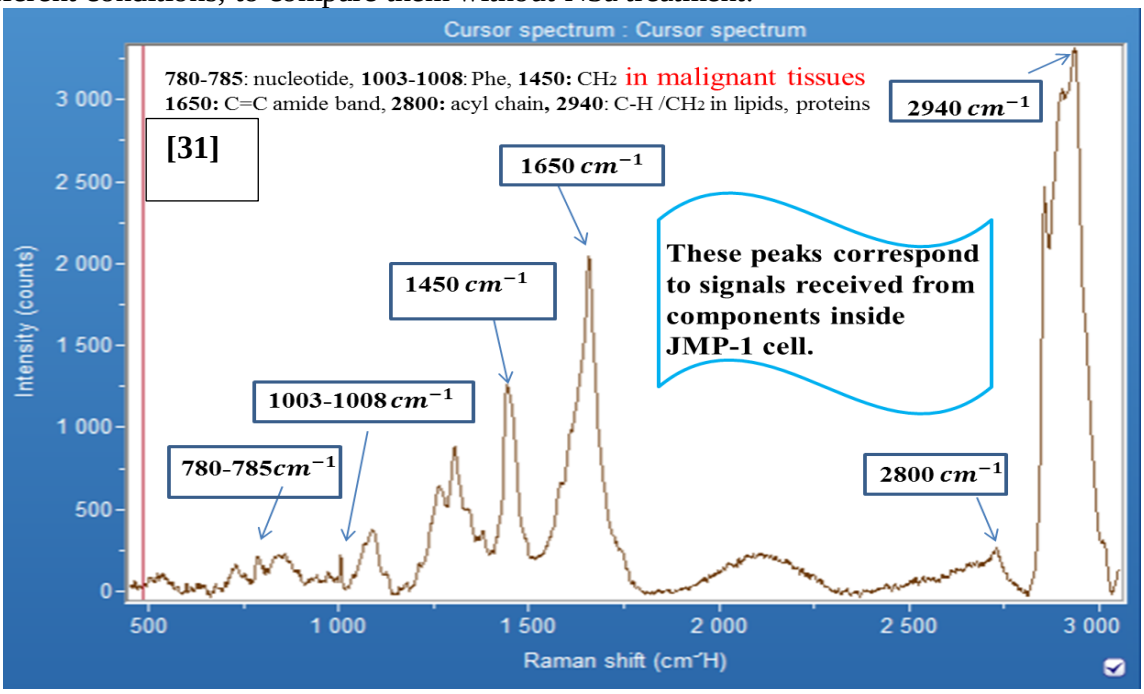


**Figure 3.2.1**. Raman plot with some important biological peaks from the **cytoplasm** of JMP-1/MCL cell.

As we faced many experimental difficulties, we decided to follow the PR3.

For the next step, the lymphoma cell lines were examined with Raman spectroscopy at the nucleus, membrane, and cytoplasm without N3a treatment, in order to create a comparative Raman signal profile.

### 3.2.1 Raman measurements of live JMP-1/MCL cells in RPMI (phenol-free) at T=18°C without N3a treatment

In order to minimize evaporation (RPMI evaporation) from our sample, the temperature was regulated at T=18°C. Initially we tested the environmental humidity liquidation, and we found out that drops started to appear on the plate at T=16°C, so to avoid this phenomenon we used T=18°C as a minimal evaporation condition for our sample. This way we measured for over 1h with no visual losses of the sample. This temperature reduction gives a lower chance of cell movement which allows better and faster Raman measurements.

**Cell 1: JMP-1/MCL**

One live cell was measured with a laser intensity of 25%. One measuring position **in the center of the cell** was observed for a total of 5 min. Each point measurement was set to have exposure time of 50 sec and 3 accumulations (how many times the laser "hits" the same specific spot), resulting to 150 sec of total measurement time.

**Figure 3.2.2.** JMP-1/MCL cell before Raman measurements.

**Figure 3.2.3.** JMP-1/MCL cell immediately after Raman measurements.

**Observation:** Cell's shape was slightly changed but not lysed after the measurements.

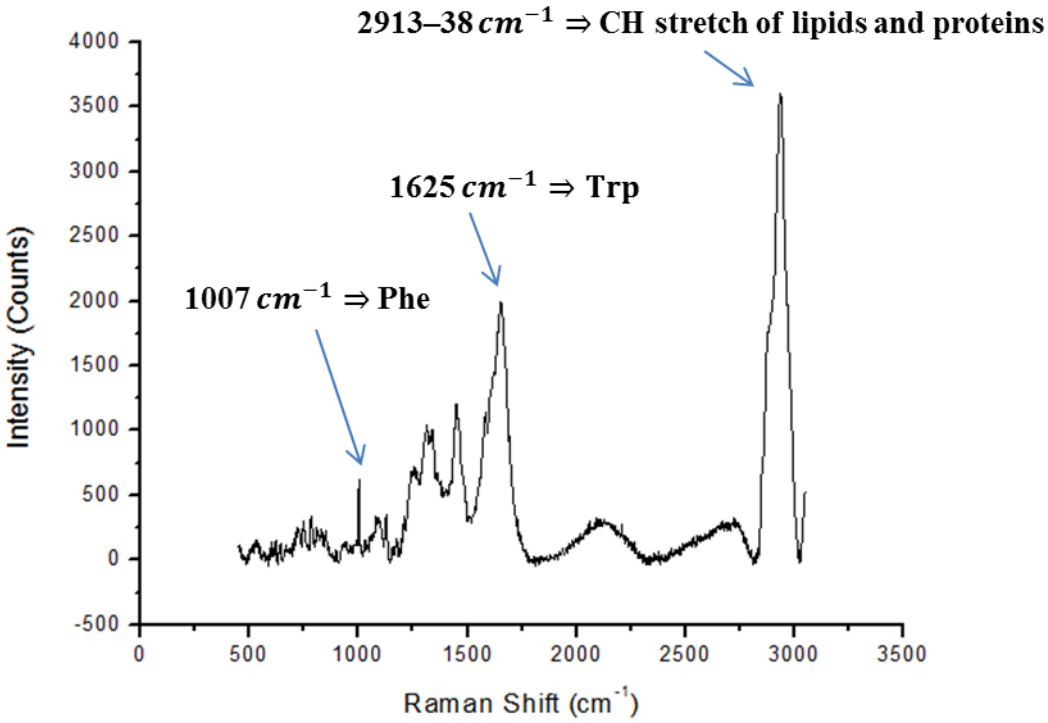


**Figure 3.2.4.** Raman plot of Cell 1 measurement, in the center of the cell.

Immediately afterwards, **the same cell** was measured **on the membrane** for a total of 2.5 min, with double laser intensity (50%) and half the acquisition time (25 sec), the accumulation number remained 3.

**Observation:** The measurement was not accurate because the cell was moved but not lysed; as a result cytoplasm was measured instead of the membrane. As we can see in fig 3.2.5 the supposed membrane plot presents more similarities to a cytoplasm plot (fig 3.2.1) instead of a

membrane plot due to the cell's displacement. It's worth noting that this plot is not an indicative representation of a membrane plot.

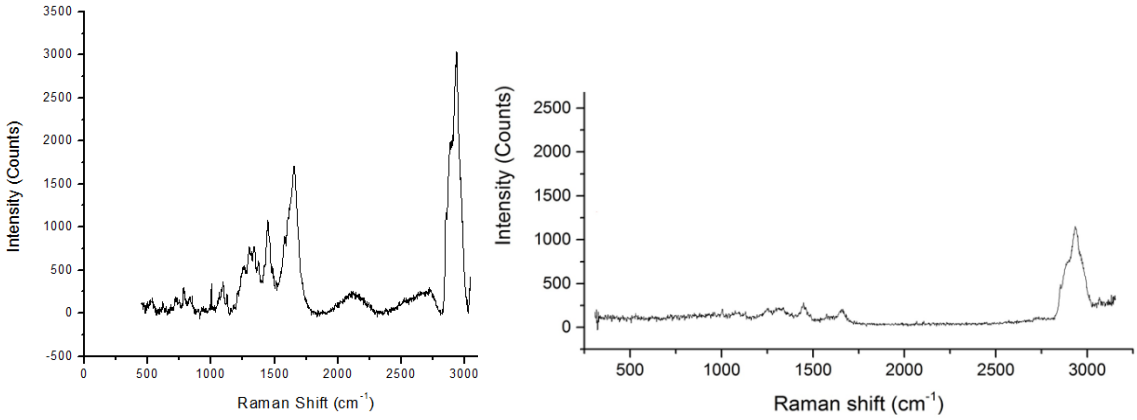


**Figure 3.2.5.** Typical Raman plots of JMP-1/MCL cells from membranes. The one on the right is an indicative Raman plot from a membrane in contrast to the one on the left which corresponds to cytoplasm. The important difference is in the intensity of the peaks.

Subsequently, **the same live cell** was measured with the maximum laser intensity (100%) of~ 40mW and continuously decreasing acquisition times (reached 13 sec).

**Observation:** The cell wasn't damaged at all with 100% laser intensity.

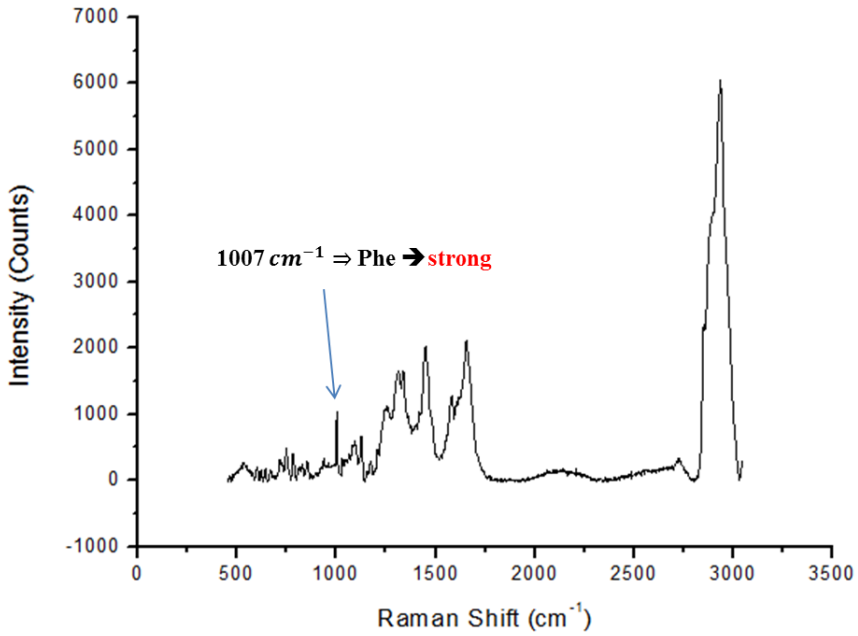


**Figure 3.2.6.** Raman plot of Cell 1 measurement, in the center of the cell, with 100% laser intensity.

With the new methodology conditions, signals were strong and peaks were very distinct with lower exposure times, which allowed us to increase the laser to maximum intensity (~40mW). The reason for this is that there are no interferences, due to the lack of interfaces in between the sample and the lens which could cause laser power and Raman signal intensity losses.

We proceeded with some **mapping measurements** on live cells following the new methodology conditions.

We drew a horizontal line in the middle of the cell as it is shown in fig 3.2.7.

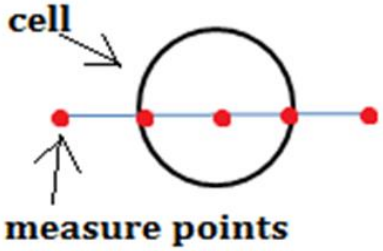


**Figure 3.2.7.** Representation of laser points for Raman measurements.

Raman measurements were made in live JMP-1/MCL cells at 9 different measurement positions at 100% (~40mW) laser intensity. An indicative measurement is presented below.

**Cell measured: JMP-1/MCL**

Theoretical measuring time: 9 points **x** 15sec/point **x** 3(in each point) **x** 2(spectral time windows➔ 2 measurements) = 810sec➔900sec=15min measurement

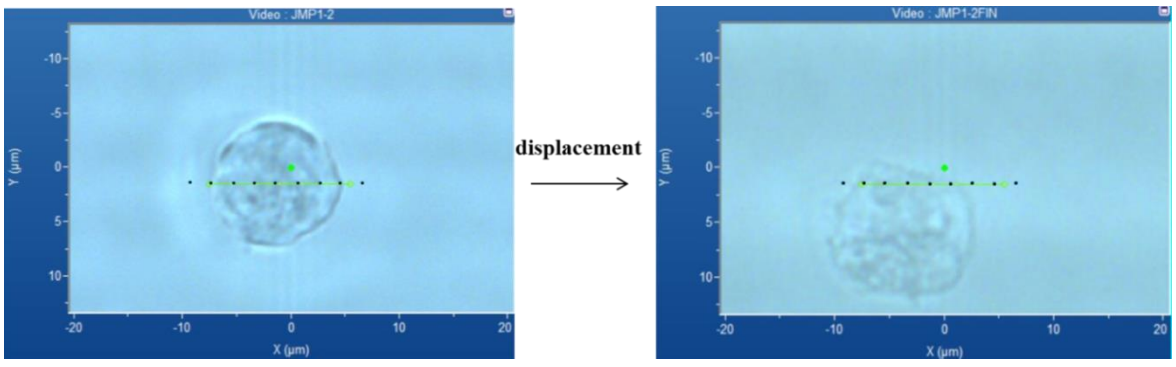


**Figure 3.2.8.** Illustration of JMP-1/MCL cell before and after Raman measurements, at 9 different measurement positions. Unfortunately we observed a displacement of the cell.

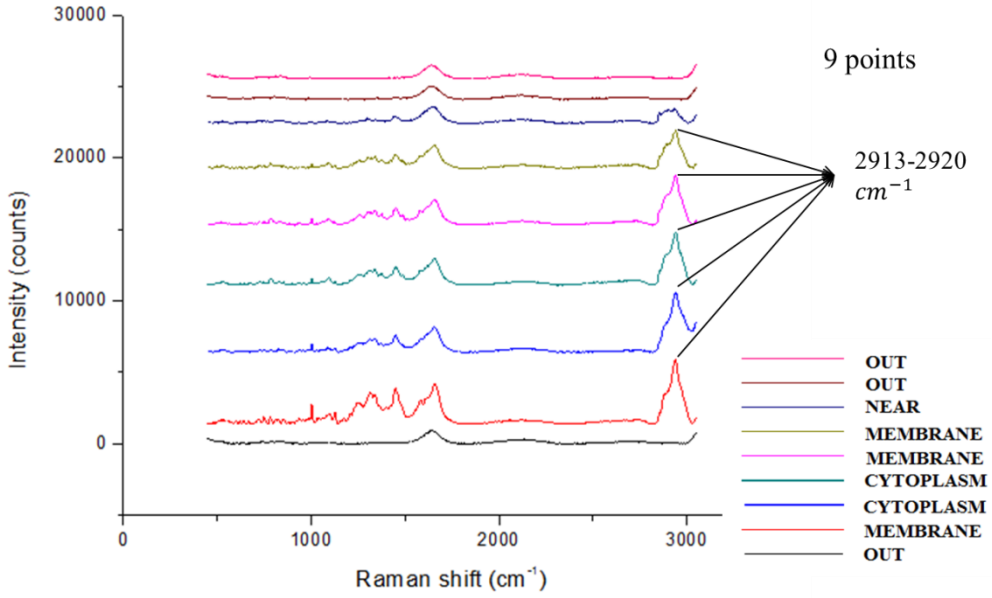


**Figure 3.2.9.** Indicative Raman plot of JMP-1/MCL cell in fig 3.2.8.

**Observations:**

- **2913-2920 $cm^{-1}$** Raman band (➔2913–38 CH stretch of lipids and proteins) was observed. **The intensity of this band was lower in the cytoplasm, but higher close to the membrane.**
- Cell was moving.
- Cell's shape was slightly altered after the measurements.

**Conclusions:**

- Shorter times/point were examined and we concluded that a **15 min measurement with 100% laser intensity** was the ideal Raman measuring time for JMP-1/MCL lymphoma cells, with no visible cell damage, less cell mobility and no visual losses of the sample.
- Our purpose was to measure the cells as fast as possible to achieve a lower chance of cell movement in order to get better Raman measurements.
- High temperatures transfer a lot of energy to cells during the measurements, combined with the high laser intensity, cell damage is possible. We proposed that **T=18°C** is an appropriate measuring temperature for the JMP-1/MCL cell line.

### 3.2.2 Raman measurements of live JMP-1/MCL cells in RPMI (phenol-free) at T=15°C without N3a treatment

The temperature was regulated at T=15°C and not T=18°C to avoid further RPMI evaporation and cell mobility. Under those conditions we measured for over 3h with no visual losses of the sample.

24 live JMP-1/MCL cells were analyzed Confocal Raman spectroscopy imaging. In each JMP-1/MCL cell, 5 different points were measured: surrounding area, cell membrane, cytoplasm, nuclear membrane and nucleus.

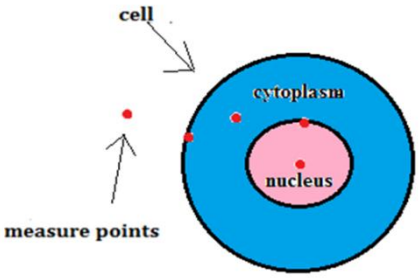


**Figure 3.2.10.** Representation of laser points for Raman measurements.

Laser intensity was set at 100% (~40mW), acquisition time was 5 sec, accumulation number was 3, the distance from the microscope slide surface was 14μm and finally the total measuring time was calculated as follows:

Theoretical measuring time: 5 points **x** 5 sec/point **x** 3(in each point) **x** 2(spectral time windows➔ 2 measurements) = 150 sec = 2.5 min

Practical measuring time: {[((5x3) + 5) x 2] +2} x 5 = 210 sec = 3.5 min

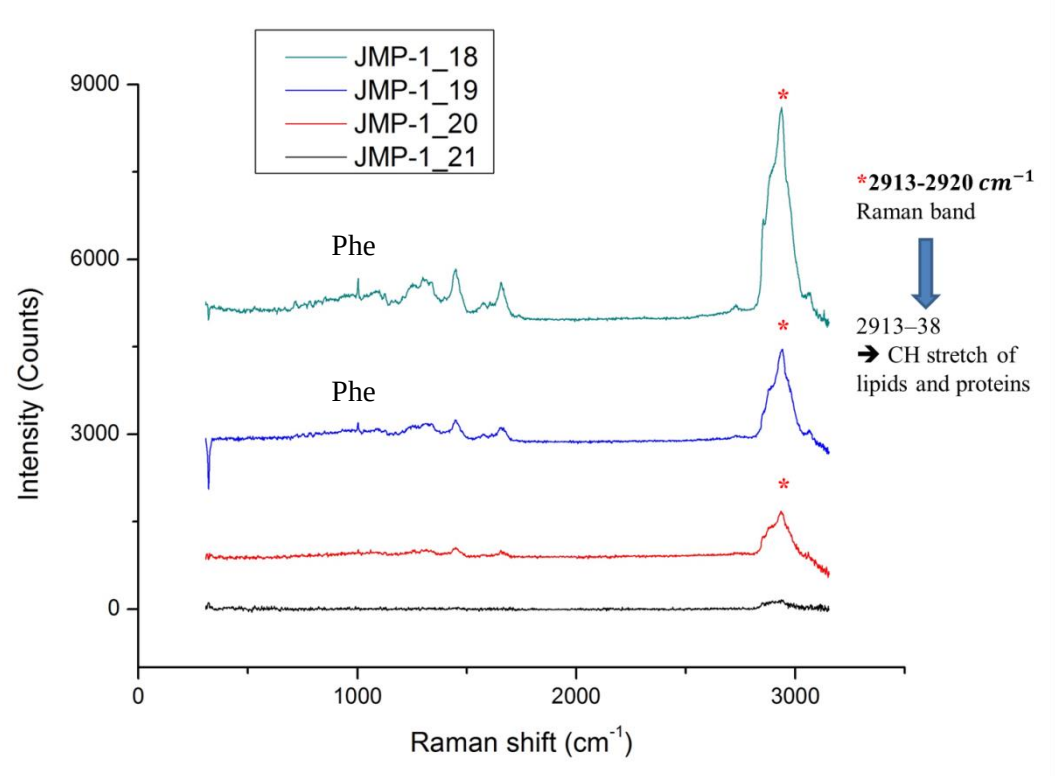


**Figure 3.2.11.** Indicative Raman signaling from **membrane** spots of different JMP-1/MCL cells. Comparison Raman plots.

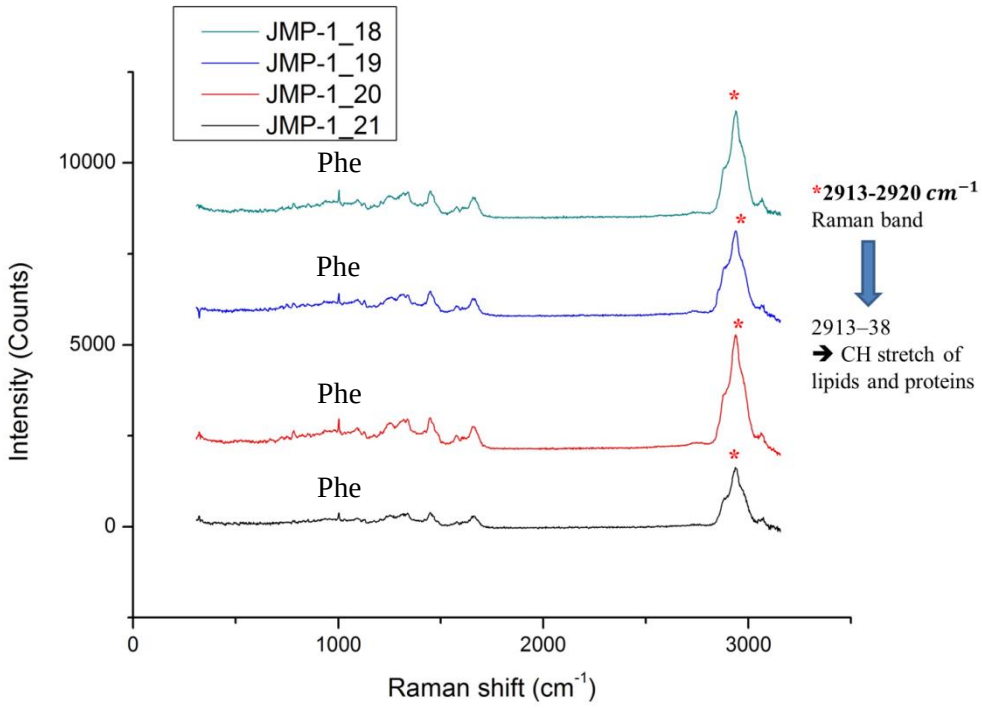


**Figure 3.2.12.** Indicative Raman signaling from **nucleus** spots of different JMP-1/MCL cells. Comparison Raman plots.

**General observations:**

- **2913-2920 $cm^{-1}$** Raman band (➔2913–38 CH stretch of lipids and proteins) was observed in almost all membranes and nucleuses.
- Raman spectra were comparable to previous spectra of JMP-1/MCL cells (T=18°C). Nevertheless the intensity was reduced.
- Cells before, during and after the measurements remained uniform.
- Most of the cells remained alive and almost immovable during the measurements.

**Conclusions:**

- With the new methodology conditions, signals were as strong as the previous measurements of JMP-1/MCL cells (T=18°C). Raman peaks, especially of lipids, were very distinct in lower exposure times, which allowed us to increase the laser intensity to maximum.
- T=15°C was appropriate for cell stabilization and negligible evaporation of RPMI.

### 3.2.3 Raman measurements of live SUP-M2/ALCL cells in RPMI (phenol-free) at T=15°C without N3a treatment

Under the same experimental conditions SUP-M2/ALCL NH lymphoma cells were measured with Raman spectroscopy.

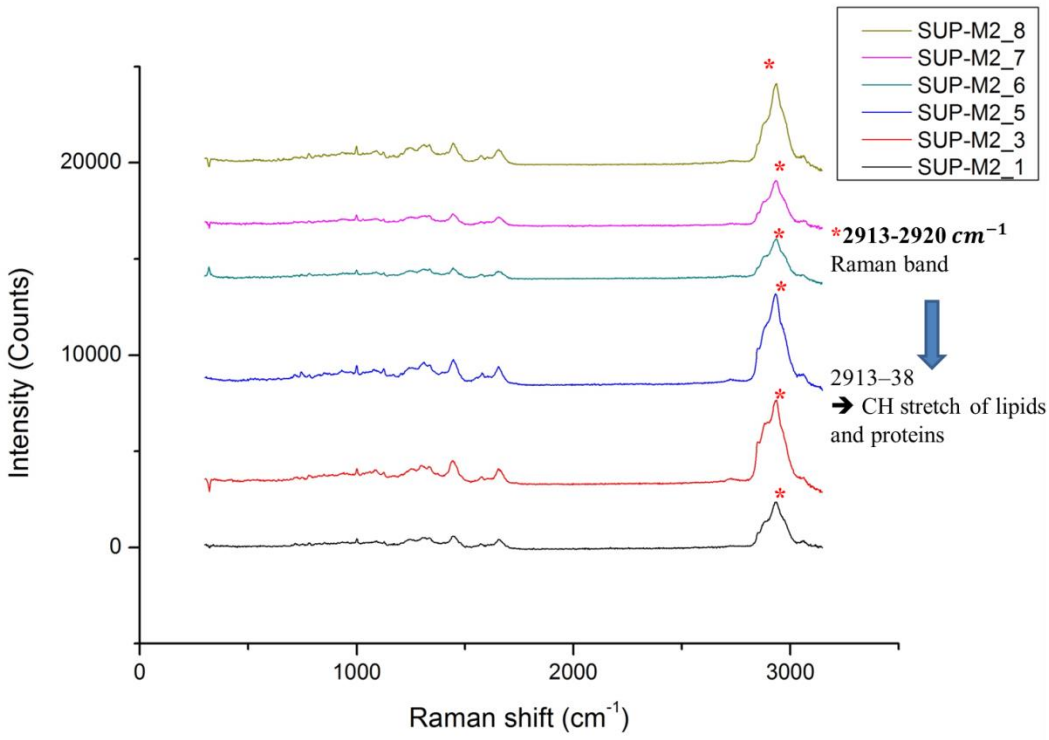


**Figure 3.2.13.** Indicative Raman signaling from **nucleus** spots of different SUP-M2/ALCL cells. Comparison Raman plots.

**Observations:**

- SUP-M2/ALCL cells maintained high mobility at T=15°C compared to JMP-1/MCL.
- Most of SUP-M2/ALCL cells were lysed after the Raman measurements which means they are not as resilient as JMP-1/MCL.

For the reasons mentioned previously, concerning SUP-M2/ALCL cells, we decided to continue the Raman measurements only with JMP-1/MCL and MDA-V/HL cells.

*The methodology conditions have now been determined, which concern laser intensity, number of spots, spot measuring time, total measurement time, protocol and use of confocal imaging.* ***We can now proceed to our first objective****, the experiments to be presented aim to compare the NHL (JMP-1/MCL) and HL (MDA-V/HL) cell lines.*

## 3.3 Raman measurements of NHL and HL cell lines at different temperatures

### 3.3.1 JMP-1/MCL cells

In each JMP-1/MCL cell (NHL) of the following Raman measurements, 4 different measuring points were observed: cell membrane, cytoplasm, nucleus and the surrounding area. At first the laser targeted the nucleus, afterwards the cytoplasm, the membrane and the surrounding area of the cell. All cells were alive, the laser was at maximum intensity (100%) of 40 mW, acquisition time was 5 sec, accumulation number was 3, the distance from the microscope slide surface was 10-20μm and the measuring time was:

Theoretical measuring time: 4 points **x** 5 sec/point **x** 3(in each point) **x** 2(spectral time windows➔ 2 measurements) = 120 sec = 2 min measurement

Practical measuring time: {[((5x3) + 5) x 2] +2} x 5 = 210 sec = 2.8 min

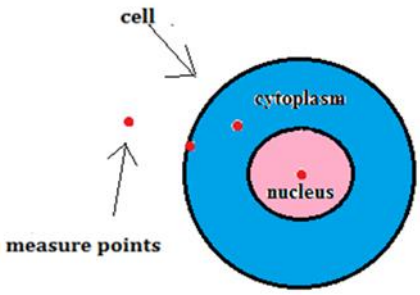


**Figure 3.3.1.** Representation of laser points for Raman measurements.

It is worth noting that the measurement of the surrounding area of the cells was used as a starting point. The frequencies measured from that area, were then removed from the remaining measurements (noise abatement).

- **JMP-1/MCL Experiment (BR1)**

Initially we tried to measure at T=15°C which proved impossible due to the high moisture content of the atmosphere (54%). Even though the microscope slide was ethanol sterilized, atmospheric particles were deposited due to high moisture content. To counter that, we raised the temperature to T=18°C where JMP-1/MCL cells were measured, after that we were able to measure at T=15°C. Subsequently, we wanted to measure the cells at their physiological temperature (T=37°C), we allowed 5min for the cells to relax slowly raising the temperature to T=37°C. We measured the cells at that temperature and finally at T=30°C. The measurements lasted for 1.5 h with no visual losses of the sample. For each temperature 4 JMP-1/MCL cells were measured. In fig. 3.3.2 the best indicative Raman plots are presented.

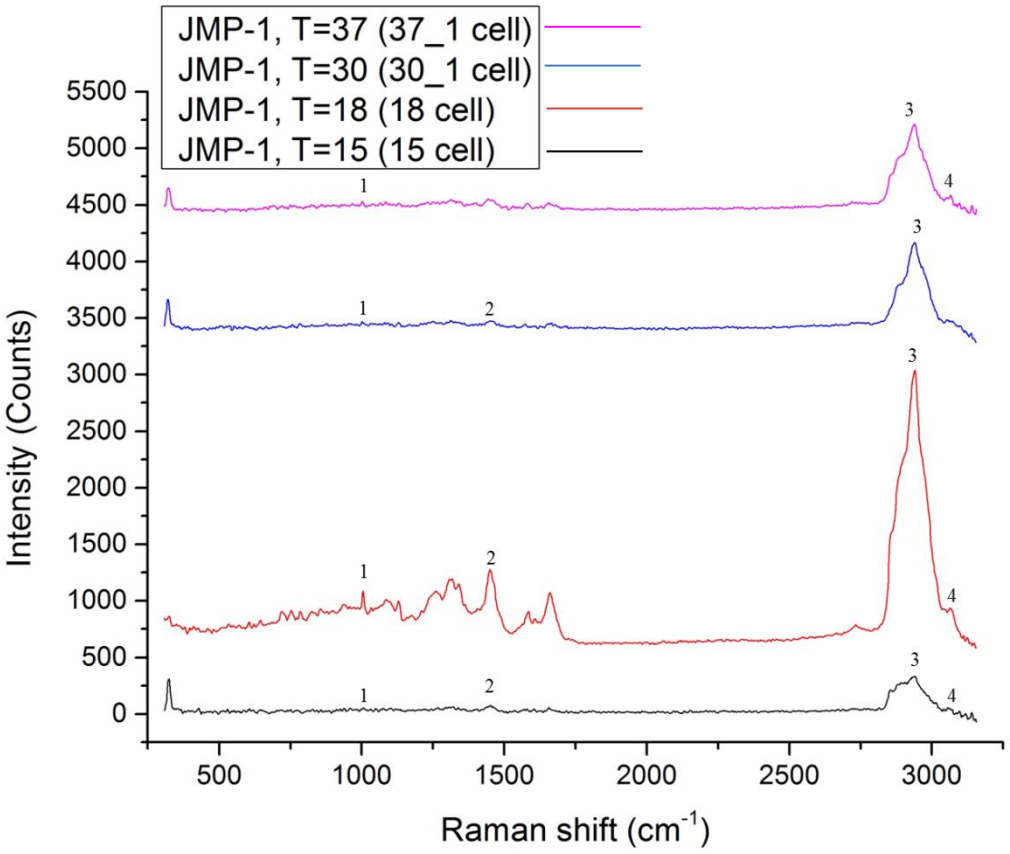


**Figure 3.3.2.** Indicative Raman signaling from **membrane** spots of JMP-1/MCL cells in different temperatures. Comparison Raman plots.

**Table 3.3.1.** Table of the same Raman signaling peaks from **membranes** in JMP-1/MCL cells [45].

| **No** | **Raman Shift ($cm^{-1}$)** | **Assignment** |
|---|---|---|
| 1 | 1001-1007 | Symmetric ring breathing mode of phenylalanine |
| 2 | 1451-1452 | $CH_2CH_3$ deformation (collagen assignment-protein band)<br>Structural protein modes of tumors |
| 3 | 2939-2940 | $CH_2$ asymmetric stretch<br>C-H vibrations in lipids and proteins<br>v as $CH_2$, lipids, fatty acids |
| 4 | 3063-3067 | Region of the OH-NH-CH stretching vibrations |

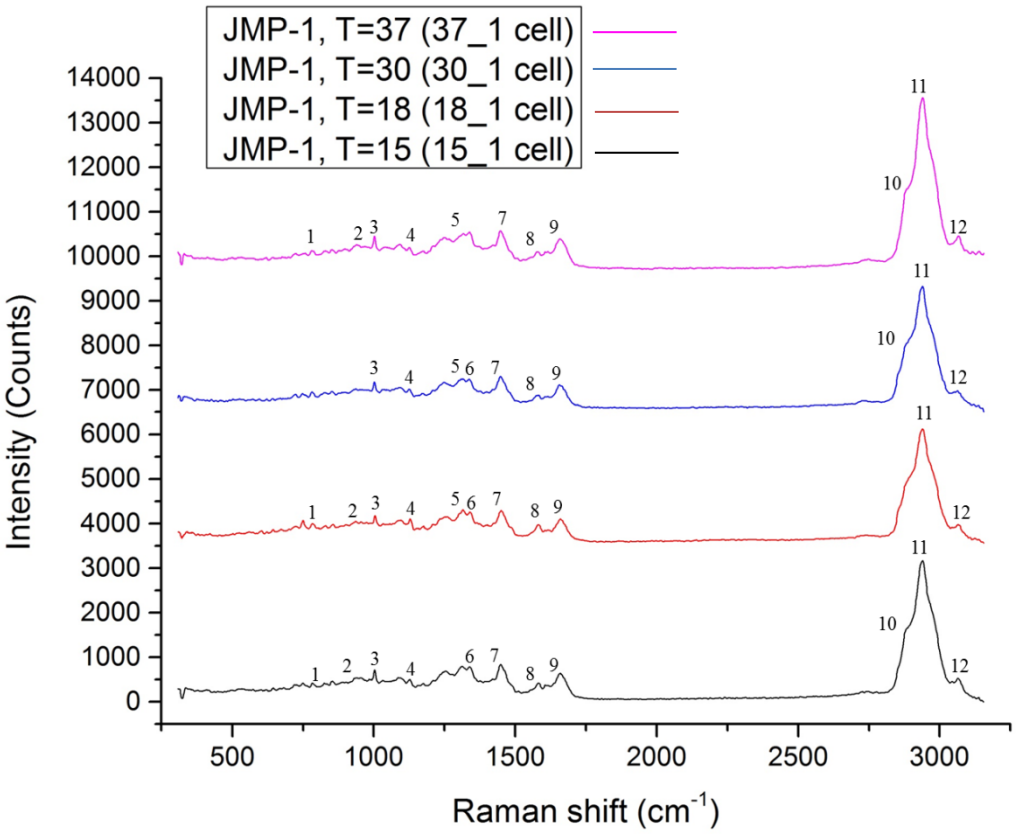


**Figure 3.3.3.** Indicative Raman signaling from **nucleus** spots of JMP-1/MCL cells in different temperatures. Comparison Raman plots.

**Table 3.3.2.** Table of the same Raman signaling peaks from **nucleuses** in JMP-1/MCL cells [45].

| No | Shift ($cm^{-1}$) | Assignment |
|---|---|---|
| **1** | 782-784 | Ring breathing modes in the DNA/RNA bases, Phosphodiester |
| **2** | 936-941 | Skeletal modes (polysaccharides, amylose),C-O-C glycodides (carbohydrates)<br>C-C backbone (collagen assignment) |
| **3** | 1004 | Phenylalanine |
| **4** | 1126-1129 | C-N stretching (proteins)<br>C-O stretching (carbohydrates)<br>ν(C-C) skeletal of acyl backbone in lipid (trans conformation) |
| **5** | 1312-1318 | $CH_3CH_2$ twisting mode of collagen/lipid<br>G (ring breathing modes of the DNA/RNA bases)<br>C-H deformation (protein), Amide III (α-helix) |
| **6** | 1338-1341 | C-C stretch of phenyl<br>$C_3$-$C_3$ stretch and $C_5$-$O_5$ stretch CHα in-plane bend<br>nucleic acid and tryptophan<br>$CH_2/CH_3$ wagging<br>twisting and/or bending mode of collagens and lipids |
| **7** | 1448-1451 | CH vibration (proteins, lipids) |

| | | |
|---|---|---|
| | | $CH_2CH_3$ deformation (collagen assignment) |
| **8** | 1581-1584 | C=C bending mode of phenylalanine<br>C-C stretching |
| **9** | 1656-1661 | Amide I band, C=C (lipids) |
| **10** | 2881-2884 | CH, $CH_2$, and $CH_3$ symmetric and antisymmetric stretching of lipids and proteins |
| **11** | 2939-2940 | C-H vibrations in lipids and proteins<br>$CH_2$ asymmetric stretch |
| **12** | 3064 | 2300–3800 Region of the OH-NH-CH stretching vibrations |

**Observations:**

- Nucleuses have more similar peaks between the different temperatures compared to membranes.
- All nucleus plots of JMP-1/MCL cells at all the different temperatures (15°,18°,30°,37°) are **visually identical and signals (peaks) are also the same.** So, there probably isn't any signal heterogeneity between nucleuses of JMP-1/MCL cells at different temperatures.
- At higher temperatures (T=37°C and T=30°C) most of the cells were lysed after the measurements in contrast to the cells at lower temperatures (T=18°C and T=15°C) where they remained alive.

➢ **JMP-1/MCL Experiment (BR2)**

In the previous experiment our first plan was to measure at T=15°C, T=20°C, T=25°C, T=30°C and T=37° but we didn't manage to measure at T=20°C and T=25°C because of false time calculations. For this reason we conducted another Raman experiment with JMP-1/MCL cells to include those temperatures in our measurements.

Initially we measured at T=20°, afterwards at T=25°C, T=30° and finally after allowing 5min of waiting for the cells to relax at T=15°C. Before measuring at T=15°, we changed the sample (cleaned the microscope slide and added 20μl of the sample on it), because most of the cells were already dead. The measurements lasted for 2 h with no visual losses of the sample. For each temperature 4 JMP-1/MCL cells were measured. Unfortunately we didn't manage to measure at T=37°C because most of the cells were lysed. In fig 3.3.4 and 3.3.5 the best indicative Raman plots are presented.

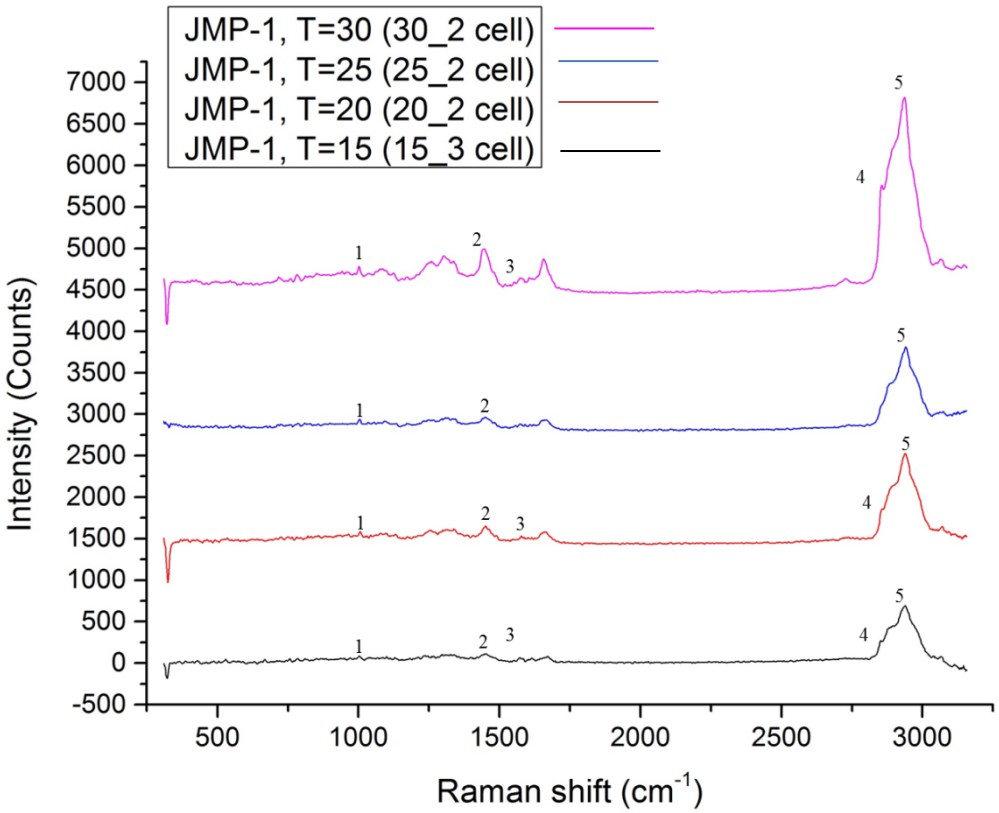


**Figure 3.3.4.** Indicative Raman signaling from **membrane** spots of JMP-1/MCL cells in different temperatures. Comparison Raman plots.

**Table 3.3.3.** Table of the same Raman signaling peaks from **membranes** in JMP-1/MCL cells [45].

| No | Raman Shift ($cm^{-1}$) | Assignment |
|---|---|---|
| **1** | 1002-1004 | Symmetric ring breathing mode of phenylalanine |
| **2** | 1448-1454 | CH, $CH_2CH_3$ deformation<br>Collagen and phospholipids |
| **3** | 1573-1574 | Guanine, adenine, TRP (protein) |
| **4** | 2853-2856 | CH, $CH_2$, and $CH_3$ symmetric and antisymmetric stretching<br>(lipids, proteins) |
| **5** | 2936-2940 | $CH_2$ asymmetric stretch of lipids, fatty acids<br>C-H vibrations in lipids and proteins, |

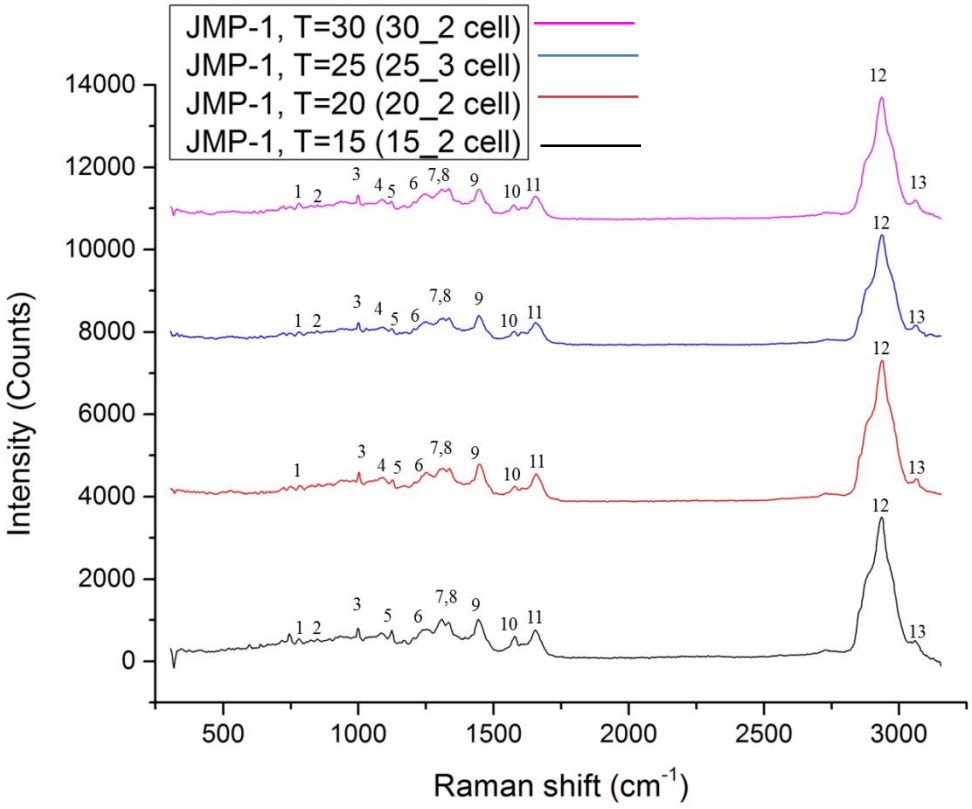


**Figure 3.3.5.** Indicative Raman signaling from **nucleuses** spots of JMP-1/MCL cells in different temperatures. Comparison Raman plots.

**Table 3.3.4.** Table of the same Raman signaling peaks from **nucleuses** in JMP-1/MCL cells [45].

| No | Raman Shift ($cm^{-1}$) | Assignment |
|---|---|---|
| **1** | 780-782 | DNA, Thymine, cytosine, uracil, RNA U, T, C (ring breathing modes in the DNA/RNA bases) |
| **2** | 847-848 | Monosaccharides (α-glucose) and Disaccharide (maltose) (C-O-C) skeletal mode |
| **3** | 999-1002 | $\nu_{45}$(CC) in the spectra of single human Red blood cell<br>Bound and free NADH<br>C-C aromatic ring stretching<br>Phenylalanine |
| **4** | 1090-1093 | Symmetric $PO_2^-$ stretching vibration of the DNA backbone<br>C-N of proteins |
| **5** | 1121-1127 | ν(C-C) skeletal of acyl backbone in lipid (trans conformation)<br>ν(C-N)<br>Several bands of moderate intensity, belonging to amide III and other groups (proteins) |
| **6** | 1245-1252 | Amide III<br>$C\text{-}O_4$ aromatic stretch<br>Guanine, cytosine ($NH_2$) |
| **7** | 1304-1308 | C-N asymmetric stretching in asymmetric aromatic amines |

| | | |
|---|---|---|
| | | $CH_2$ deformation (lipid)<br>adenine, cytosine |
| **8** | 1334-1336 | $CH_3CH_2$ wagging mode of collagen and polynucleotide chain (DNA purine bases) |
| **9** | 1444-1447 | Cholesterol band, $\delta(CH_2)$, lipids, fatty acids<br>$CH_2$ bending mode and deformation of proteins and lipids |
| **10** | 1572-1578 | Guanine ($N_3$), adenine<br>Transient Receptor Potential protein<br>Bound and free NADH |
| **11** | 1652-1658 | Amide I (C=O stretching mode of proteins (collagen assignment),<br>α-helix conformation)/C=C lipid stretch<br>Triglycerides (fatty acids) |
| **12** | 2935-2937 | $CH_2$ asymmetric stretch<br>Chain end $CH_3$ symmetric band |
| **13** | 3059-3063 | Region of the OH-NH-CH stretching vibrations |

**Observations:**

- Nucleuses have more similar peaks between the different temperatures compared to membranes.
- Raman signals between nucleus spots in JMP-1/MCL cells, at T=15°C and T=30°C, were visually similar at different experimental days under the same experimental conditions.
- Most of the cells at higher temperatures (T=30°C and T=25°C) were lysed after the measurements in contrast to cells at lower temperatures (T=20°C and T=15°C) which remained alive.
- We received both satisfactory and non-satisfactory Raman spectra. Specifically, at T=20°C and T=30°C signals had fairly minimal noise and acceptable spatial resolution. At T=25°C signals also had fairly minimal noise and acceptable spatial resolution, but there were some Raman plots that were not satisfactory to us. Finally at T=15°C signals were excellent.

### 3.3.2 MDA-V/HL cells

MDA-V/HL cell line is divided into big and small cells which have different responses to stress. Small MDA-V/HL cells are more resilient than the big ones, for this reason they tolerate much more stress without any apoptotic tendencies. At this experiment small cells had a diameter of 10-16 μm and big cells had a diameter greater than 17 μm.

- **MDA-V/HL Experiment (BR3)**

MDA-V/HL cells were measured at 6 different temperatures under the same conditions as the previous measurements of JMP-1/MCL cells.

For each temperature 4 MDA-V/HL cells were measured. The measurements lasted for 2 h with no visual losses of the sample.

The initial temperature was T=37°C, since it is close to the physiological human temperature so cells were less stressed, and was then gradually lowered to T=15°C.

Temperature change order: T=37°C➔ T=30°C➔ T=25°C➔ T=20°C➔ T=18°C➔ T=15°C

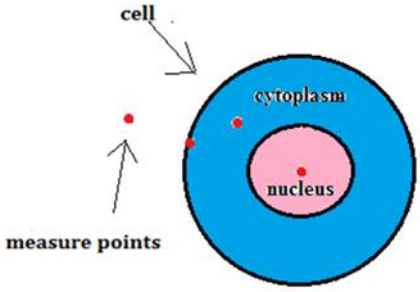


**Figure 3.3.6.** Representation of laser points for Raman measurements.

It is worth noting that the measurement of the surrounding area of the cells was used as a starting point. The frequencies measured from that area, were then removed from the remaining measurements (noise abatement).

In fig 3.3.7, 3.3.8, 3.3.9 and 3.3.10 the best indicative Raman plots are presented.

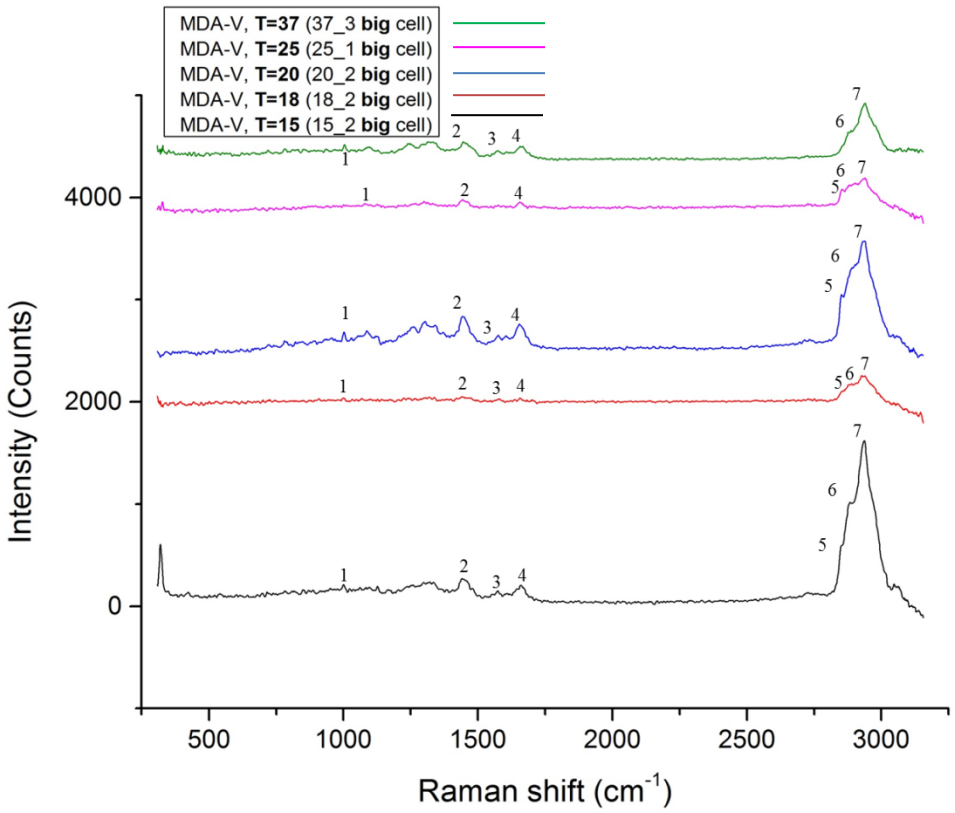


**Figure 3.3.7.** Indicative Raman signaling from **membrane** spots of **MDA-V/HL big** cells in different temperatures. Comparison Raman plots.

**Table 3.3.5.** Table of the same Raman signaling peaks from **membranes** in **MDA-V/HL big** cells [45].

| No | Raman Shift ($cm^{-1}$) | Assignment |
|---|---|---|
| **1** | 999-1004 | $\nu_{45}$(CC) in the spectra of single human Red blood cell (C-C) phenylalanine(collagen assignment), Phenyl breathing mode |
| **2** | 1443-1446 | Cholesterol band, δ($CH_2$), lipids, fatty acids $CH_2$ bending mode and deformation of proteins and lipids |
| **3** | 1573-1579 | Guanine ($N_3$), adenine<br>Pyrimidine ring (nucleic acids) and heme protein<br>Transient Receptor Potential protein |
| **4** | 1656-1666 | C=C (lipids), Triglycerides (fatty acids)<br>Amide I (proteins)<br>T, G, C (ring breathing modes of the DNA/RNA bases) |
| **5** | 2851-2854 | CH, $CH_2$, and $CH_3$ symmetric and antisymmetric stretching (lipids) |
| **6** | 2884-2892 | $CH_2$ as str of lipids and proteins |
| **7** | 2926-2940 | $CH_2$ as str in lipids, fatty acids C-H v in lipids and proteins |

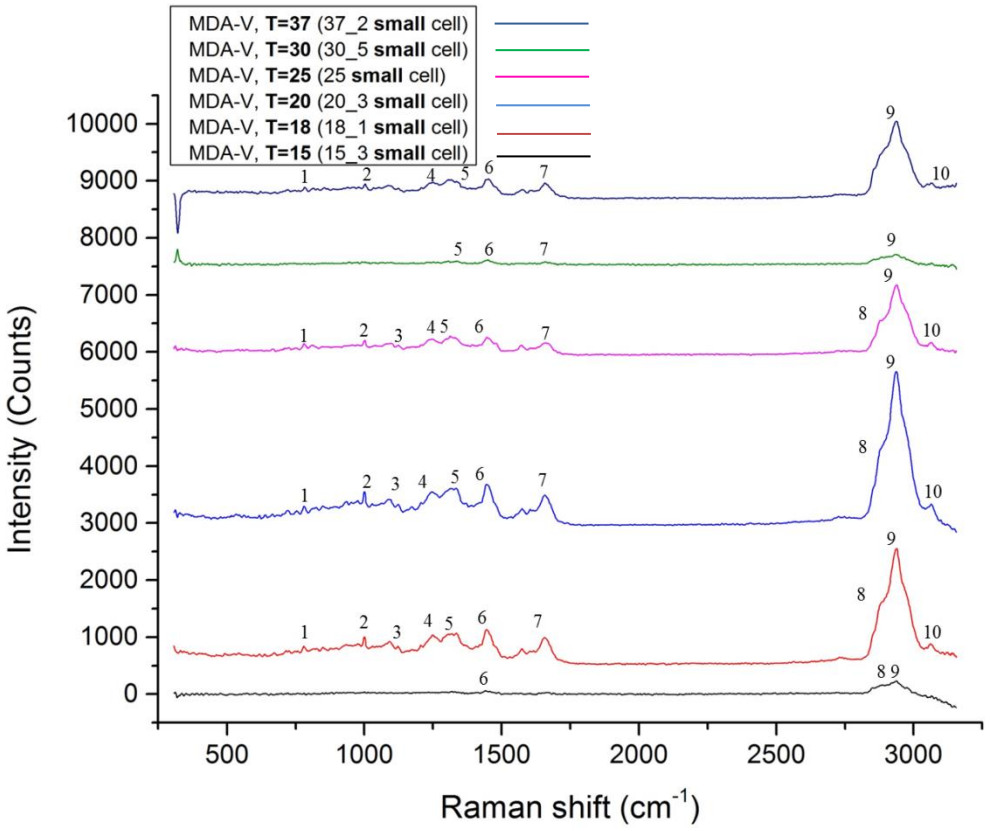


**Figure 3.3.8.** Indicative Raman signaling from **membrane** spots of **MDA-V/HL small** cells in different temperatures. Comparison Raman plots.

**Table 3.3.6.** Table of the same Raman signaling peaks from **membranes** in **MDA-V/HL small** cells [45].

| No | Raman Shift ($cm^{-1}$) | Assignment |
|---|---|---|
| **1** | 780-783 | Ring breathing modes in the DNA/RNA bases, Uracil-based ring breathing mode |
| **2** | 1000-1003 | Phenylalanine<br>Bound and free NADH<br>C-C aromatic ring stretching |
| **3** | 1123-1126 | ν(C-C) skeletal of acyl backbone in lipid (trans conformation),C-C stretching mode of lipids and proteins<br>Glucose<br>C-N stretching |
| **4** | 1246-1251 | Guanine, cytosine ($NH_2$)<br>Amide III (of collagen) |
| **5** | 1331-1338 | $CH_3CH_2$ wagging, deformation of collagen (protein assignment) and polynucleotide chain (DNA purine bases)<br>Guanine, Tryptophan<br>$CH_2/CH_3$ wagging, twisting and/or bending mode of collagens and lipids |
| **6** | 1441-1452 | $CH_2$ scissoring and $CH_3$ bending in lipids, Cholesterol and its esters<br>$CH_2$ bending mode of proteins and lipids, $CH_2$ deformation of |

| | | |
|---|---|---|
| | | proteins<br>C H vibration (proteins), C H vibration (lipids), Lipids<br>Structural protein modes of tumors |
| **7** | 1655-1661 | ν(C=O) amide I, α-helix, collagen, Amide I<br>ν(C=C) cis, lipids, fatty acids C=C groups in unsaturated fatty acids, Ceramide backbone, |
| **8** | 2879-2887 | CH, $CH_2$ (lipids and proteins), and $CH_3$ (lipids) symmetric and antisymmetric stretching,<br>Contributions from acyl chains |
| **9** | 2934-2943 | $CH_2$ asymmetric stretch<br>$CH_3$ stretching vibrations |
| **10** | 3062-3065 | Region of the OH-NH-CH stretching vibrations |

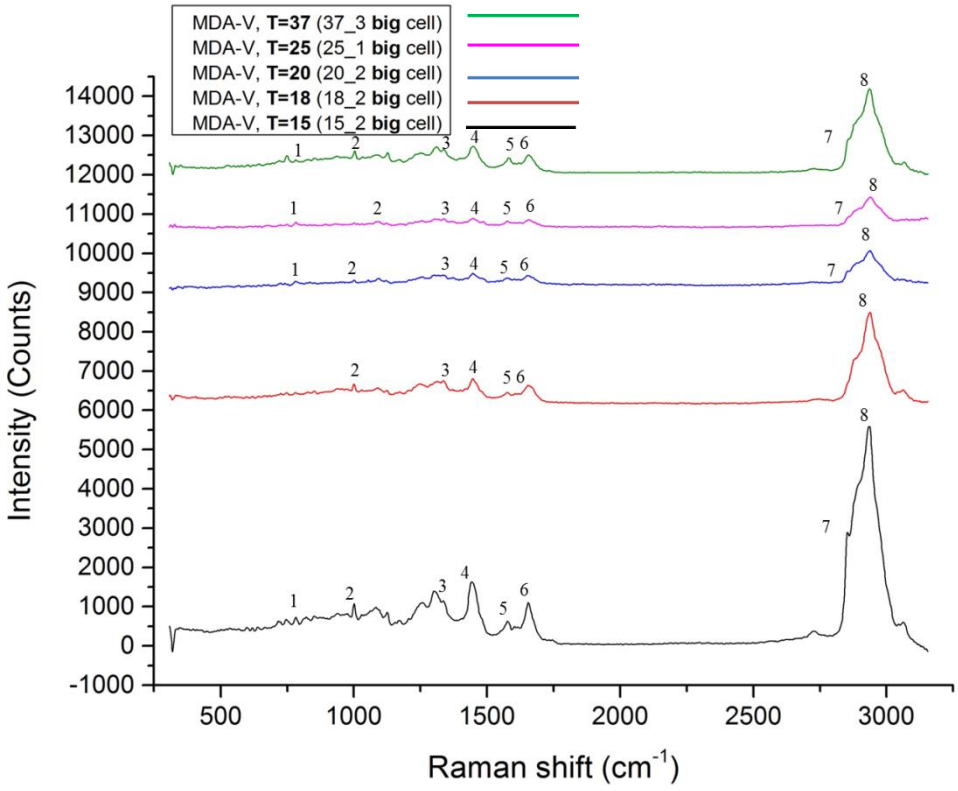


**Figure 3.3.9.** Indicative Raman signaling from **nucleus** spots of **MDA-V/HL big** cells in different temperatures. Comparison Raman plots.

**Table 3.3.7.** Table of the same Raman signaling peaks from **nucleuses** in **MDA-V/HL big** cells [45].

| No | Raman Shift ($cm^{-1}$) | Assignment |
|---|---|---|
| **1** | 780-783 | Ring breathing modes in the DNA/RNA bases |
| **2** | 1002-1004 | C-C aromatic ring stretching, Phenylalanine (collagen assignment) |
| **3** | 1336-1339 | C-C stretch of phenyl and $C_3$-$C_3$ stretch and $C_5$-$O_5$ stretch<br>CHα in-plane bend<br>Polynucleotide chain (DNA purine bases), Amide III, $\delta(CH_3)$ $\delta(CH_2)$ twisting, collagen (protein assignment), $CH_2$ wagging vibrations from glycine backbone and proline side chain C H deformation (protein) |
| **4** | 1444-1450 | $CH_2$ bending mode and deformation of proteins, lipids, fatty acids, Cholesterol band<br>δ as$(CH_3)$ $\delta(CH_2)$ of proteins<br>C H vibration proteins and lipids<br>C-H deformation bands (CH functional groups in lipids, amino acid side chains of the proteins and carbohydrates)<br>$\nu_{28}$ (CαCm), observed in the spectra of single human RBC,<br>$CH_2$ bending mode in malignant tissues, Bending modes of methyl groups (one of the vibrational modes of collagen)<br>Methylene deformation in biomolecules |
| **5** | 1574-1582 | δ(C=C), phenylalanine, Phenylalanine<br>Guanine ($N_3$)<br>Bound and free NADH |
| **6** | 1653-1659 | Lipid (C=C stretch), Carbonyl stretch (C=O), Cholesterol band, fatty acids (Triglycerides)<br>Amide I vibration (collagen like proteins), Glutathione |
| **7** | 2852-2861 | Contributions from acyl chains<br>CH, $CH_2$ (lipids), and $CH_3$(lipids) symmetric and proteins) antisymmetric stretching |
| **8** | 2934-2938 | CH stretch of lipids and proteins<br>$CH_2$ asymmetric stretch |

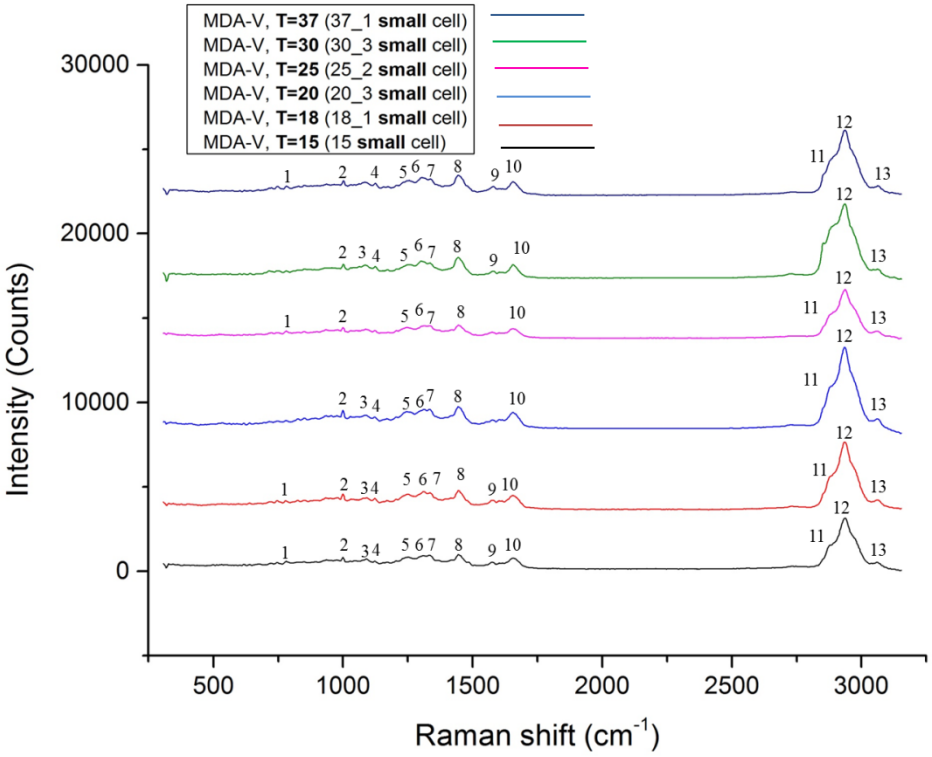


**Figure 3.3.10.** Indicative Raman signaling from **nucleus** spots of **MDA-V/HL small** cells in different temperatures. Comparison Raman plots

**Table 3.3.8.** Table of the same Raman signaling peaks from **nucleuses** in **MDA-V/HL small** cells [45].

| No | Raman Shift ($cm^{-1}$) | Assignment |
|---|---|---|
| **1** | 779-782 | Ring breathing modes in the DNA/RNA bases |
| **2** | 1000-1001 | Symmetric ring breathing mode of phenylalanine<br>Bound and free NADH |
| **3** | 1086-1092 | ν(C-C) gauche<br>$PO_2^-$ stretch<br>Phosphodioxy |
| **4** | 1123-1126 | C-N stretching vibration proteins (protein assignment)<br>C-C stretching mode of lipids and protein<br>ν(C-C) skeletal of acyl backbone in lipid (trans conformation),<br>ν(C-O)+ν(C C), disaccharides, sucrose, glucose |
| **5** | 1249-1256 | Lipids<br>A, T (ring breathing modes of the DNA/RNA bases)<br>Amide III (protein) |
| **6** | 1303-1315 | $CH_3/CH_2$ twisting, wagging, and/or bending mode of collagens and lipids<br>Guanine (B, Z-marker) |
| **7** | 1335-1338 | $CH_3CH_2$ wagging, collagen (protein assignment), |

| | | |
|---|---|---|
| | | polynucleotide chain (DNA purine bases),<br>$CH_3CH_2$ deforming modes of collagen and nucleic acids<br>Guanine<br>Tryptophan |
| **8** | 1445-1446 | $\delta(CH_2)$, $\delta(CH_3)$, collagen (protein assignment), $\delta(CH_2)$, $\delta(CH_3)$, scissoring, phospholipids (lipid assignment)<br>$CH_2CH_3$ bending modes of collagen and phospholipids,<br>$CH_2$ bending mode of proteins and lipids being of diagnostic significance<br>Methylene bending mode (a combination of proteins and phospholipids)<br>$CH_2$ deformation |
| **9** | 1578-1581 | Guanine ($N_3$), adenine (nucleic acids)<br>C=C bending mode of phenylalanine Pyrimidine ring ,C-C stretching phenylalanine<br>heme protein |
| **10** | 1656 | C=C (lipids), Amide I (proteins) |
| **11** | 2880-2883 | Contributions from acyl chains<br>$CH,CH_2$ (lipids, proteins), $CH_3$(lipids) symmetric and antisymmetric stretching |
| **12** | 2936-2937 | $CH_2$ asymmetric stretch |
| **13** | 3059-3065 | Region of the OH-NH-CH stretching vibrations |

**Observations:**

- Most of the cells at higher temperatures (T=37°C, T=30°C and T=25°C) were lysed after the measurements in contrast to cells at lower temperatures (T=20°C, T=18°C T=15°C) which remained alive. This happens because at higher temperatures cells receive higher energy amounts from their environment.
- The measurements of big MDA-V/HL cell membranes did not give us satisfactory Raman spectrums, which is unjustifiable because, big MDA-V/HL cells have a higher content of lipids in their membranes compared to small MDA-V/HL cells, so lipid detection should have been easier.

**Conclusions:**

- Since MDA-V/HL cell line is divided into big and small cells, at the same temperature they have obvious heterogeneity compared to JMP-1/MCL cells. We will attempt to verify this with PCA analysis mentioned in Chapter 3 (3.5).
- In all temperatures most of the Raman spectra were satisfactory, especially at T=15°C where signals were **excellent**. This is the reason why **T=15°C remains the ideal measuring time** for minimum cell mobility and RPMI evaporation regarding Raman measurements; but not from a biological point of view. Based on Raman theory the temperature reduction in a biological system, like lymphoma cells, besides immobilization, also causes a lower metabolic response which does not influence the received signals from the molecules. As we observed in the previous JMP-1/MCL and MDA-V/HL Raman plots, regardless of the temperature, concerning the membranes

and the nucleus, in the majority of them we received the same Raman peaks. Even though some peaks were displaced, they were corrected with the appropriate calibration prior to the measurements.

- The most significant same peaks between the membranes and the nucleuses in BR1, BR2 and BR3 experiments, based on the tables 3.3.1-3.3.8, are at 1000-1007 corresponding to Phe, at 1448-1454 corresponding to CH2CH3 def (deformations) of protein structures in tumors and at 2935-2940 corresponding to CH2, CH asymmetric vibrations of mainly lipids in the total methylation area.

- **MDA-V/HL Experiment (BR4)**

MDA-V/HL cells were measured at **T=15°C**, under the same conditions as the previous measurements.

We will **only use these data for the JMP-1/MCL and MDA-V/HL cell line comparison for PCA analysis.**

**General conclusion:** Raman plots from the nucleus area, gave us more distinct peaks which we are certain they correspond to the nucleus. Measurements in the membrane and the cytoplasm, especially in the cytoplasm, are not as accurate as the nucleus measurements; due to the cell's mobility, some measurements in the cytoplasm corresponded to either membrane or nucleus Raman assignments. Raman signals received from the nucleus area presented higher repeatability, compared to those received from the cytoplasm and the membrane. This is the reason why we **are going to compare and analyze nucleus spots between JMP-1/MCL and MDA-V/HL cells.**

## 3.4 Raman measurements-comparison nucleus of HL (MDA-V/HL) and NHL (JMP-1/MCL) cell lines in RPMI (phenol-free) at different temperatures.

For the nucleus comparisons between JMP-1/MCL and MDA-V/HL cells, it was necessary to make an average of all the nucleus signals from all the cells for each BR1, BR2, BR3 and BR4 for each temperature (T= 15, 18, 20, 25, 30, 37 °C).

Afterwards we decided to **subtract the average of JMP-1/MCL nucleus data signals from the average of MDA-V/HL nucleus data signals**, so their divergence will produce a Raman plot where its peaks correspond to the Raman signaling differences of JMP-1/MCL and MDA-V/HL cell lines which is presented in fig. 3.4.

From all Raman plots (HL-NHL), the most intense and strong peaks were detected (with the help of Origin 9 Data Analysis software), analyzed and documented in an excel file for each temperature separately. The results are presented in the table 3.4.1.

**Table 3.4.1.** Table of the most important signaling differences between HL and NHL lymphoma

| Raman Shift ($cm^{-1}$) | BR3-BR1 | BR3-BR2 | BR4-BR1 | BR4-BR2 | Assignment |
|---|---|---|---|---|---|
| 743-749 | T=18,30,37 | T=15,25 | T=15 | T=15 | DNA, Tryptophan |
| 1000-1007 | T=15,18,30,37 | T=20,30 | T=15 | T=15 | C-C aromatic ring (**Benzene)** stretching Phenylalanine |
| 1125-1131 | T=30,37 | T=15,25,30 | T=15 | T=15 | ν(C-C) skeletal of acyl backbone in lipid (trans conformation) C-N str. (proteins) C-O str. (carbohydrates) |
| 1433-1450 | T=18,37 | T=15,25 | | T=15 | $CH_2$ scissoring (of lipids) |
| 1581-1587 | T=37 | T=15,25 | T=15 | T=15 | C=C str. (protein assignment) |
| 1652-1658 | T=15,30,37 | T=30 | T=15 | | Lipid (C=C stretch) Amide I (α-helix) |
| 2844-2855 | T=15,30 | T=15,20,25, 30 | T=15 | T=15 | $CH_3$ symmetric stretch of lipids |
| 2887-2898 | T=15,30 | T=15,25,30 | T=15 | | $CH_2$ asymmetric stretch of lipids and proteins |
| 2935-2944 | T=30,37 | T=20,30 | T=15 | T=15 | Chain end $CH_3$ symmetric band C-H vibrations in lipids and proteins v as $CH_2$, lipids, fatty acids |

➢ **T=37°C**

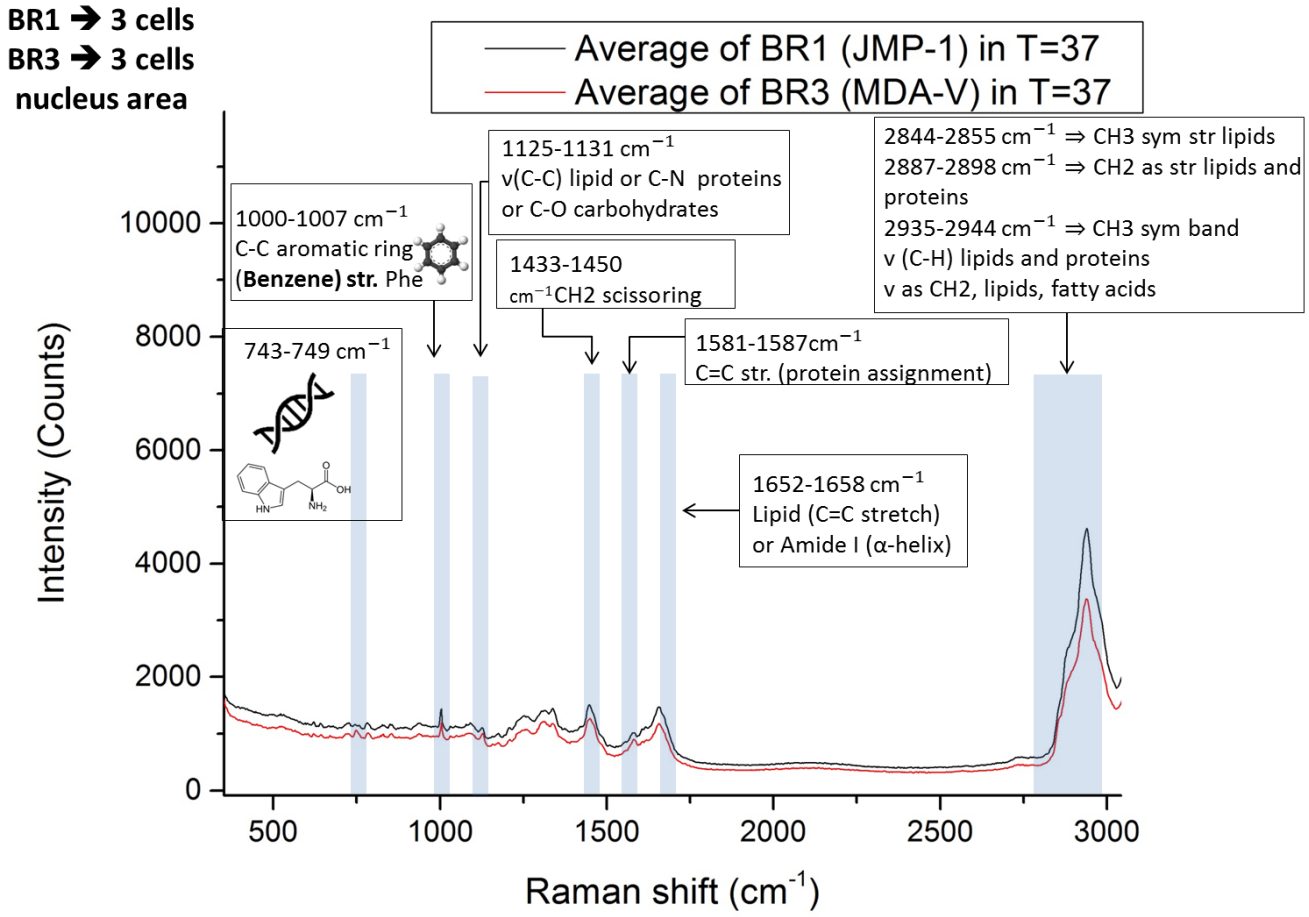


**Figure 3.4.1.** Raman signaling average plots of JMP-1/MCL and MDA-V/HL cells for T=37°C.

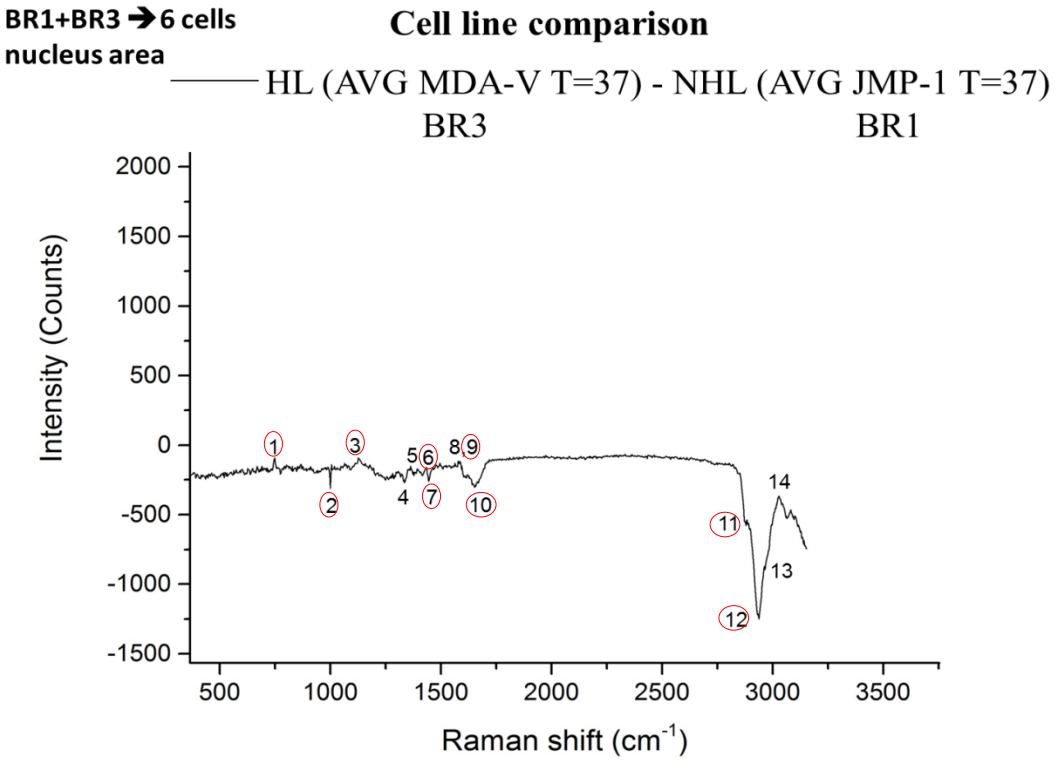


**Figure 3.4.2.** Raman signaling differences between JMP-1/MCL and MDA-V/HL cell lines in T=37°C. The circled numbers indicate the most important peaks based on the blue shaded areas (see fig 3.4.1).

**Assignment of peaks ( $cm^{-1}$)**

| | | | |
|---|---|---|---|
| 1)➔749 | 5)➔1364 | 9)➔1587 | 13)➔2963 |
| 2)➔1000 | 6)➔1436 | 10)➔1652 | 14)➔3029 |
| 3)➔1128 | 7)➔1444 | 11)➔2881, 2884 | |
| 4)➔1336 | 8)➔1578 | 12)➔2938 | |

**Observation:** The peak no12, at wn 2938$cm^{-1}$, has the strongest Raman intensity, where it corresponds to $CH_3$ symmetric band, C-H vibration of lipids and proteins and $CH_2$ asymmetric vibration of lipids and fatty acids. Also, the peak no2, at wn 1000$cm^{-1}$, is a very distinct peak which corresponds to Phenylalanine.

➢ **T=30°C**

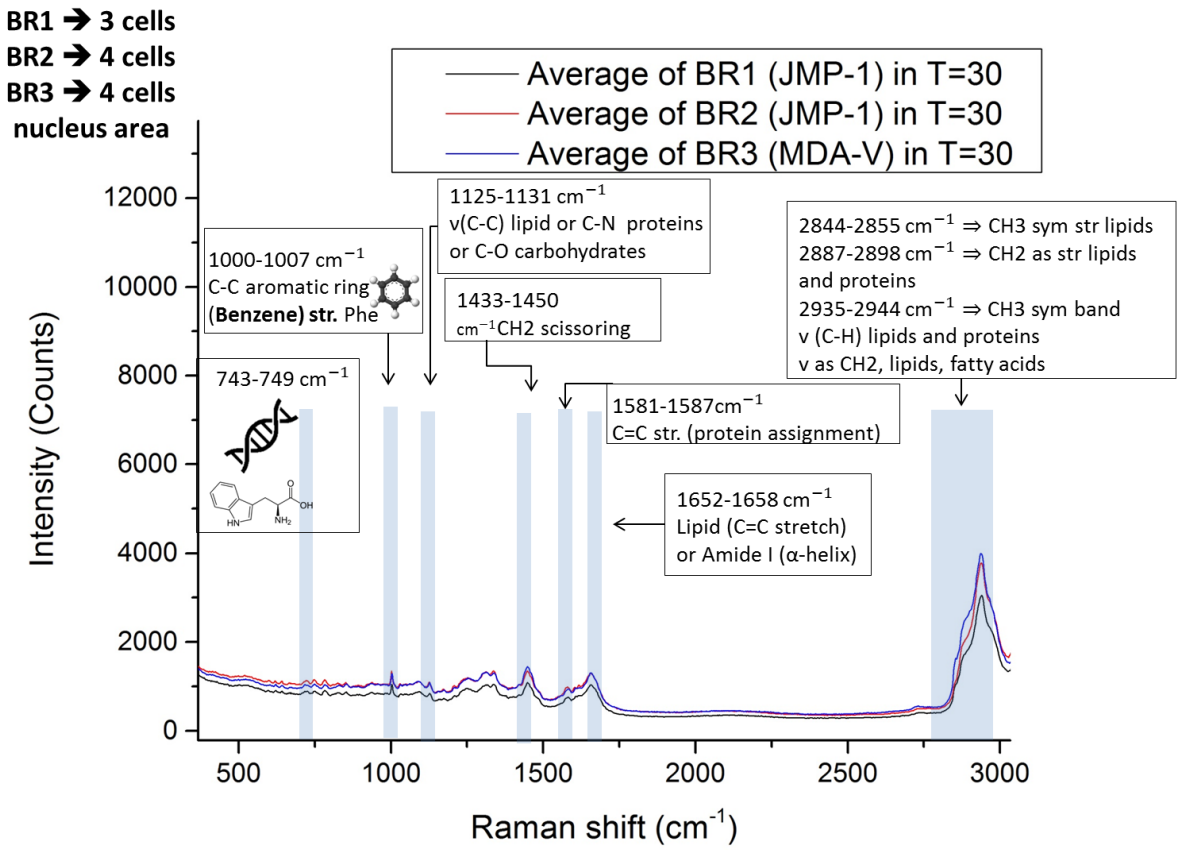


**Figure 3.4.3.** Raman signaling average plots of JMP-1/MCL and MDA-V/HL cells for T=30°C.

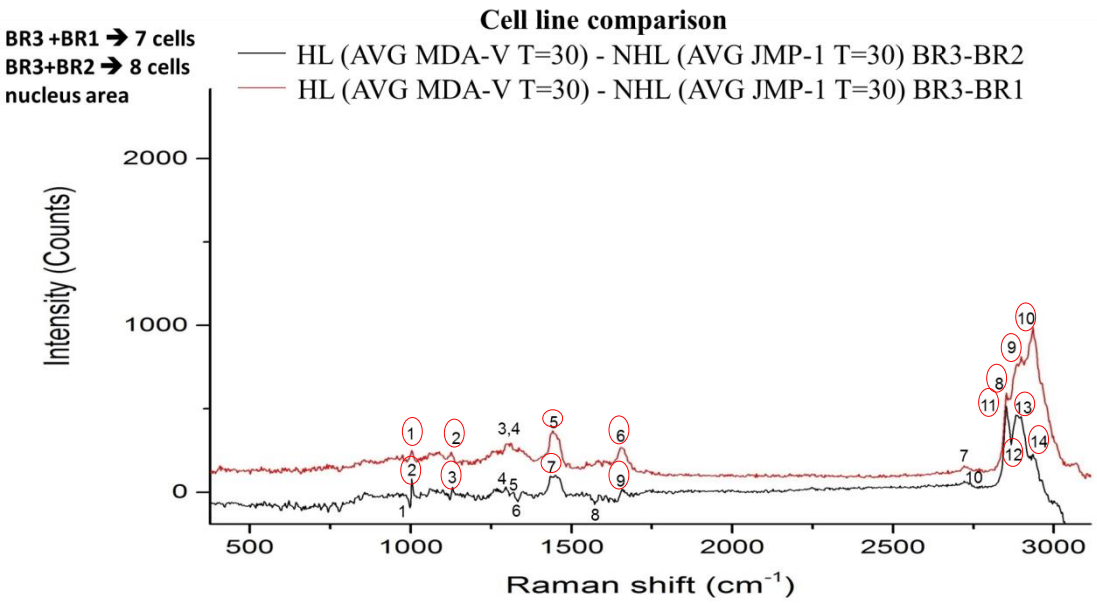


**Figure 3.4.4.** Raman signaling differences between JMP-1/MCL and MDA-V/HL cell lines in T=30°C. The circled numbers indicate the most important peaks based on the blue shaded areas (see fig 3.4.3).

**Assignment of peaks ( $cm^{-1}$)**

**BR3-BR2:**

| | | | |
|---|---|---|---|
| 1)➔997 | 5)➔1319 | 9)➔1658 | 13)➔2898 |
| 2)➔1002 | 6)➔1331 | 10)➔2721 | 14)➔2935 |
| 3)➔1131 | 7)➔1450 | 11)➔2852 | |
| 4)➔1296 | 8)➔1573 | 12)➔2867 | |

**BR3-BR1:**

| | | | |
|---|---|---|---|
| 1)➔1002 | 4)➔1310-1313 | 7)➔2721 | 9)➔2898 |
| 2)➔1125 | 5)➔1441 | 8)➔2852 | 10)➔2935 |
| 3)➔1296 | 6)➔1655 | | |

**Observation:** For the (BR3-BR1) curve, the peak no10, at wn 2935$cm^{-1}$, has the strongest Raman intensity, where it corresponds to $CH_3$ symmetric band, C-H vibration of lipids and proteins and $CH_2$ asymmetric vibration of lipids and fatty acids.

For the (BR3-BR2) curve, the peak no11 at wn 2852$cm^{-1}$, has the strongest Raman intensity, where it corresponds to $CH_3$ symmetric stretching of lipids. Also the peak no2, at wn 1002 $cm^{-1}$, is a very distinct peak which corresponds to Phenylalanine.

➢ **T=25°C**

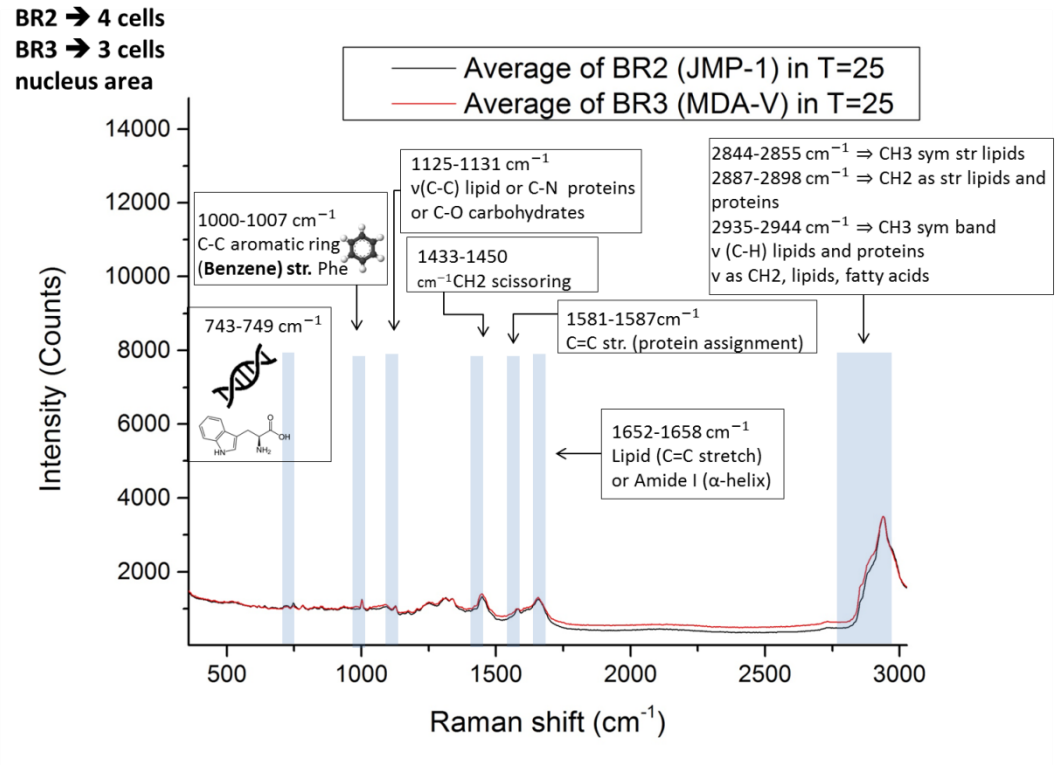


**Figure 3.4.5.** Raman signaling average plots of JMP-1/MCL and MDA-V/HL cells for T=25°C.

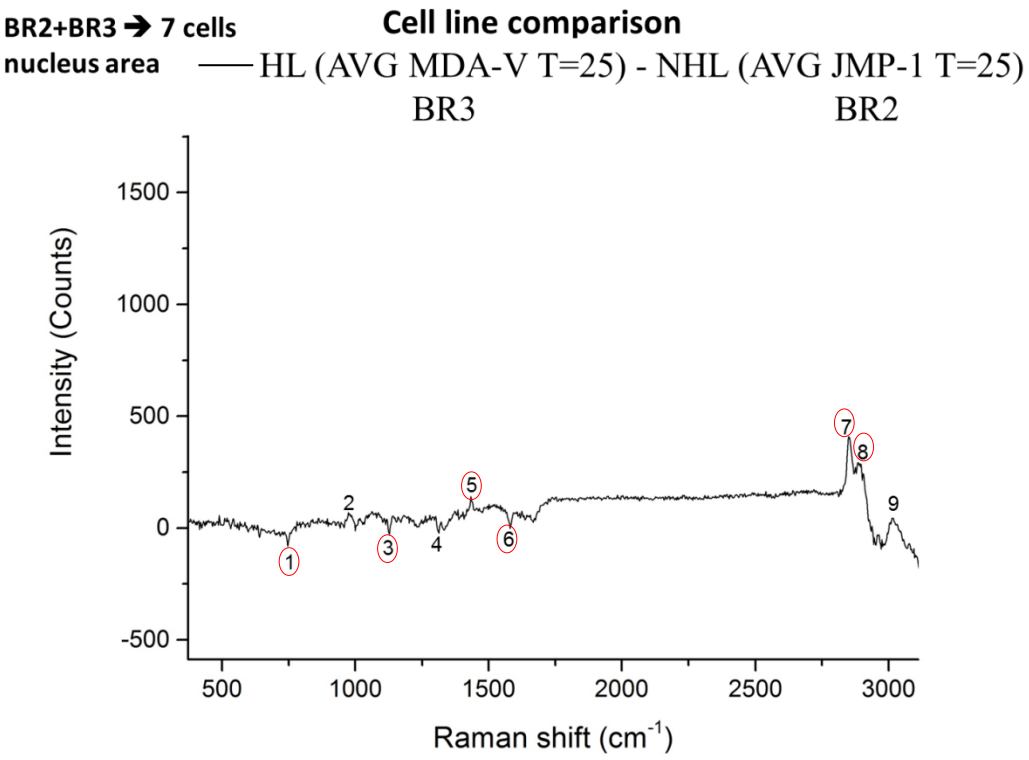


**Figure 3.4.6.** Raman signaling differences between JMP-1/MCL and MDA-V/HL cell lines in T=25°C. The circled numbers indicate the most important peaks based on the blue shaded areas (see fig 3.4.5).

**Assignment of peaks ( $cm^{-1}$)**

| | | |
|---|---|---|
| 1)➔746 | 4)➔1313 | 7)➔2849 |
| 2)➔974 | 5)➔1433 | 8)➔2887 |
| 3)➔1128 | 6)➔1581 | 9)➔3012 |

**Observation:** The peak no7, at wn 2849$cm^{-1}$, has the strongest Raman intensity, where it corresponds to $CH_3$ symmetric stretching of lipids. Also the peaks with the numbers 1,3,5,6 at wn 746, 1128, 1433 and 1581 $cm^{-1}$, are very distinct peaks which correspond to ring breathing mode of DNA/RNA bases, ν(C-C) lipid/C-N proteins/C-O carbohydrates, $CH_2$ scissoring and C=C str. (protein assignment) respectively.

➢ **T=20°C**

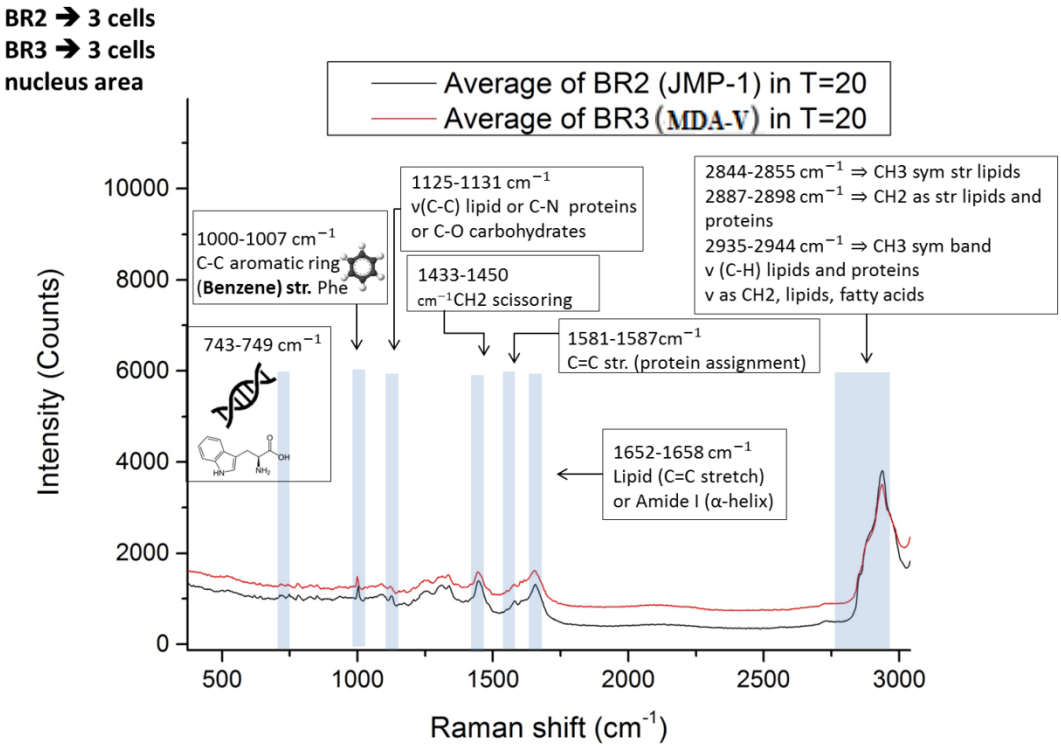


**Figure 3.4.7.** Raman signaling average plots of JMP-1/MCL and MDA-V/HL cells for T=20°C.

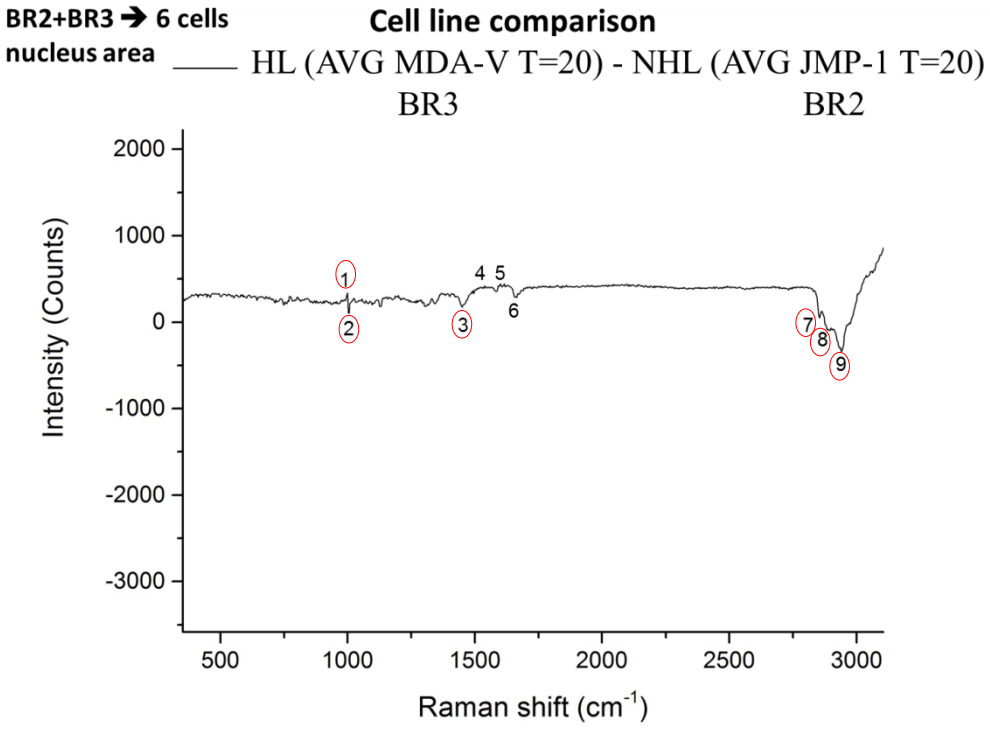


**Figure 3.4.8.** Raman signaling differences between JMP-1/MCL and MDA-V/HL cell lines in T=20°C. The circled numbers indicate the most important peaks based on the blue shaded areas (see fig 3.4.7).

**Assignment of peaks ( $cm^{-1}$)**

| | | |
|---|---|---|
| 1)➔1000 | 4)➔1538 | 7)➔2855 |
| 2)➔1002 | 5)➔1615 | 8)➔2884 |
| 3)➔1450 | 6)➔1664 | 9)➔2941 |

**Observation:** The peak no9, at wn 2941$cm^{-1}$, has the strongest Raman intensity, where it corresponds to $CH_3$ symmetric band, C-H vibration of lipids/proteins and $CH_2$ asymmetric vibration of lipids/fatty acids. Also the peak no2 at wn 1002$cm^{-1}$, is a very distinct peak which corresponds Phenylalanine.

➢ **T=18°C**

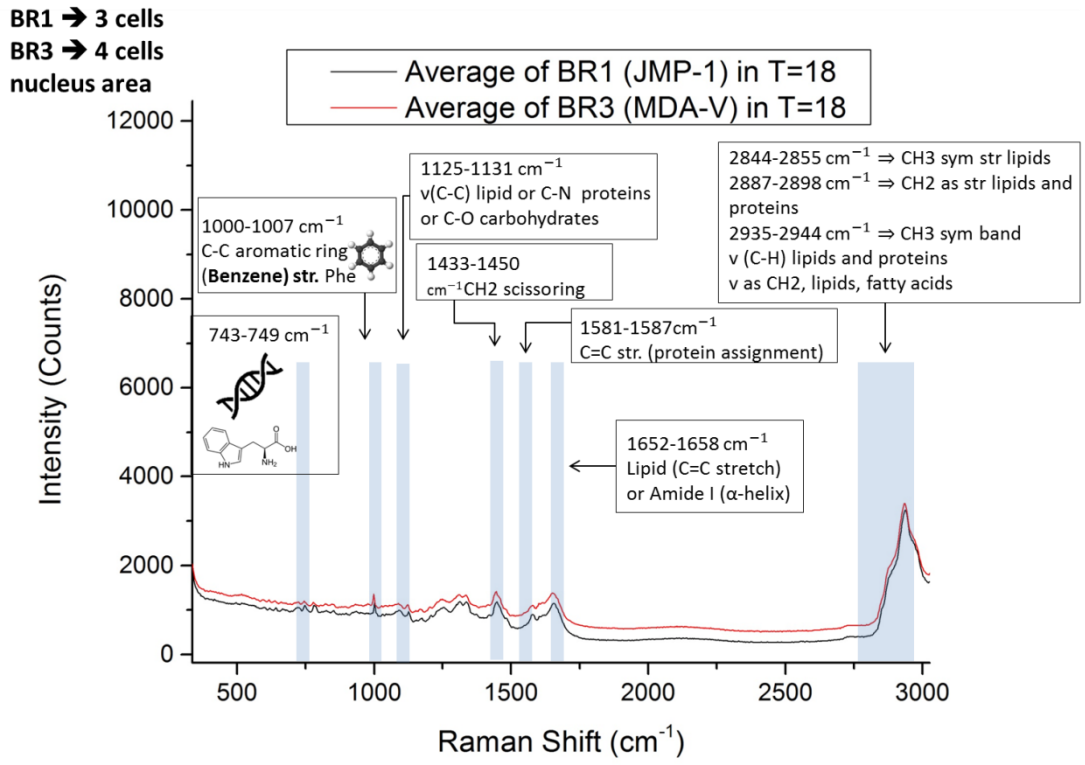


**Figure 3.4.9.** Raman signaling average plots of JMP-1/MCL and MDA-V/HL cells for T=18°C.

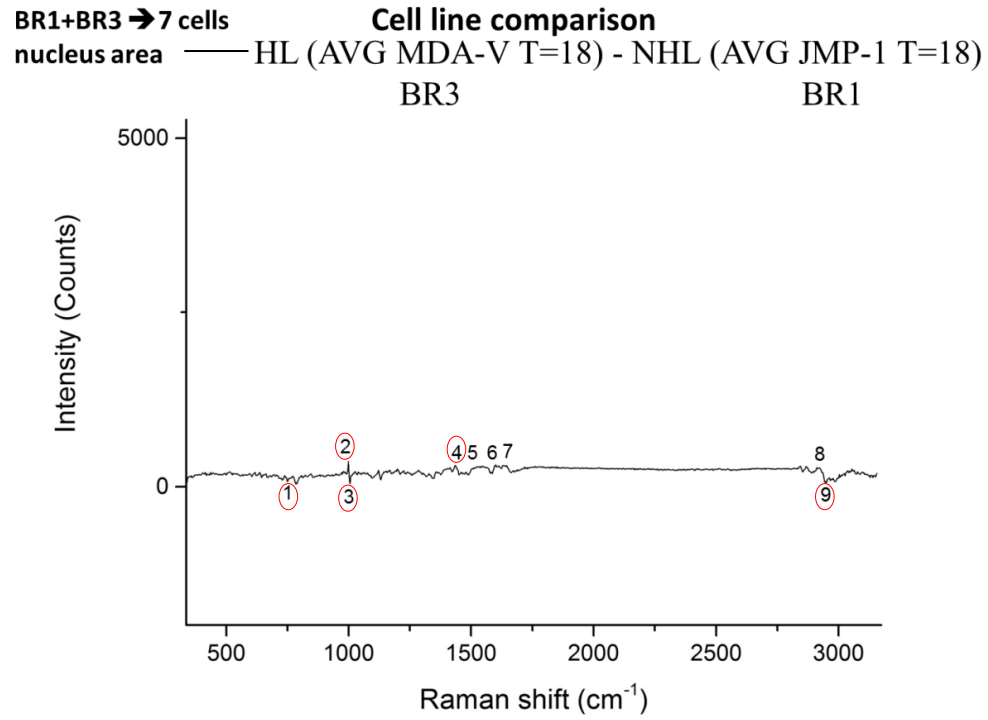


**Figure 3.4.10**. Raman signaling differences between JMP-1/MCL and MDA-V/HL cell lines in T=18°C. The circled numbers indicate the most important peaks based on the blue shaded areas (see fig 3.4.9).

**Assignment of peaks ( $cm^{-1}$)**

| | | |
|---|---|---|
| 1)➔748 | 4)➔1436 | 7)➔1629 |
| 2)➔1000 | 5)➔1547 | 8)➔2912 |
| 3)➔1002 | 6)➔1601 | 9)➔2949 |

**Observation:** The peak no2, at wn 1000$cm^{-1}$, is a very distinct peak which corresponds to Phenylalanine.

➢ **T=15°C**

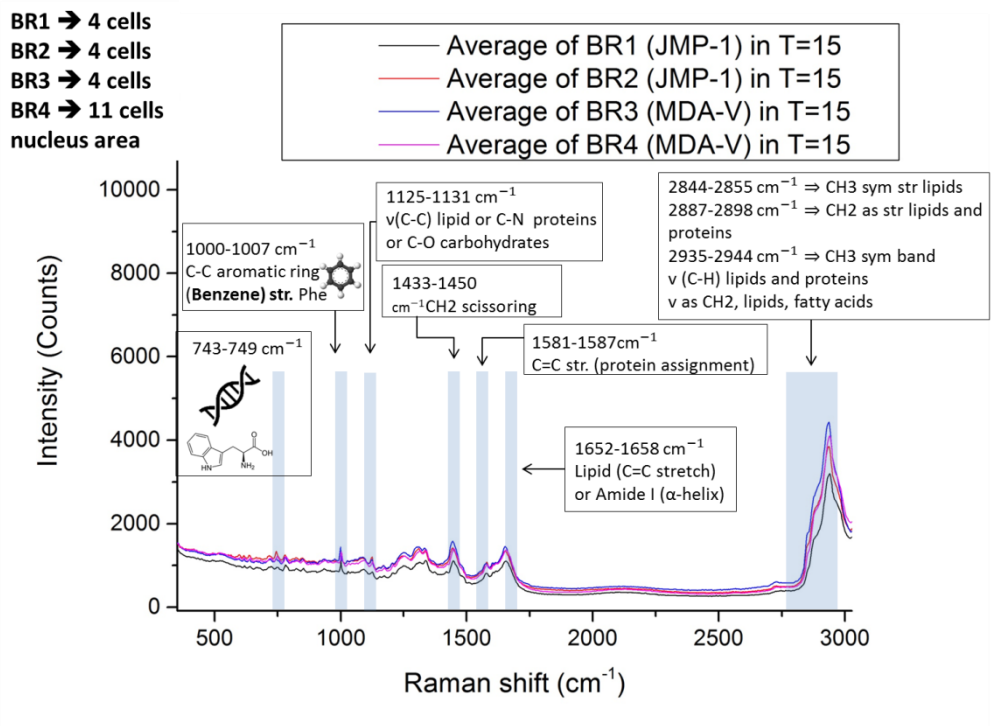


**Figure 3.4.11.** Raman signaling average plots of JMP-1/MCL and MDA-V/HL cells for T=15°C.

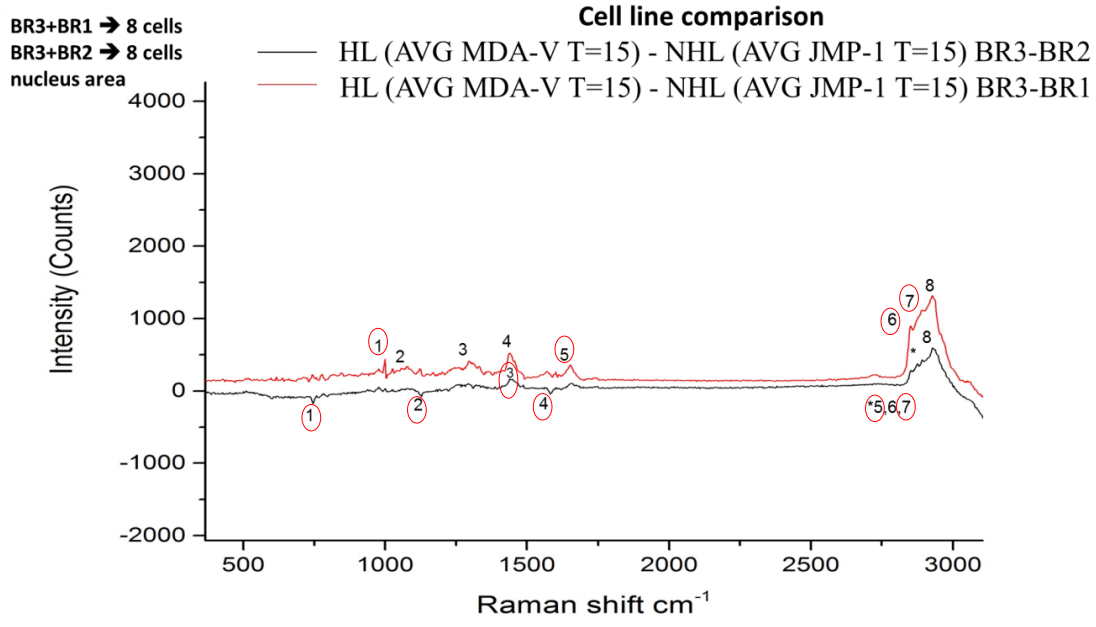


**Figure 3.4.12.** Raman signaling differences between JMP-1/MCL and MDA-V/HL (BR3) cell lines in T=15°C. The circled numbers indicate the most important peaks based on the blue shaded areas (see fig 3.4.11).

**Assignment of peaks ( $cm^{-1}$)**

**BR3-BR2:**

| | | | |
|---|---|---|---|
| 1)➔746 | 3)➔1439 | 5)➔2852 | 7)➔2892 |
| 2)➔1128 | 4)➔1581 | 6)➔2875 | 8)➔2929 |

**BR3-BR1:**

| | | | |
|---|---|---|---|
| 1)➔1000 | 3)➔1293 | 5)➔1652 | 7)➔2892 |
| 2)➔1079 | 4)➔1330 | 6)➔2852 | 8)➔2929 |

**Observation:** For the (BR3-BR1) curve, the peak no8, at wn 2929$cm^{-1}$, has the strongest Raman intensity, despite the fact that it does not belong to the important Raman peaks, it corresponds to $CH_2$ asymmetric stretch. Also the peak no1, at wn 1000$cm^{-1}$, is a very distinct peak which corresponds to Phenylalanine.

For the (BR3-BR2) curve, the peak no8, at wn 2929$cm^{-1}$, has the strongest Raman intensity, despite the fact that it does not belong to the important Raman peaks, it corresponds to $CH_2$ asymmetric stretch.

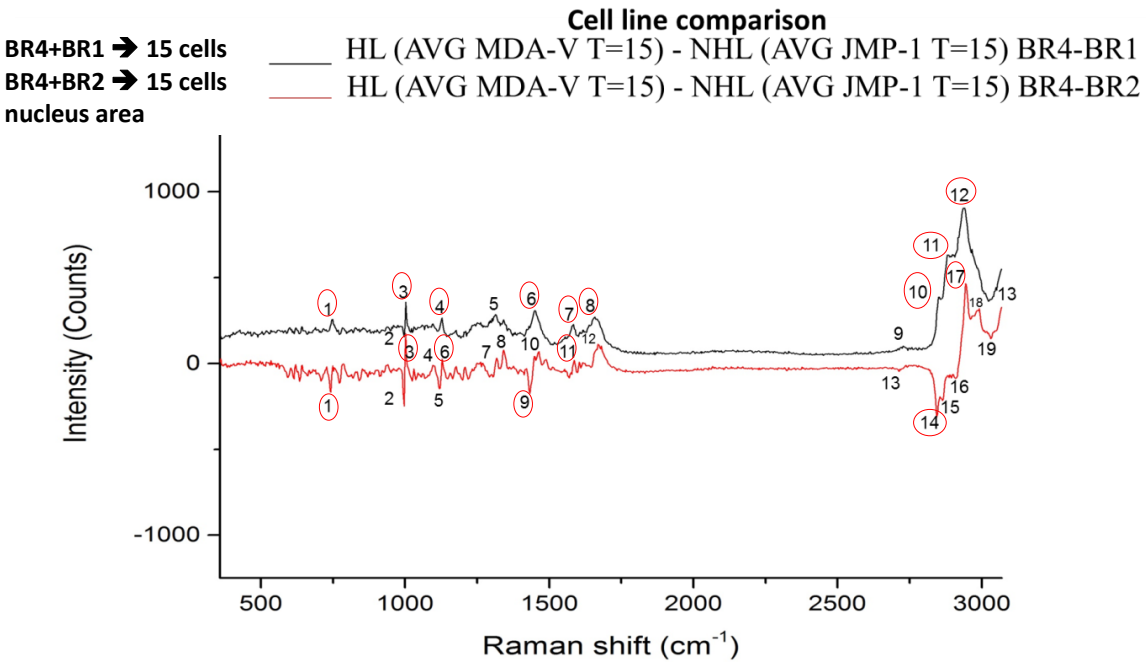


**Figure 3.4.13.** Raman signaling differences between JMP-1/MCL and MDA-V/HL (BR4) cell lines in T=15°C. The circled numbers indicate the most important peaks based on the blue shaded areas (see fig 3.4.11)

**Assignment of peaks**

**BR4-BR1:**

| | | | |
|---|---|---|---|
| 1)➔749 | 5)➔1313 | 9)➔2727 | 12)➔2941 |
| 2)➔997 | 6)➔1450 | 10)➔2853 | 13)➔3024 |
| 3)➔1003 | 7)➔1584 | 11)➔2892 | |
| 4)➔1128 | 8)➔1658 | | |

**BR4-BR2:**

| | | | |
|---|---|---|---|
| 1)➔743 | 6)➔1128 | 11)➔1587 | 16)➔2910 |
| 2)➔997 | 7)➔1319 | 12)➔1670 | 17)➔2944 |
| 3)➔1003 | 8)➔1342 | 13)➔2713 | 18)➔2992 |
| 4)➔1097 | 9)➔1433 | 14)➔2844 | 19)➔3032 |
| 5)➔1119 | 10)➔1464 | 15)➔2864 | |

**Observation:** For the (BR4-BR1) curve, the peak no12, at wn 2941$cm^{-1}$, has the strongest Raman intensity, where it corresponds to $CH_3$ symmetric band, C-H vibration of lipids/proteins and $CH_2$ asymmetric vibration of lipids/fatty acids. Also, the peak no3, at wn 1003$cm^{-1}$, is a very distinct peak which corresponds to Phenylalanine.

For the (BR4-BR2) curve, the peaks with the numbers 14 and 17 at wn 2844$cm^{-1}$ and 2944$cm^{-1}$ respectively have the strongest Raman intensity, where they correspond to $CH_3$ symmetric stretching of lipids and to $CH_3$ symmetric band, C-H vibration of lipids/proteins, $CH_2$ asymmetric vibration of lipids/fatty acids respectively. Also, the peaks with the numbers 1 and 9 , at wn 743$cm^{-1}$ and 1433$cm^{-1}$ are very distinct peaks which correspond to ring breathing mode of DNA/RNA bases and to $CH_2$ scissoring respectively. Finally, the peaks with the numbers 2 and 3 at wn 997$cm^{-1}$ and 1003$cm^{-1}$ respectively are more distinct than the rest of them and correspond to Phenylalanine.

**Comments-Conclusions**

- At T=37°C and T=30°C there are a lot of Raman signaling differences between HL and NHL lymphoma cell lines, but the most important ones are the peaks of $CH_3/CH_2/CH$ stretches (lipids) ("total methylation signaling area" at about 2800-3000$cm^{-1}$) and the Phenylalanine peak (1000-1007$cm^{-1}$).

- At T=25°C there are a lot of Raman signaling differences too, but some of the peaks are more distinct and represent DNA/RNA, lipids, carbohydrates and proteins. However, these peaks are more distinct but not as intense as those at T=30°C.
- At T=20°C peaks are less distinct and less intense but the most important peaks are the same as T=37°C and T=30°C.
- At T=18°C Raman signaling differences between HL and NHL lymphoma cell lines are few where the only intense peak is that of Phenylalanine, which means that at this temperature we don't have a lot of Raman signaling differences.

- At T=15°C we have the most Raman signaling differences between HL and NHL lymphoma cell lines where the most important ones are the same as T=37°C and T=30°C and also DNA/RNA peaks.

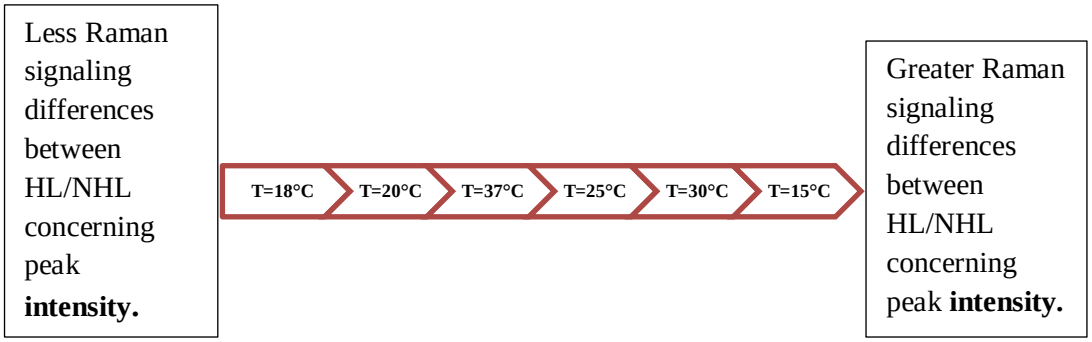


- Concluding, HL and NHL lymphoma cell lines have Raman signaling differences when they are measured with Raman spectroscopy in the same conditions. The most important and intense differences are presented at about 2800-3000cm$^{-1}$, where the "total methylation signaling area" and lipids are and at 1000-1007 cm$^{-1}$ where Phenylalanine is detected.

## 3.5 PCA analysis of HL (MDA-V/HL) and NHL (JMP-1/MCL) cell lines.

Our PCA analysis of HL and NHL lymphoma cell lines are presented fig. 3.5.

- **T=15°C**

**MDA-V/HL compared to JMP-1/MCL cells**

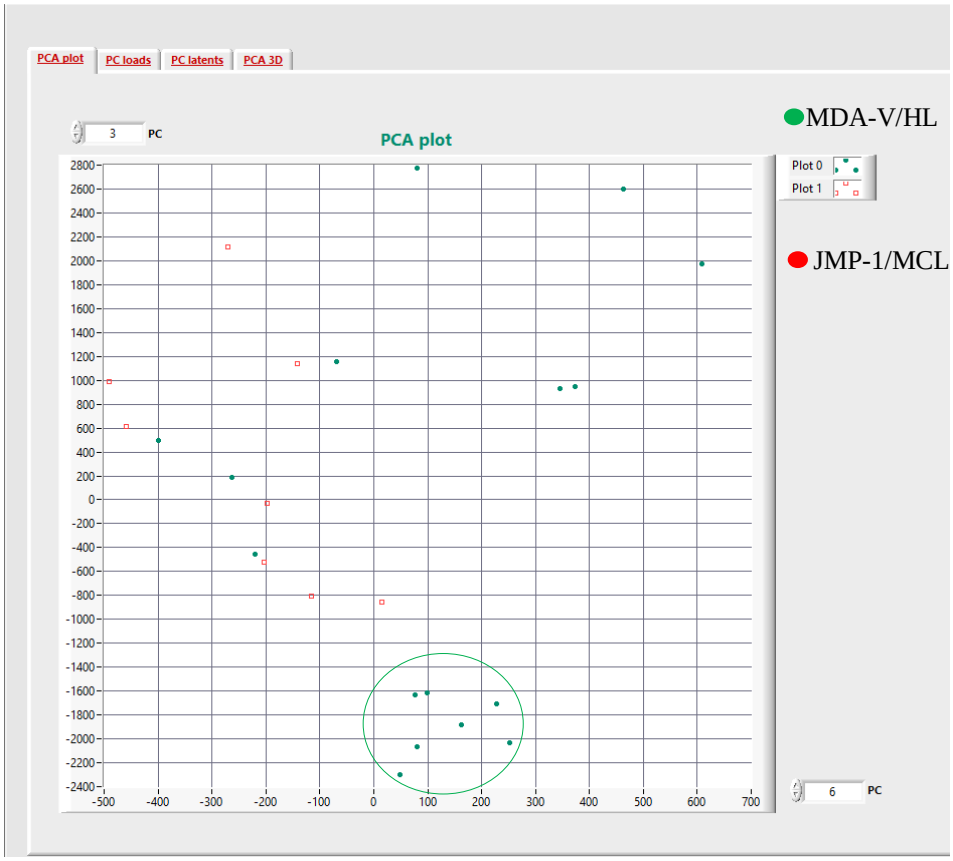


**Figure 3.5.1.** MDA-V/HL to JMP-1/MCL cells comparison.

**Observation:** In the **horizontal** principal component axis we can see a differentiation between MDA-V/HL and JMP-1/MCL cells, as we can observe in the cluster in fig 3.5.1, in contrast to the vertical principal component axis, where there isn't any differentiation between MDA-V/HL and JMP-1/MCL cells.

**MDA-V/HL big compared to MDA-V/HL small cells**

As we didn't observe **any big** differentiation between MDA-V/HL and JMP-1/MCL cells, we tried PCA analysis between MDA-V/HL big and MDA-V/HL small cells.

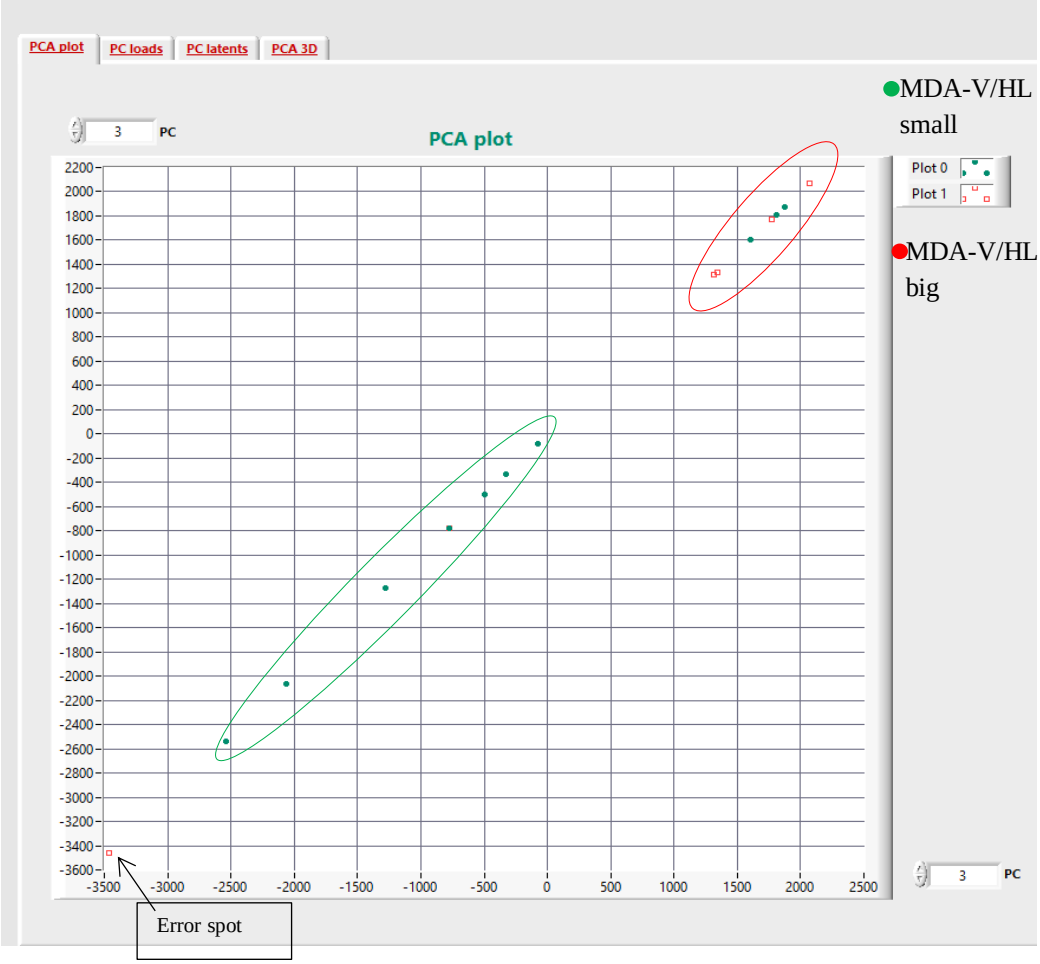


**Figure 3.5.2.** MDA-V/HL big to MDA-V/HL small cells comparison.

**Observation:** In both the horizontal and the vertical principal component axis we can see a **distinct differentiation between MDA-V/HL big and MDA-V/HL small cells** as we can observe in the clusters in fig 3.5.2. Only one spot is out of the cluster (one cell), which can be considered an error. This means that MDA-V/HL big and MDA-V/HL small cells are distinguishable with Raman spectroscopy and offer different Raman signal identities. The green spots in the red cluster may be a middle size closer to big MDA-V/HL cell size. The fact that in fig 3.5.1 many of the green dots (MDA-V/HL cells) are scattered is normal. Due to the fact that MDA-V/HL big cells are completely differentiated from the MDA-V/HL small cells, we proceeded to use MDA-V/HL big and JMP-1/MCL cells at T=15 for our PCA (fig 3.5.3).

**MDA-V/HL big compared to JMP-1/MCL cells**

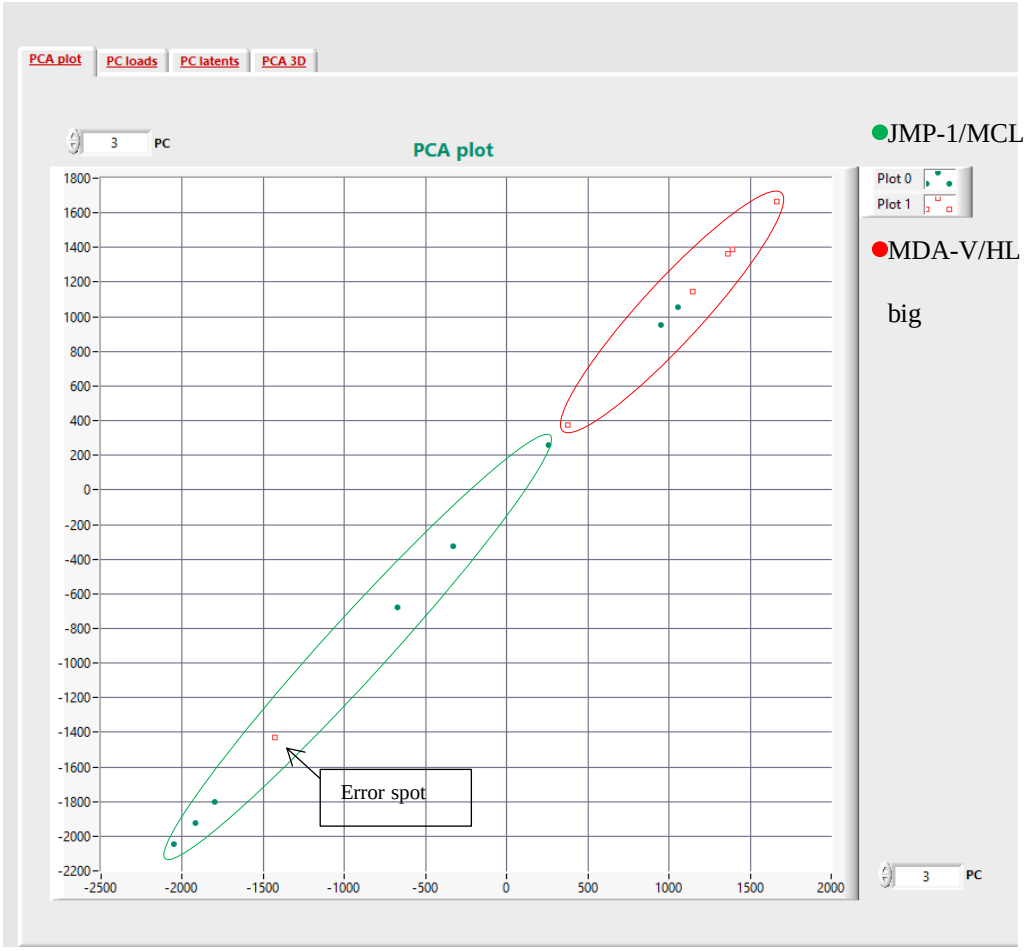


**Figure 3.5.3.** MDA-V/HL big to JMP-1/MCL cells comparison.

**Observation:** In both the horizontal and the vertical principal component axis we can see a **distinct differentiation between MDA-V/HL big and JMP-1/MCL cells** as we can observe in the clusters fig 3.5.3. Only one spot (one cell) can be considered an error. This means that MDA-V/HL big and JMP-1/MCL cells are distinguishable with Raman spectroscopy and offer different Raman signal identities. For the two green spots (JMP-1/MCL) in the red cluster, they appear to have more similarities with the red ones (MDA-V/HL big) which means that MDA-V/HL big and JMP-1/MCL cells obviously have Raman similarities.

**PCA analysis of MDA-V/HL small cells compared to JMP-1/MCL cells didn't give us any differentiation.**

**Conclusion:** At T=15°C only MDA-V/HL big cells are differentiated from JMP-1/MCL cells, based on the PCA analysis of their **nucleus** Raman plots.

## ➢ T=30°C

### MDA-V/HL small compared to JMP-1/MCL cells

At T=30°C we were unable to measure any MDA-V/HL big cells.

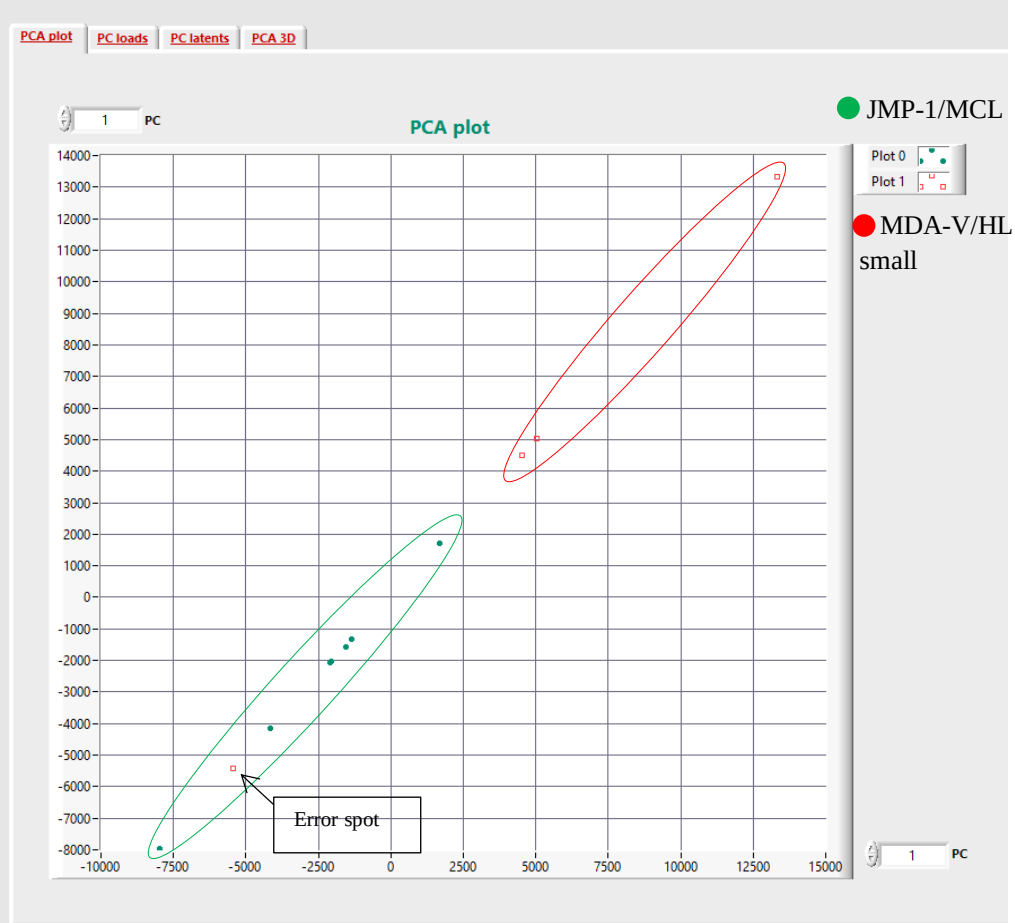


**Figure 3.5.4.** MDA-V/HL small to JMP-1/MCL cells comparison.

**Observation:** In both the horizontal and the vertical principal component axis **we can see a distinct differentiation between MDA-V/HL small and JMP-1/MCL cells** as we can observe in the clusters in fig 3.5.4. Only one spot (one cell) can be considered an error. This means that MDA-V/HL small and JMP-1/MCL cells are distinguishable with Raman spectroscopy and offer different Raman signal identities.

Another PCA analysis with increased vertical principal component was created.

**MDA-V/HL small compared to JMP-1/MCL cells**

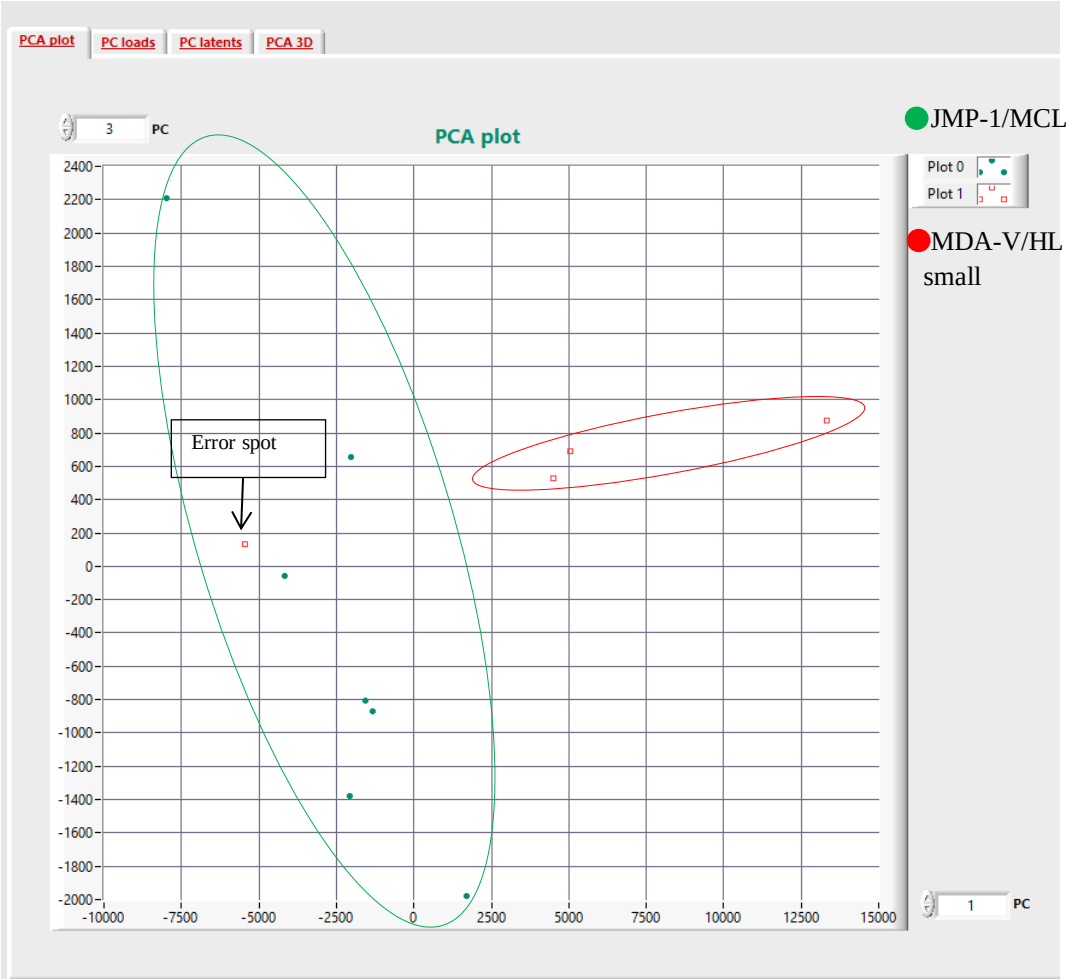


**Figure 3.5.5.** MDA-V/HL small to JMP-1/MCL cells comparison.

**Observation:** In the **horizontal** principal component axis we can see a **distinct differentiation between MDA-V/HL small and JMP-1/MCL cells** as we can observe in the clusters fig 3.5.5. Only one spot (one cell) can be considered an error. This means that MDA-V/HL small and JMP-1/MCL cells are distinguishable with Raman spectroscopy and offer different Raman signal identities.

PCA analysis of MDA-V/HL small cells compared to JMP-1/MCL cells gave us distinct differentiations in this temperature.

**Conclusion:** At T=30°C only MDA-V/HL small cells are differentiated from JMP-1/MCL cells, based on the PCA analysis of their **nucleus** Raman plots. Unfortunately we were unable to measure any MDA-V/HL big cell, so we have no results.

- **PCA comparison of BR1 (JMP-1/MCL) and BR3 (MDA-V/HL) experiments**

In the BR1 experiment JMP-1/MCL cells were measured in T=15, 18, 30, 37 °C and in the BR3 experiment MDA-V/HL cells were measured in T=15, 18, 20, 25, 30, 37 °C.

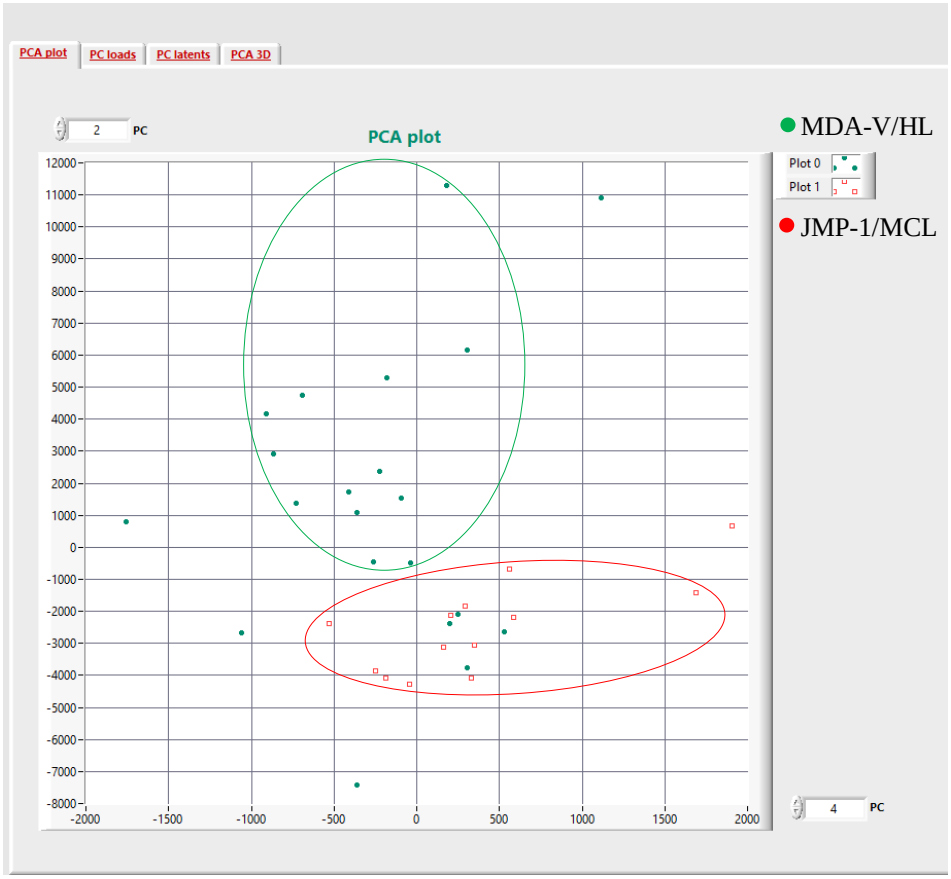


**Figure 3.5.6.** BR3 MDA-V/HL to BR1 JMP-1/MCL cells comparison.

**Observation:** In the **vertical** principal component axis we can see a differentiation between MDA-V/HL and JMP-1/MCL cells as we can observe in the clusters in fig 3.5.6. For the four green spots (MDA-V/HL) in the red cluster, they appear to that have more similarities with the red ones (JMP-1/MCL) which means that these two cell lines obviously have Raman similarities.

- **PCA comparison of BR2 (JMP-1/MCL) and BR3 (MDA-V/HL) experiments**

In the BR2 experiment JMP-1/MCL cells were measured in T=15, 20, 25, 30°C and in the BR3 experiment MDA-V/HL cells were measured in T=15, 18, 20, 25, 30, 37°C.

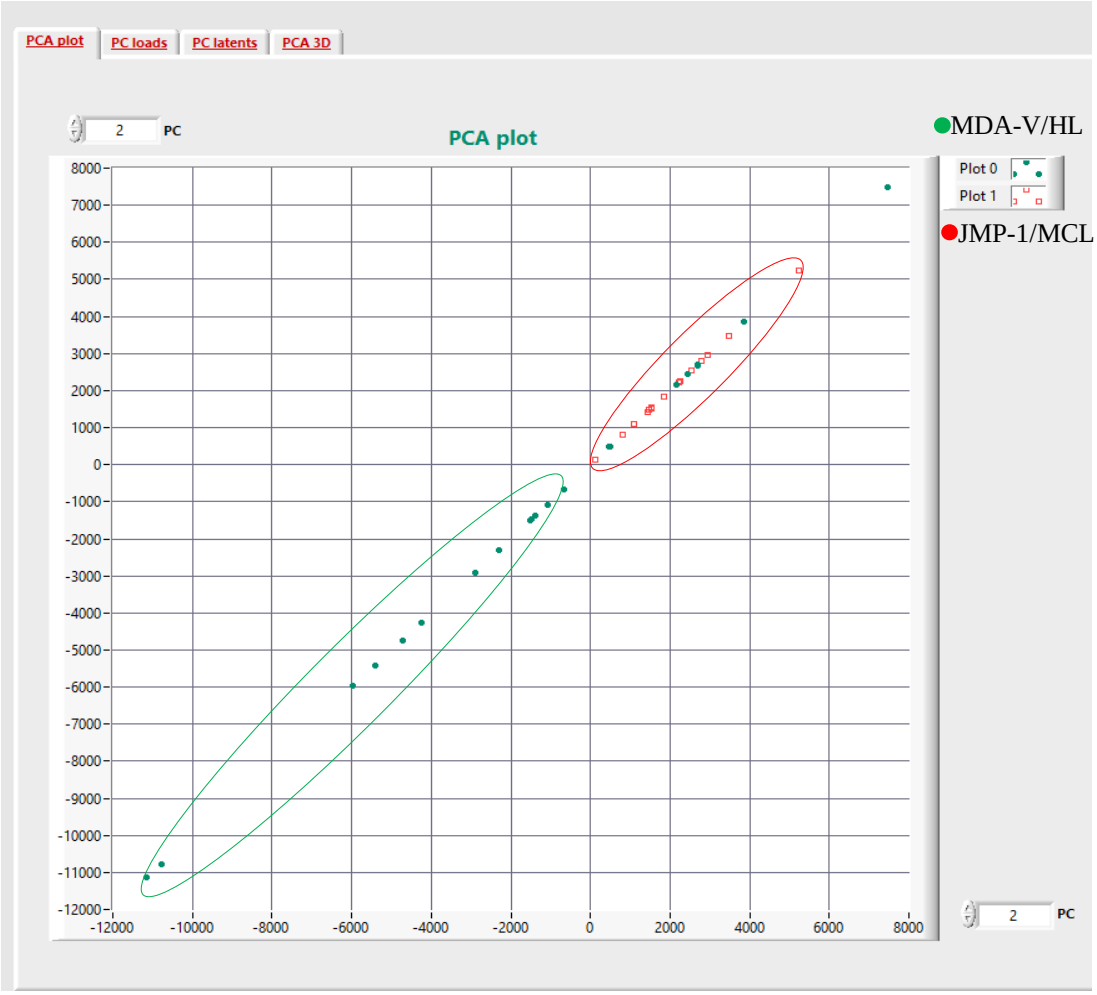


**Figure 3.5.7.** BR3 MDA-V/HL to BR2 JMP-1/MCL cells comparison.

**Observation:** In both the horizontal and the vertical principal component axis we can see a **differentiation between MDA-V/HL and JMP-1/MCL cells** as we can observe in the clusters in fig 3.5.7. For the five green spots (MDA-V/HL) in the red cluster, they appear to have more similarities with the red ones (JMP-1/MCL) which means that these two cell lines obviously have Raman similarities.

- **PCA comparison between BR1, BR2 (JMP-1/MCL) and BR3, BR4 (MDA-V/HL) experiments**

In the BR1/BR2 experiments JMP-1/MCL cells were measured in T= 15, 18, 30, 37°C/T=15, 20, 25, 30 °C respectively and in the BR3/BR4 experiments MDA-V/HL cells were measured in T=15, 18, 20, 25, 30, 37 °C/15°C respectively.

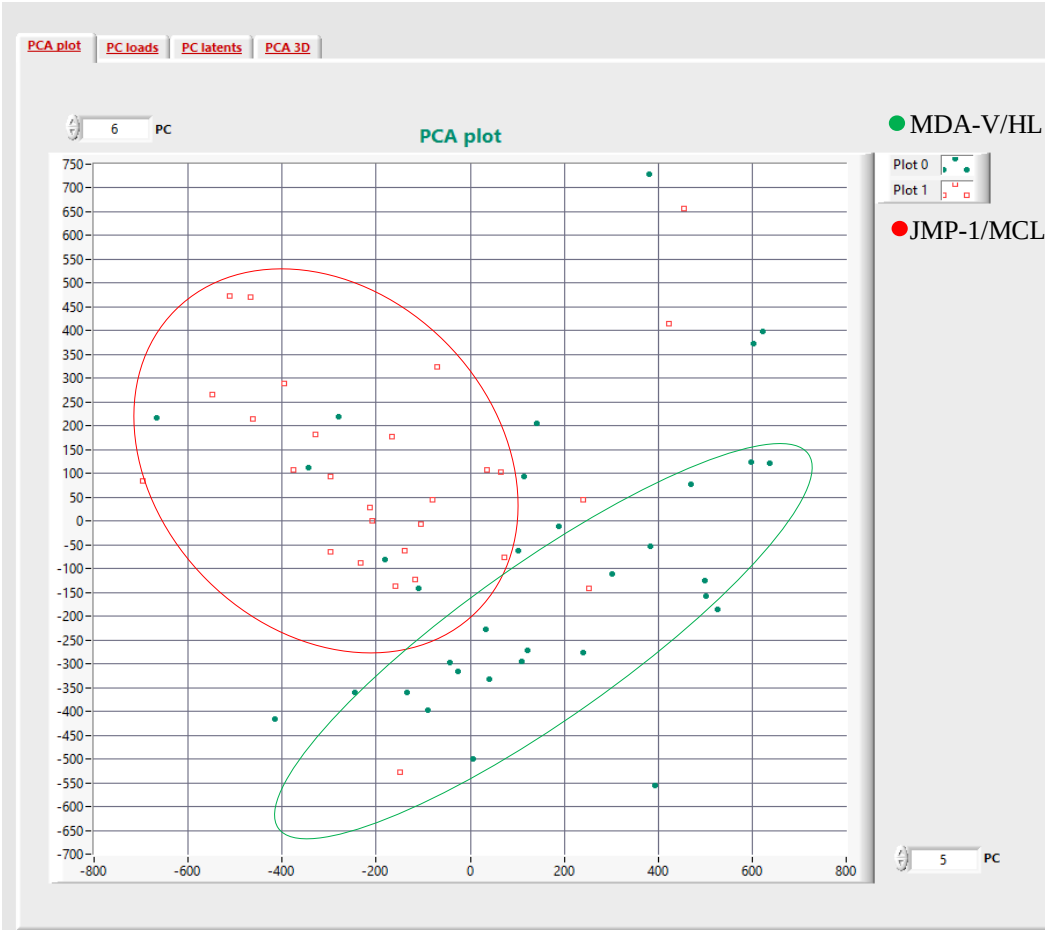


**Figure 3.5.8.** MDA-V/HL to JMP-1/MCL cells – all measurements comparison between in all the different temperatures.

**Observation:** In both the horizontal and the vertical principal component axis **we can see a differentiation between MDA-V/HL and JMP-1/MCL cells** as we can observe in the clusters fig 3.5.8.

**Conclusions:**

- **MDA-V/HL big cells in T= 15°C are more preferable for PCA comparison** with JMP-1/MCL cells because the differentiation is more distinct.

- **MDA-V/HL small cells in T= 30°C are preferable for PCA comparison** with JMP-1/MCL cells because they have distinct differentiations.
- MDA-V/HL and JMP-1/MCL cells are somewhat distinguishable with PCA analysis using Raman spectrums but they have a lot of similarities as well. It is preferable to make PCA comparisons of the different HL/NHL cell lines under the same temperature, for a better comparison.
- Results may be different if we carry out PCA analysis based on different cell areas and not just the nucleus.

## 3.6 N3a measurements

After the HL and NHL comparison we measured N3a using Raman spectroscopy in order to allow the detection of N3a in treated lymphoma cells.

### 3.6.1 Determination of N3a's Raman signature peaks

#### *Sample preparation for Raman spectroscopy*

Our stock solution was $c_i = 10$mM N3a in DMSO (N3a's solvent)

We need to have

$c_f = 5\mu$M of N3a in

$V_f$= 800μl solution (PBS with stock)

$V_i$= 0.4μl of stock solution

We made 3 different solutions:

- 1st solution of N3a: 0.4 μl of the stock solution was dissolved in 800 μl PBS
- 2nd solution of DMSO (control 1): 0.4 μl DMSO was dissolved in 800 μl PBS
- 3rd solution of PBS (control 2): 20μl PBS

Each sample was 10μl of the corresponding solution and was analyzed with Raman spectroscopy for 1 min and 35 sec.

**Information worth noting**

- Raman spectrometer is very photosensitive so the area was protected with a dark cover during the measurements.
- The vertical axis in a Raman plot (intensity) correlates to the number of bonds detected.

As presented in Table 3.6.1. we detected distinct N3a shifts. N3a's strong unique peaks were found at **480-481 and 2436-2438 $cm^{-1}$ for the first time, according to our knowledge,** which are not commonly found in other biological molecules.

**Table 3.6.1.** Distinct peaks of N3a.

| Samples | Unique Raman peaks ($cm^{-1}$) | Comments |
|---|---|---|
| **N3a in DMSO and PBS** | **2438***<br>481<br>1466* (weak) | **Raman peaks correspond to N3a** |
| DMSO in PBS (control 1) | 700-800<br>2900<br>1400 | Raman peaks correspond to DMSO Raman spectral assignments |
| PBS (control 2) | 1600 | Raman peaks correspond to PBS Raman spectral assignments |

*not corresponding to known biological compounds

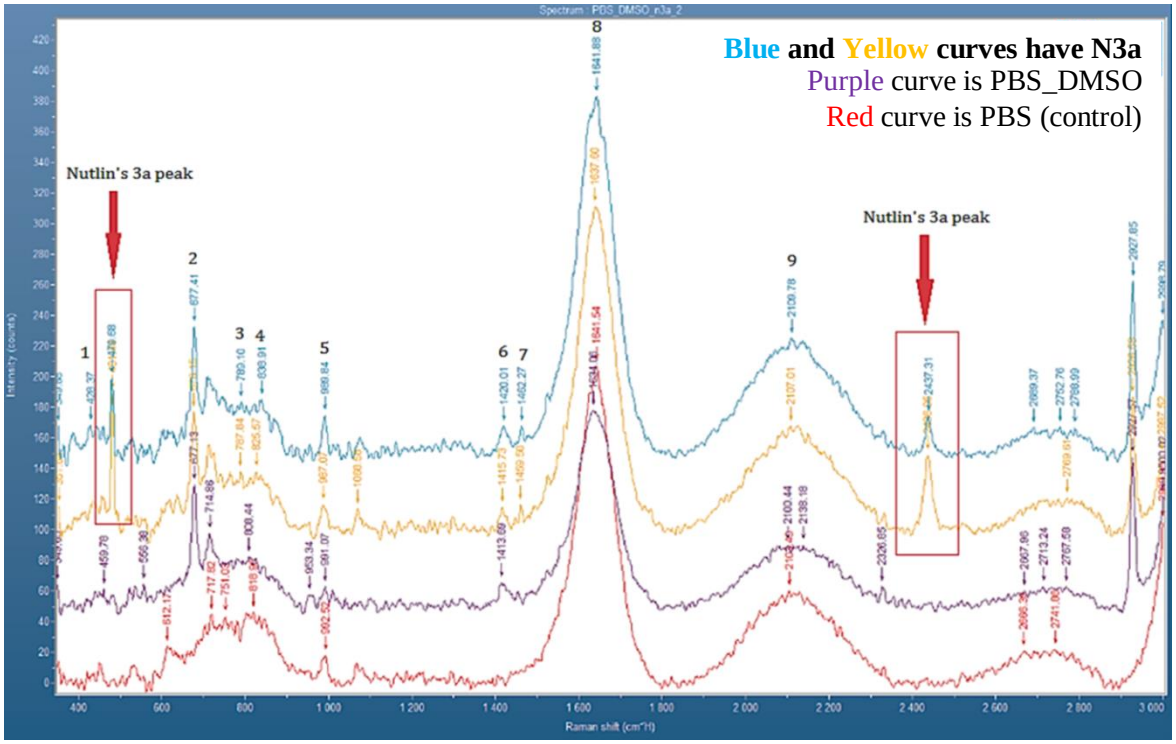


**Figure 3.6.1.** N3a Raman Spectrum – Reference, where y axis is Intensity (Counts) and x axis is Raman shift ($cm^{-1}$). The yellow and blue curves represent the solution of N3a, the purple PBS_DMSO and the Red one PBS. N3a's unique peaks are in the red boxes.

**N3a's Raman peaks found in biological compounds**

According to the Raman signaling library for biological compounds [45], Raman peaks of **N3a s spectrum** (fig 3.6.1), corresponding to known biomolecules. Raman signals as presented in Table 3.6.2, were rejected as unique N3a Raman signals.

**Table 3.6.2.** Raman peaks of N3a's spectrum (fig 3.6.1) corresponding to biological Raman signals.

| No | Shift ($cm^{-1}$) | Assignment |
|---|---|---|
| 1 | 428 | C-C-O bend alcohols/phenols, C-C skeleton, $vPO_4^{-3}$ |
| 2 | 677-678 | G ring breathing in DNA, ribose v, monoalkyl cis C-H wag |
| 3 | 789 | C-C-O strength tertiary alcohols, C-C-C branched alkanes $CHR_2$ |
| 4 | 839 | Amine groups def. v, C-C skeleton branched alkanes $CHR_2$, Triacyl C-H wag |
| 5 | 990 | Pyridine ring breathing, C-H bend, poly(L-Histidine) imidazole chain |
| 6 | 1420 | Deoxyribose (B,Z-marker), $NH_3$ bend Uracil, $CH_2$ cyclopropane derivatives |
| 7 | 1462 | $\delta CH_2$ disaccharides sucrose, Tryptophan, purine bases |
| 8 | 1642 | Heme proteins, amide I bands collagen |
| 9 | 2110 | No biological signal |

Even though some of the peaks in N3a's graph correspond to biological compounds, after thorough signal research we determined that N3a's **2 strong peaks** (**481 $\mathbf{cm^{-1}}$**, **2438 $\mathbf{cm^{-1}}$**) were not commonly found in other biological compounds. Especially **2436-2438 shifts were not detected in any biological molecule.** For this reason, it was safe to assume that N3a detection in lymphoma cell lines would be possible, using Raman spectroscopy.

**Table 3.6.3.** N3a's strong Raman peaks found in other biological molecules.

| N3a's peak | Compound | Bond(s) |
|---|---|---|
| 481 | (+) Camphor in Cytochrome P-450 | CO-P (12C-16O) CO-Fe [46] |
| **2436, 2438** | **No biological signaling** | - |

A Raman peak library was created consisting of N3a's peaks **in other non-biological molecules,** for additional confirmation of our results. Based on those findings, a possible matching of N3a's peaks with its chemical formula is presented (fig 3.6.2).

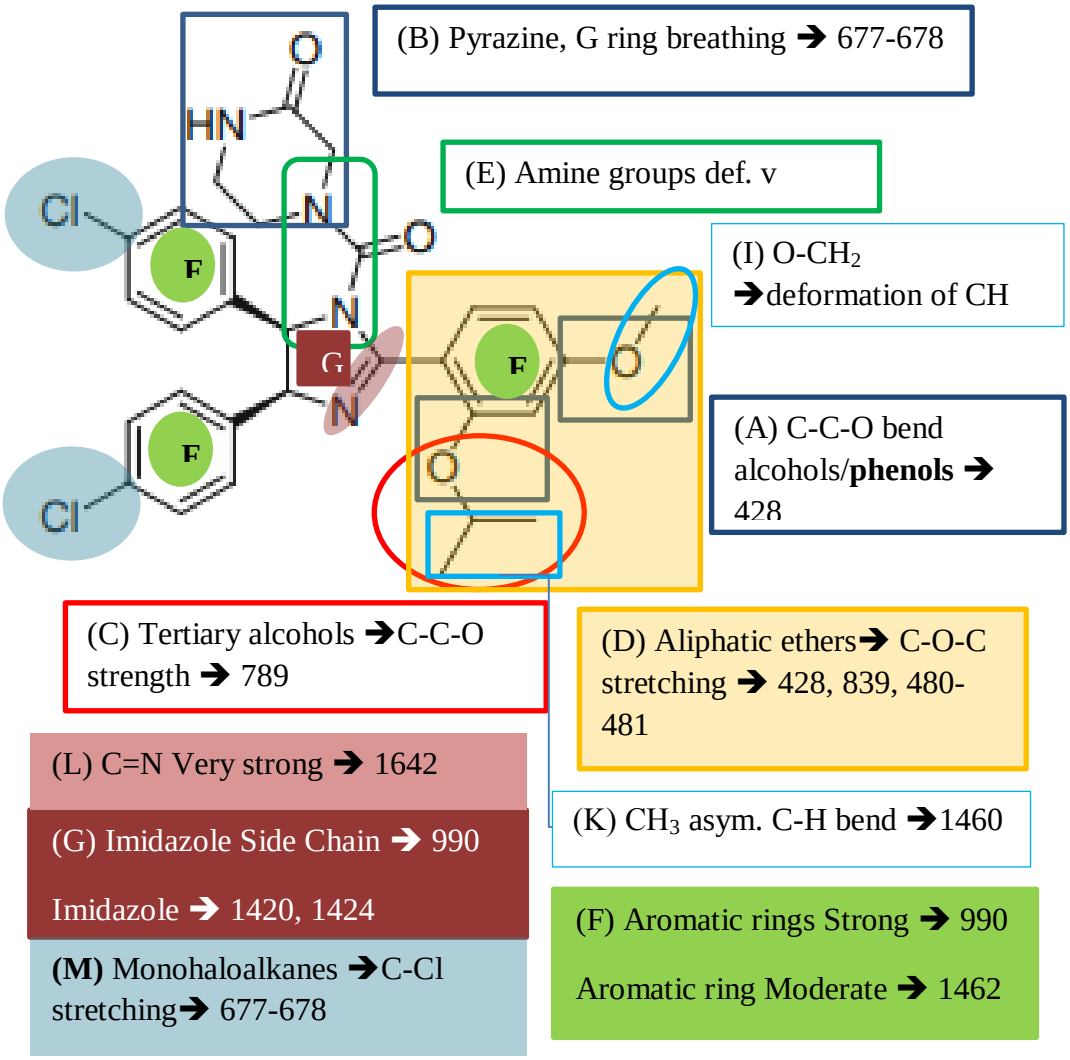


**Figure 3.6.2.** Possible matching of N3a's Raman peaks with its chemical formula: N3a {=(2-piperazinone, 4-[[(4S,5R)-4,5-bis(4-chlorophenyl)-4,5-dihydro-2-[4 methoxy-2-(1-methylethoxy)phenyl]-1H-imidazol-1-yl]carbonyl]-}. Color coded areas correspond to the colored boxes.

**Table 3.6.4.** Possible matching of N3a's peaks with its chemical formula, referring to the illustration fig 3.6.2

| No | Raman Shift ($cm^{-1}$) | Assignment |
|---|---|---|
| 1 | 480-481 | **(D)** Aliphatic Ethers ➔ COC, N3a strong peak [47] |
| 2 | 428 | **(A)** C-C-O bend alcohols/phenols, C-C skeleton [47]<br>**(D)** Aliphatic ethers ➔ $CH_3$-O-$CH_3$➔δ(C-O-C) [47] |
| 3 | 677-678 | **(B)** Assignment of Ground State Fundamental of Pyrazine ➔ pyrazine d4 [48]<br>**(M)** Monohaloalkanes ➔C-Cl stretching [47]<br>G ring breathing in DNA |
| 4 | 789 | **(C)** Branched alkanes ➔ $CHR_2$➔sym C-C-C stretching [45]<br>tertiary alcohols C-C-O strength [47] |
| 5 | 839 | **(D)** Aliphatic ethers➔sym stretching C-O-C [47]<br>**(E)** Amine groups def. v C-C skeleton branched alkanes $CHR_2$ [45] |
| 6 | 990 | **(F)** Aromatic rings Strong [49]<br>**(G)** Imidazole Side Chain ➔ C-H in-plane bend [50]<br>**(H)** normal and defocused resonance Raman spectra of phenolate [51] |
| 7 | 1420 | **(G)** 4-Methyl-imidazole, 1424 imidazole [52] |
| 8 | 1462 | **(F)** Aromatic rings moderate [49]<br>**(I)** O-$CH_2$ deformation of CH [47]<br>**(K)** 1460 $CH_3$ asym. C-H bend [53] |
| 9 | 1642 | **(L)** C=N Very strong [49] heme proteins, amide I bands collagen |
| 10 | 2110 | No signaling |
| 11 | 2436-2438 | No signaling N3a strong peak |

## 3.6.2 The use of RPMI 1640 without phenol red

As it was mentioned before, RPMI 1640 is a medium used in cell and tissue cultures for growing a variety of mammalian cell lines such us human lymphocytes. However, Phenol Red Indicator causes fluorescence effects interfering with N3a's Raman signaling area. This is why we tried to measure RPMI 1640 without dye to avoid this situation [42].

We compared N3a's Raman peaks with RPMI 1640 without dye and as we can observe in fig 3.6.3, fig 3.6.4 and fig 3.6.5., no fluorescence interference was observed during Raman analysis. It is safe to conclude that RPMI 1640 without phenol red is appropriate for Raman analysis in lymphoma cell lines.

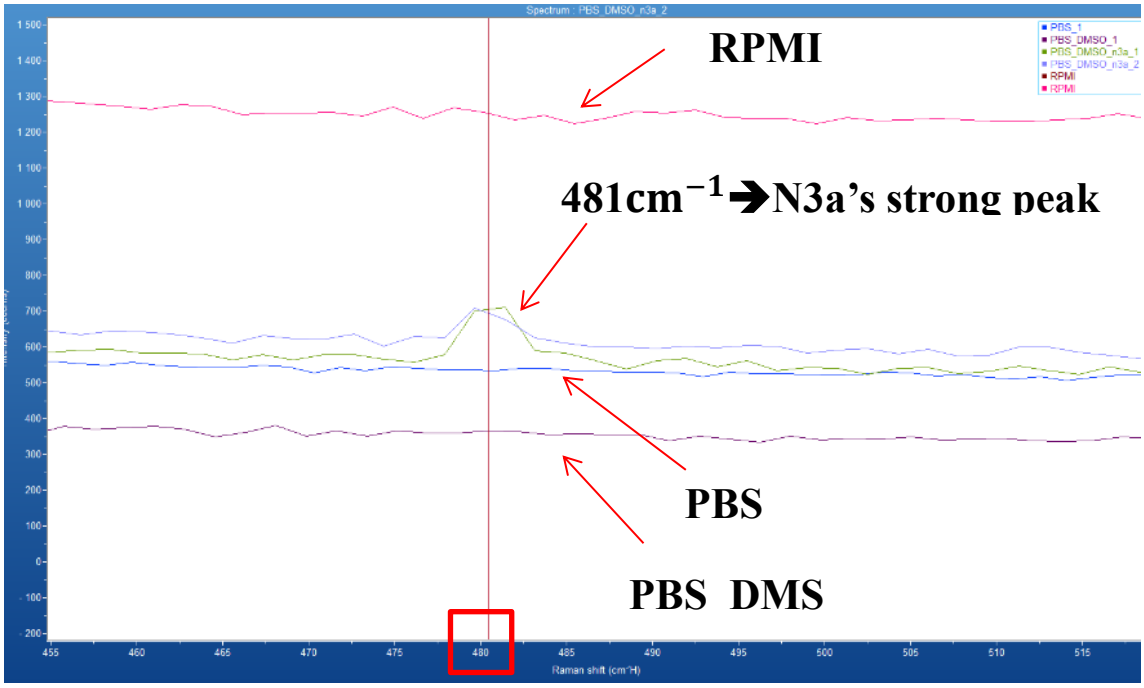


**Figure 3.6.3.** N3a's strong Raman peak compared to RPMI1640 without dye.

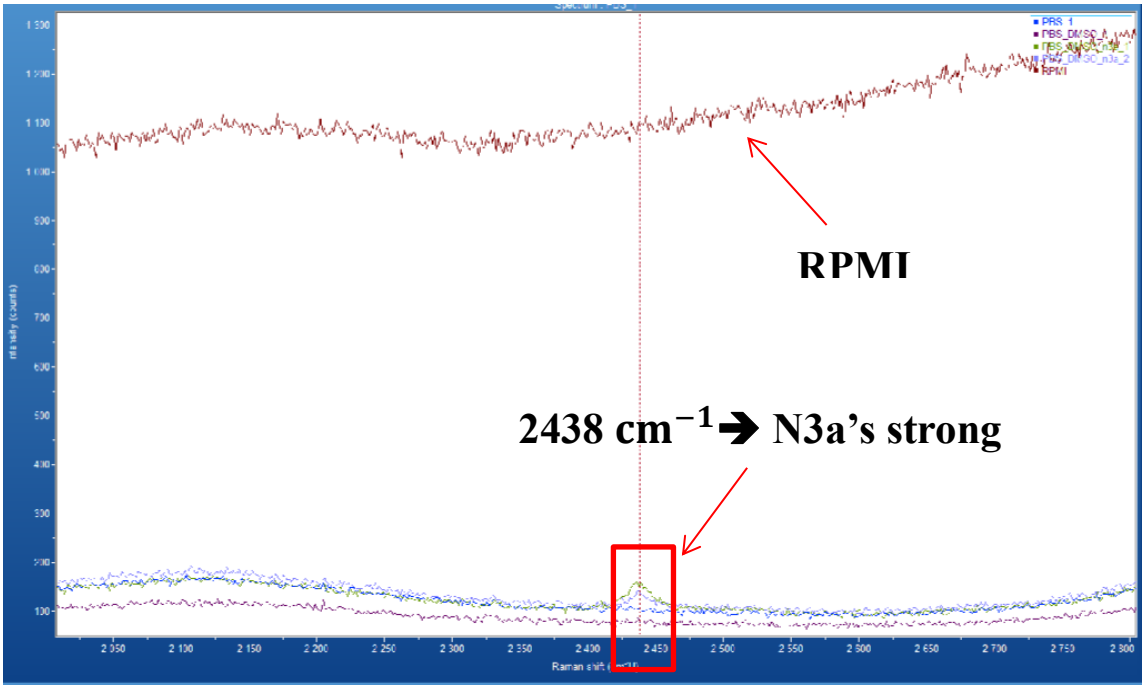


**Figure 3.6.4.** N3a's strong Raman peak compared to RPMI1640 without dye.

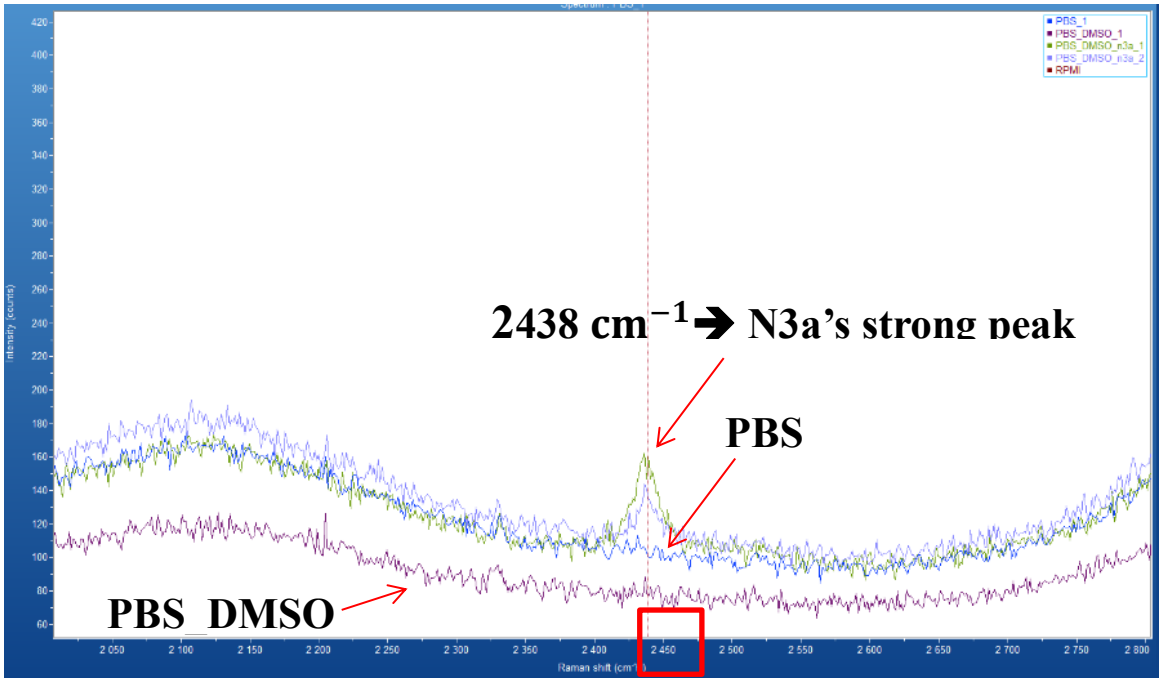


**Figure 3.6.5.** Spectrum of fig 3.2.4 in zoom, where N3a's strong Raman peak compared to RPMI1640 without dye is presented.

## 3.7 Raman measurements JMP-1/MCL cells +/- N3a.

Based on Chapter 2 (2.2.2 PR2) JMP-1/MCL cells were measured at room temperature with and without N3a treatment. Live cells and cells with altered structure were detected; the altered cells were possibly affected by N3a. Both live and affected cells were examined and measured with Raman spectroscopy.

During Raman measurements different laser intensities and measurement times were tested to find out the appropriate ones.

- **Samples:**

**1st sample solution:** JMP-1/MCL cells in DMSO and PBS without N3a treatment (control)

**2nd sample solution**: JMP-1/MCL cells in DMSO and PBS with N3a treatment.

Each measurement position was measured for 1.5 min.

## Raman measurements

### 1st sample solution (Control samples)

### Control 1

One live cell without N3a treatment was measured with a laser intensity of 50%. 9 measurement positions were observed for a total of 13.5 min.
**Observations:** N3a's peaks weren't observed inside the cell.
Indicatively a Raman shift at 1600 $cm^{-1}$ was from the PBS, a Raman shift at 1800 $cm^{-1}$ was from the cell's membrane (lipids) and a Raman shift at 2940 $cm^{-1}$ was also from a lipid band.

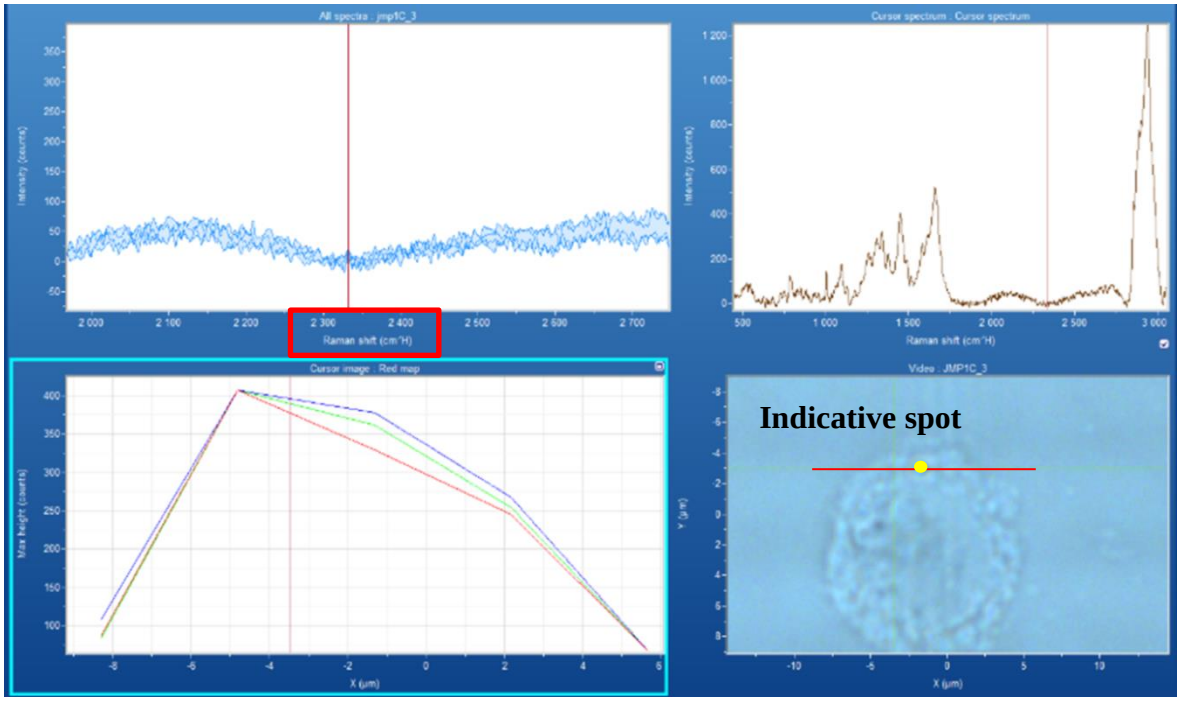


**Figure 3.7.1.** Indicative Raman plot from one spot (yellow)-Control 1. We observe that N3a's strong peak at **2436-2438 $cm^{-1}$** didn't exist.

**Control 2**

One live cell without N3a treatment was measured with a laser intensity of 100% (~ 40mW). 4 measurement positions were observed for a total of 6 min.
**Observations:** N3a's peaks weren't observed inside or in the surrounding area of the cell. Indicatively a Raman area at 1000-1500 $cm^{-1}$ was due to fluorescence.

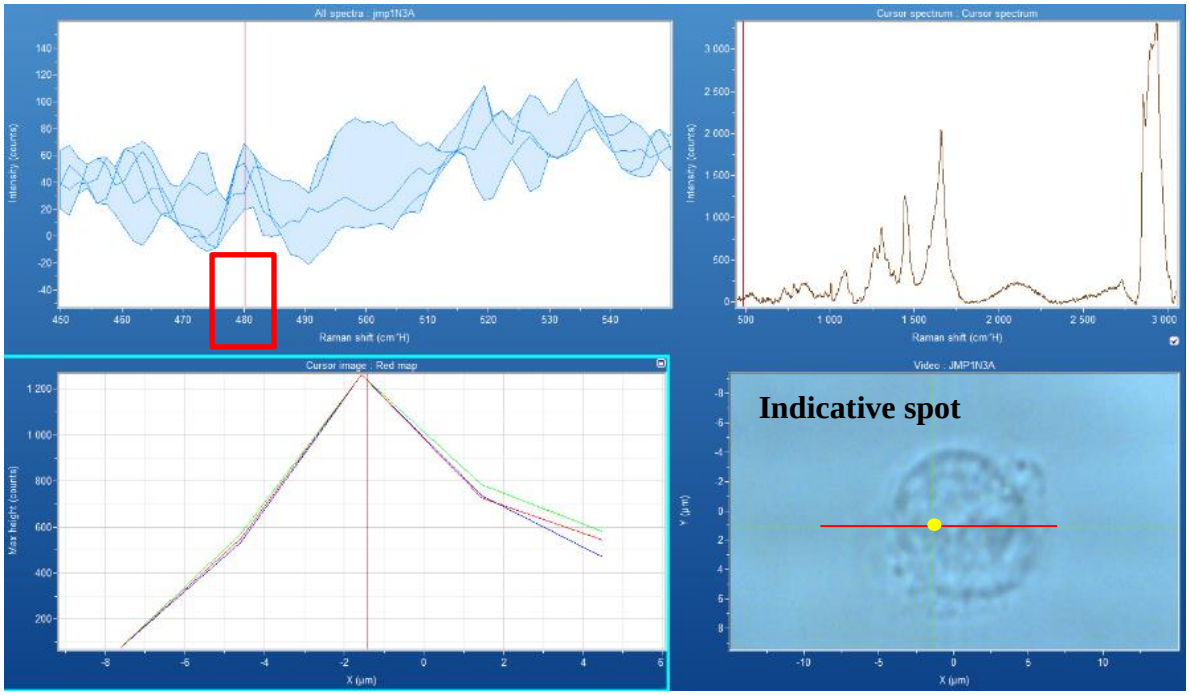


**Figure 3.7.2.** Indicative Raman plot from one spot (yellow)-Control 2. We observe that N3a's strong peak at **480 $cm^{-1}$** didn't exist.

It was observed that 100% laser intensity (~ 40mW) gives greater Raman resolution and for that reason we maintained that laser intensity.

**2nd sample solution (Treated with N3a)**

Both live and affected cells with N3a treatment were measured with a laser intensity of 100% (~40mW). 3 measurement positions were observed for a total of 4.5 min for each cell.

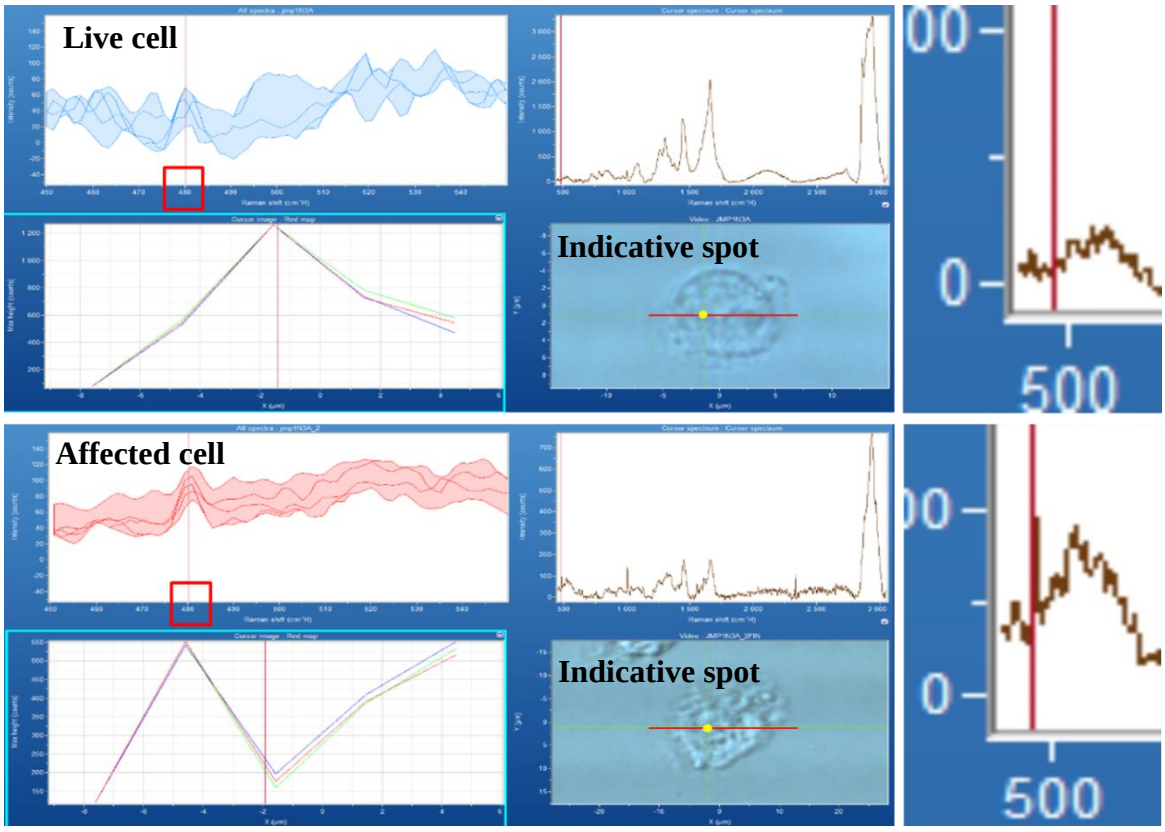


**Figure 3.7.3.** Indicative Raman plot from two spots (yellow)-Treated with N3a. For the live cell we didn't observe any N3a's strong peak. For the affected cell we can observe a N3a's strong peak at **480 $cm^{-1}$**.

**Observations:**

- For **live** cells treated with N3a, there weren't any N3a peaks observed inside the cells, but one of the strong N3a's peak (**2436 $cm^{-1}$**) was detected **out** of the cells; we hypothesized that the surrounding N3a probably did not enter the cells yet.
- For **affected** cells one of the strong N3a strong peak (**480-481$cm^{-1}$**) is visible inside and at the center of the cells. Also peaks at **500$cm^{-1}$** and **2331-2338 $cm^{-1}$** were detected inside and at the center of the cells. These peaks are probably **not shifted** N3a peaks, because Raman detection allows for a ±10 wn deviation (shift); so this shift could be a part of N3a which created a bond with another molecule inside the lymphoma cell. After extensive research, even though these peaks belong to the "silent" Raman area, it was found that thymidine analogues $N_2$ [54] and tyrosinate [55] produce Raman shifts in that area; we assumed that these shifts were caused by a probable bond formation

between a N of Nutlin and another molecule. However, this statement is only a personal assumption.

**General experimental observation:**

N3a's strong unique peaks weren't detected in untreated cells; in the case of treated cells they were detected, either inside or in the surrounding area of the cells. That fact confirms that N3a's strong unique peaks are at 480-481 and 2436-2438 $cm^{-1}$.

- **Raman measurements of MDA-V/HL cells (BR4) +/- N3a**

MDA-V/HL cells were measured at **T=15°C**, based on the PR3. We prepared 2 samples where one was treated with N3a (+) and the other was not (-). For each sample the preparation protocol was the same.

We tried to detect big cells because there is a greater chance to detect N3a inside of the cell or in the membrane, since they appear to be affected to a greater extent by N3a and become apoptotic.

In the **1st sample treated with N3a** 6 live big and 5 live small MDA-V/HL cells were examined with Raman spectroscopy. We managed to find a lot of live big cells in this sample.

In the **2nd sample without N3a** 5 live big and 7 live small MDA-V/HL cells were examined with Raman spectroscopy. We didn't manage to find a lot of live big cells at this sample.

The problem was that we couldn't detect any N3a peaks inside or in the surrounding area of the cells in the 1st sample. In the 2nd sample also there weren't any N3a peaks **(See Chapter 5 Appendix).**

(N3a peaks: 2438$cm^{-1}$strong, 481$cm^{-1}$strong, 1466 $cm^{-1}$ weak or possible shifted peaks (2331-2338$cm^{-1}$).

We examined only alive MDA-V/HL cells, where N3a probably did not enter the cells yet, so we also had to examine lysed cells, which were few in number (only 2 or 3 were lysed in the entire sample before Raman measurements). At T=15°C cells are less active, immobile and alive. Possibly a greater quantity (density) of N3a was needed in the 1st sample cell solution to increase the possibilities of N3a's detection. Finally, this experiment does not override the fact that N3a can enter and kill MDA-V/HL cells as it was mentioned in previous Raman measurements with the PR1 (fig 3.7.4). These measurements are not presented in detail because the Raman signals were not satisfactory enough for further investigation.

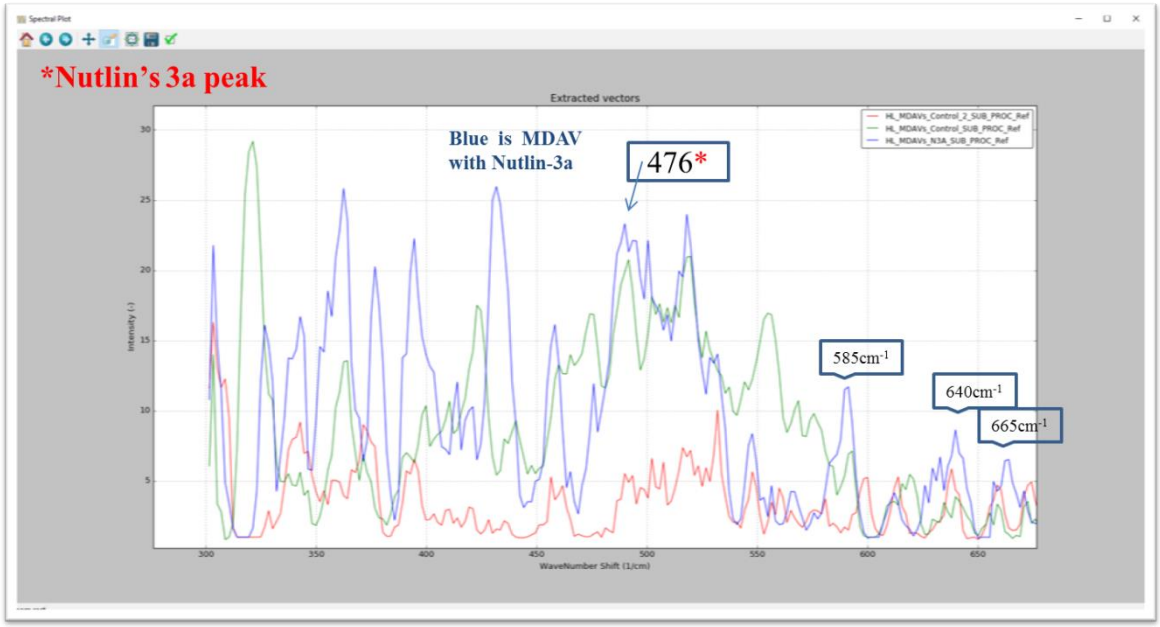


**Figure 3.7.4.** N3a's peak in treated MDA-V/HL cell. The blue graph corresponds to MDA-V/HL treated cell.

In BR4 Raman experiment, sample 2 (Control sample) was **only be examined for the comparison of the JMP-1/MCL and MDA-V/HL cell line** in T=15°C as described in PCA analysis. **Sample 1 will not be examined at all.**

## 3.8 Prototype Raman plot

A prototype Raman plot for lymphoma cells was created, based on literature as presented in fig 3.8.1. [45, 56, 57].

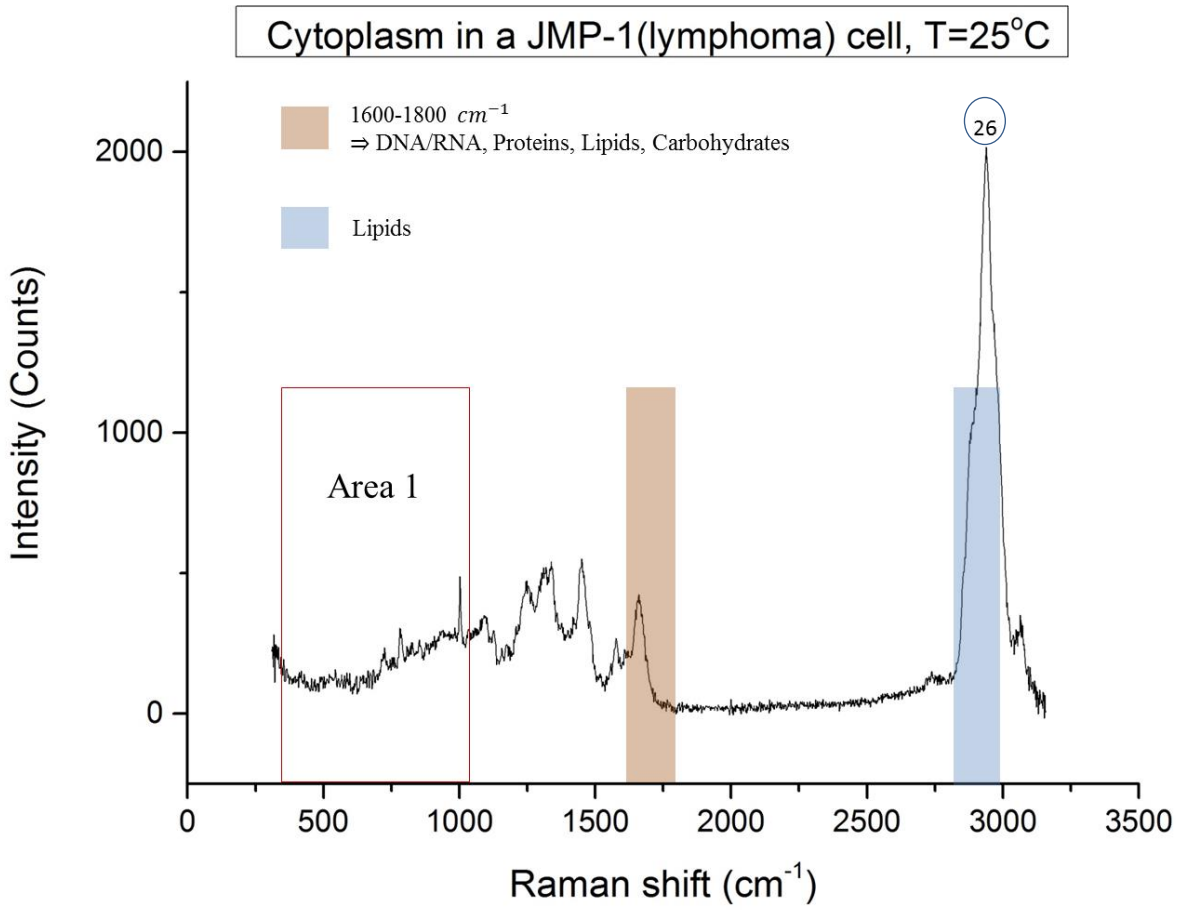


**Figure 3.8.1.** A prototype Raman plot for lymphoma cells. Area 1 is pointed out inside the red box.

At the blue area 2853-2940 $\mathbf{cm^{-1}}$ Raman assignment is $CH_2$ asym stretches and CH stretches in **lipids and proteins,** as we can also see at shift no26. Generally lipids are more often detected (blue area).

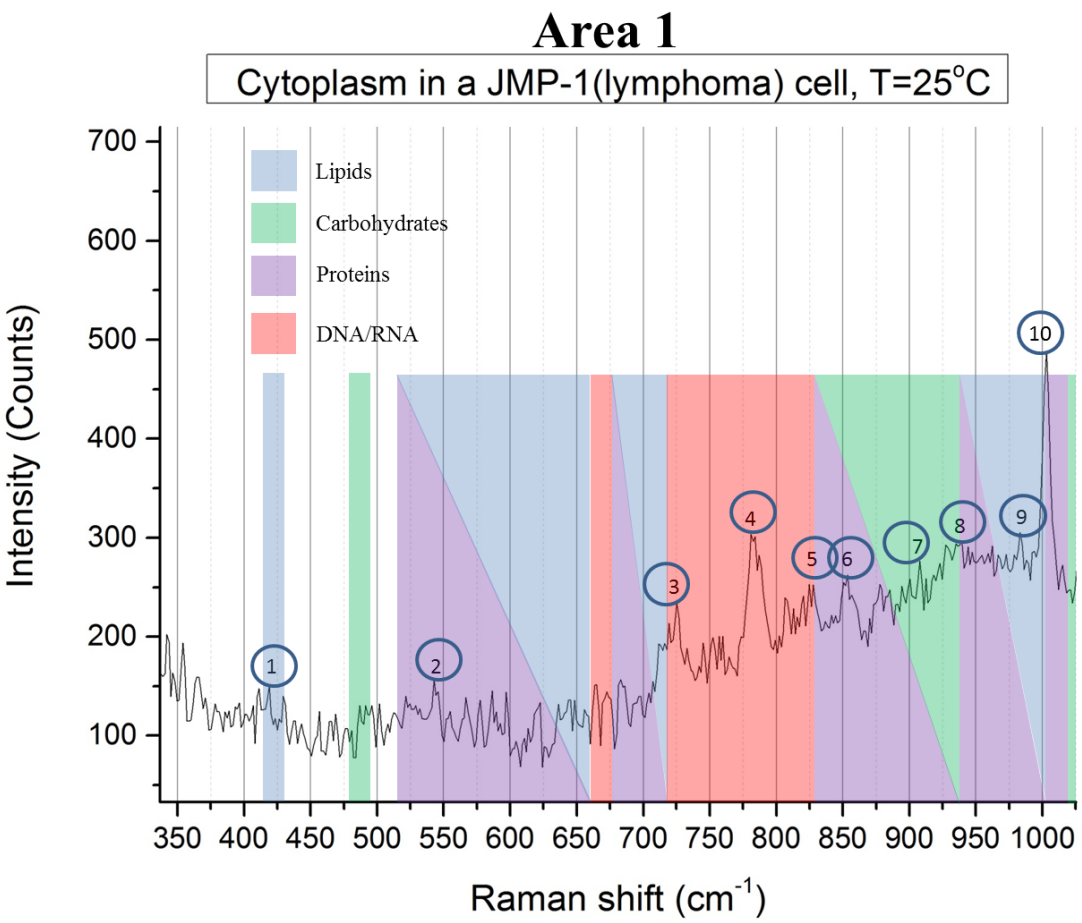


**Figure 3.8.2.** Area 1 of fig 3.8.1 in zoom.

**Table 3.8.1.** Table of Raman signaling peaks in Area 1.

| No | Raman Shift ($cm^{-1}$) | Assignment |
|---|---|---|
| **1** | 419 | **Cholesterol** |
| **2** | 543 | v(S-S) trans-gauche-gauche-trans **amino acid Cys** |
| **3** | 725 | **Adenine** |
| **4** | 781-784 | Phosphodiester, **Cytosine** |
| **5** | 825 | Phosphodiester |
| **6** | 854 | C-O-C skeletal mode of a anomers, **Polysaccharides** |

| | | |
|---|---|---|
| **7** | 908 | Ring breathing **Tyr** (proteins) |
| **8** | 940 | v(C-C) stretching of **amino acids Pro, Val** (protein band) |
| **9** | 983 | 980➔ C-C stretching **β-sheet protein** |
| **10** | 1003 | Phe C-C skeletal |

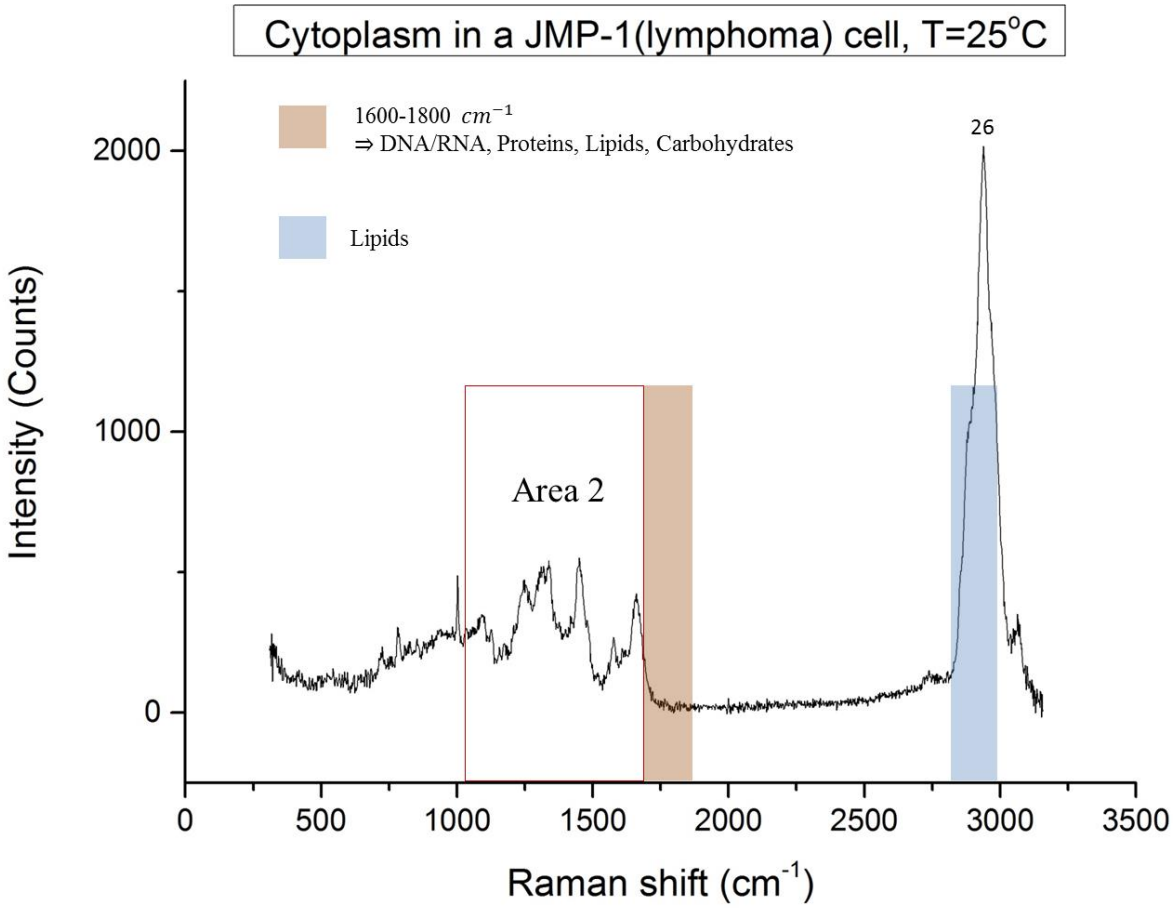


**Figure 3.8.3.** A prototype Raman plot for lymphoma cells. Area 2 is pointed out inside the red box.

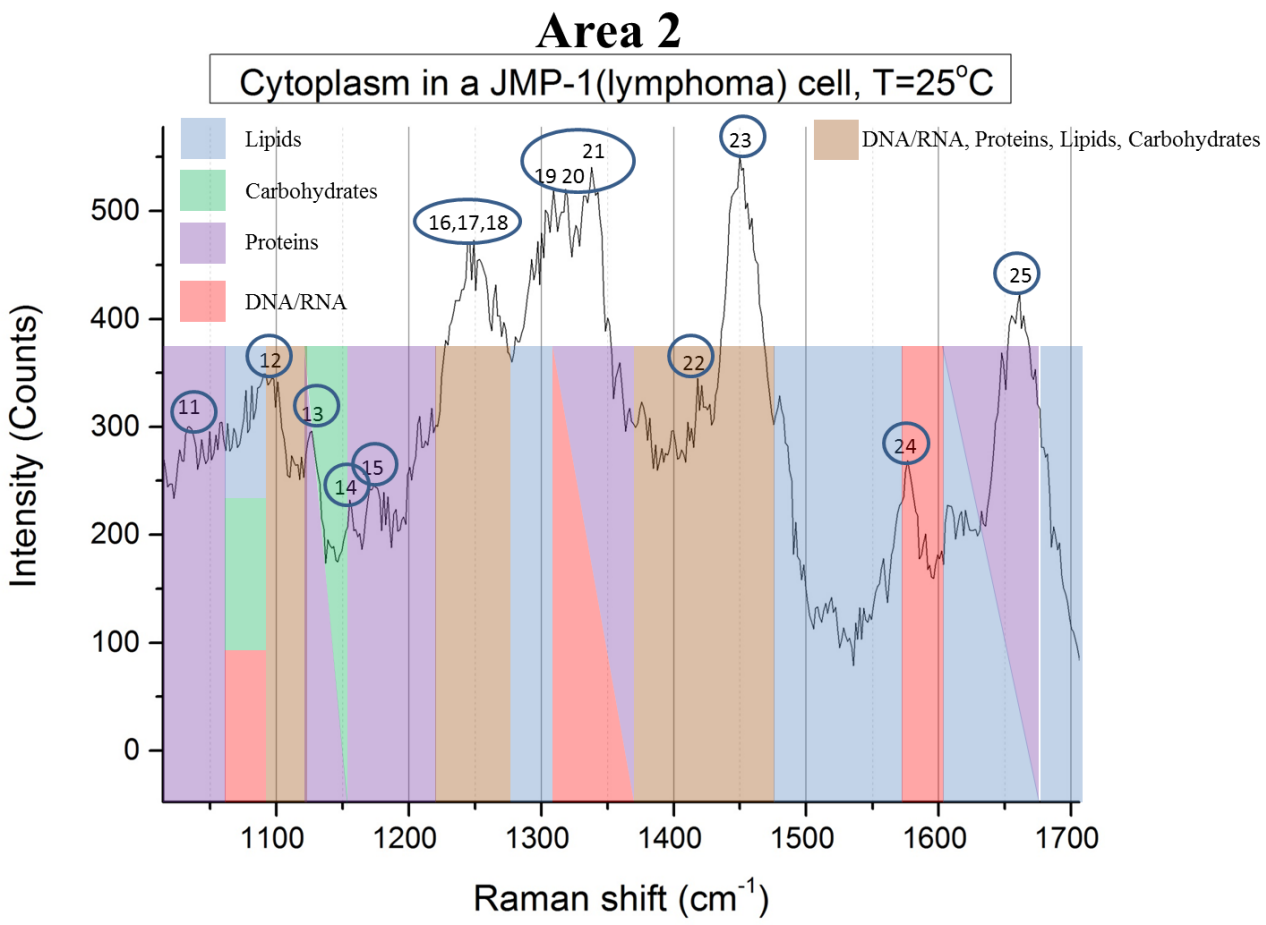


**Figure 3.8.4.** Area 2 of fig 3.8.3 in zoom.

**Table 3.8.2.** Table of Raman signaling peaks in Area 2.

| No | Raman Shift ($cm^{-1}$) | Assignment |
|---|---|---|
| 11 | 1035 | **Collagen** |
| 12 | 1092 | Phosphodioxy |
| 13 | 1127 | v(C-N) |
| 14 | 1155 | Carotenoids, C-C, (C-N) stretching of **proteins**, **Glycogen** |
| 15 | 1173 | Cytosine, Guanine, **Tyrosine (collagen type I)** |
| 16 | 1244 | **Amide III**, Pyrimidine bases **Cytosine, Thymine** |
| 17 | 1246 | Amide III of Collagen |
| 18 | 1249 | **Amide III**, **Guanine, Cytosine** ($NH_2$) |
| 19 | 1309 | $CH_3/CH_2$ twisting or bending mode of **lipid**<br>$CH_3/CH_2$ twisting or bending mode of **Collagen** |
| 20 | 1318 | **Guanine**, C-H deformation of **proteins** |
| 21 | 1338 | **Adenine** |
| 22 | 1421 | Deoxyribose, **Adenine, Guanine** |
| 23 | 1450 | $CH_2$ scissoring vibration of **lipids** |
| 24 | 1576 | Nucleic acid mode, **Guanine** ($N_3$) |
| 25 | 1661 | **Unsaturated Fatty acids of tumors** |

# Chapter 4: Conclusions and future perspectives.

## 4.1 Conclusions

HL and NHL cell lines were examined with Raman spectroscopy with/without N3a treatment. N3a's Raman spectrum was examined and analyzed in order to attempt to create a **possible** Raman peak-N3a association, to identify a Raman N3a fingerprint based on our research. N3a's strong peaks at 480-481$cm^{-1}$ and 2436 $cm^{-1}$ Raman shifts were also identified as N3a's unique peaks after research. N3a's strong unique peaks were detected **only** in treated lymphoma cells, either inside or in the surrounding area of the cells.

Membranes and nucleuses were examined with Raman spectroscopy, in different temperatures. Shorter times/point were examined, we concluded that a total practical measuring time of 2,8 min with an acquisition time of 5 sec and an accumulation number of 3, in combination with 100% laser intensity (40mV) at T=15°C, are the ideal conditions for Raman spectroscopy measurements of HL and NHL cells.

Furthermore we observed that nucleuses have more similar Raman peaks, between the different temperatures, compared to membranes and also Raman plots from the nucleus area, gave us more distinct peaks which we are certain they correspond to the nucleus. Raman signals received from the nucleus area presented higher repeatability, compared to those received from the cytoplasm and the membrane. For these reasons we chose nucleuses for further Raman analysis.

Raman bands at 2913-2920 $cm^{-1}$ and 1000-1007 $cm^{-1}$ can be detected in almost all membranes and nucleuses and correspond to CH stretch of lipids/ proteins and phenylalanine respectively. However, HL and NHL cell comparison proved that there are differences between them and the most important differences concerning signal intensities are present at about 2800-3000$cm^{-1}$ ("total methylation signaling area") and at 1000-1007 $cm^{-1}$ where Phenylalanine is detected. **We can probably say that in some way HL can be distinguishable from NHL by examination and analysis of these 2 Raman areas from their nucleuses.**

The HL and NHL cell lines used have some common peaks, those peaks differ greatly in their **intensity**. This intensity differentiation can be used to distinguish the different cell lines, although further investigation is required.

Finally PCA analysis helps us to ensure that MDA-V/HL and JMP-1/MCLcells are somewhat differentiated and possibly distinguishable with PCA analysis using Raman spectrums but they have a lot of similarities as well.

## 4.2 Future perspectives

From all these experiments we realized that it is more efficient to examine **apoptotic lymphoma cells** for N3a's detection, for this reason more experimentation is required. Furthermore, further investigation of N3a's effect inside the cell is required.

Also more Raman experiments with the MDA-V/HL cell line with/without N3a treatment are required for the discovery of the accurate location of N3a in treated lymphoma cells.

It would be preferable to find a way of cytoplasmic observation without inaccuracy, limiting the movement of the cells. Freezing cells in nitrogen and then observing them with Raman spectroscopy may be beneficial, since observation of cells in near freezing T is common practice.

Further investigation is required concerning the intensity differentiation in correlation to the distinguishability of JMP-1/MCL and MDA-V/HL lymphoma cell lines. The combination of other spectroscopic techniques for confirmation of our results is advised.

Proteomic cell analysis and observation of cell membrane proteins and biomolecule building blocks with Raman spectroscopy; may be a promising approach for distinguishing lymphoma cell lines.

Finally, Raman analysis of normal non-cancerous B cells that each cell line used originated from, in order to compare them, would be beneficial.

# Chapter 5: Appendix

## 5.1 BR4 graphs

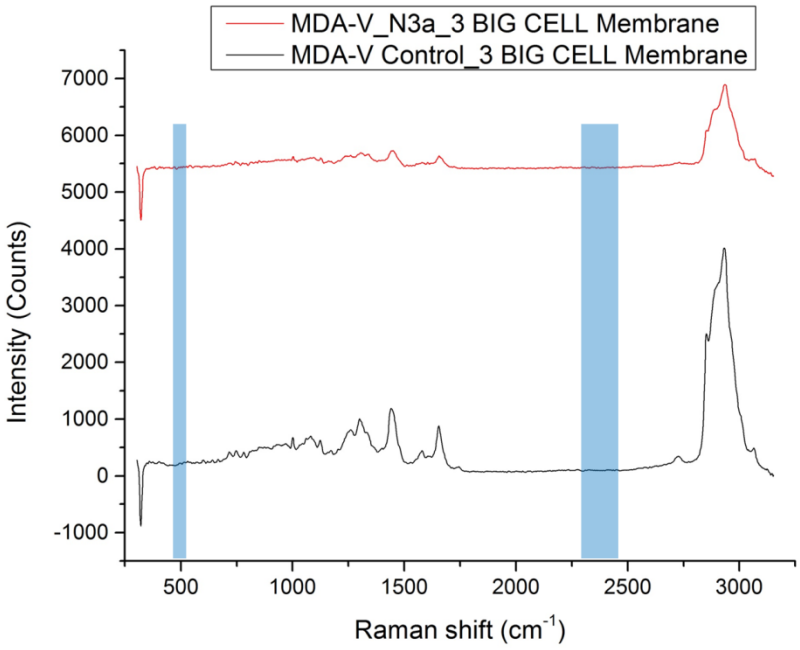


**Figure 5.1.1.** BR4 experiment. Membrane comparison between MDA-V/HL treated (red curve) and no treated (black curve) cells. Shaded areas are where N3a's strong peaks would be detected. N3a's strong peaks are not present.

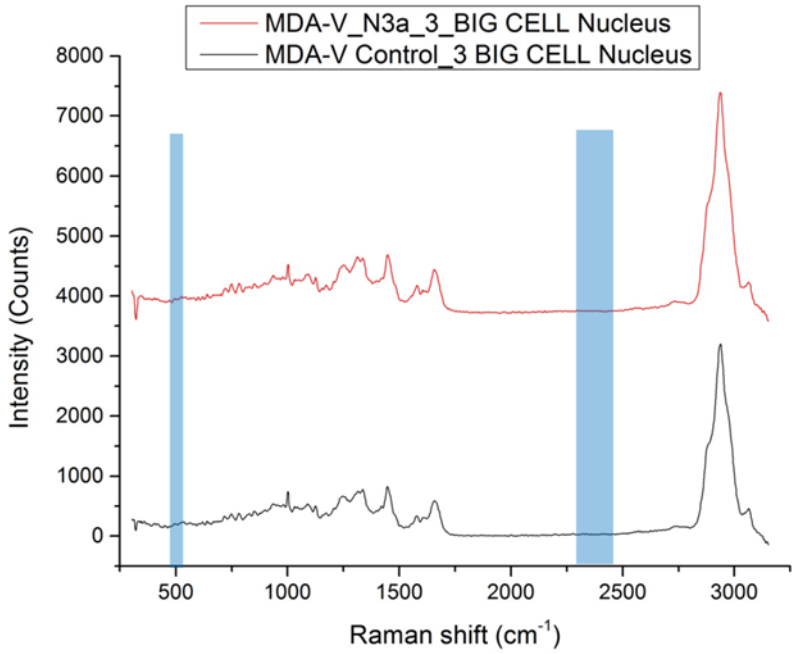


**Figure 5.1.2.** BR4 experiment. Nucleus comparison between MDA-V/HL treated (red curve) and no treated (black curve) cells. Shaded areas are where N3a's strong peaks would be detected. N3a's strong peaks are not present.

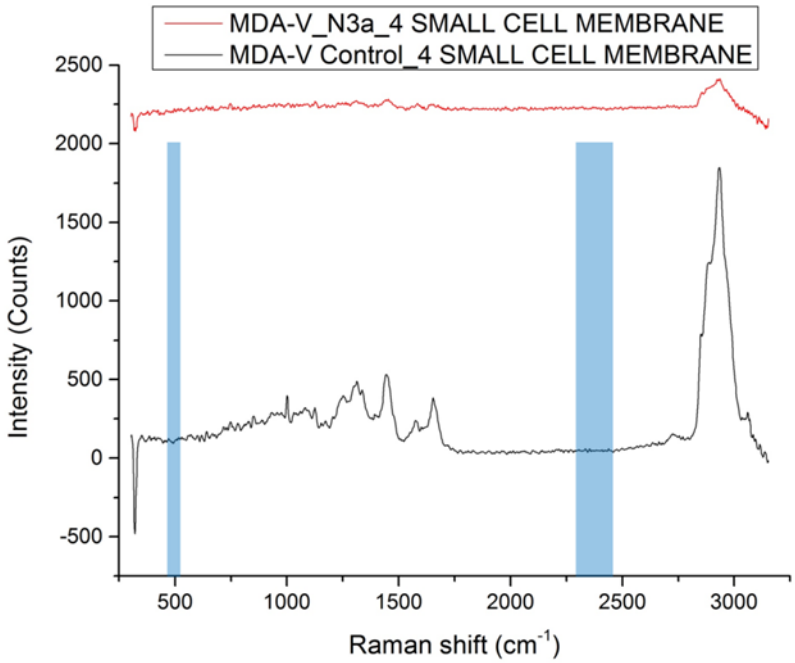


**Figure 5.1.3.** BR4 experiment. Membrane comparison between MDA-V/HL treated (red curve) and no treated (black curve) cells. Shaded areas are where N3a's strong peaks would be detected. N3a's strong peaks are not present.

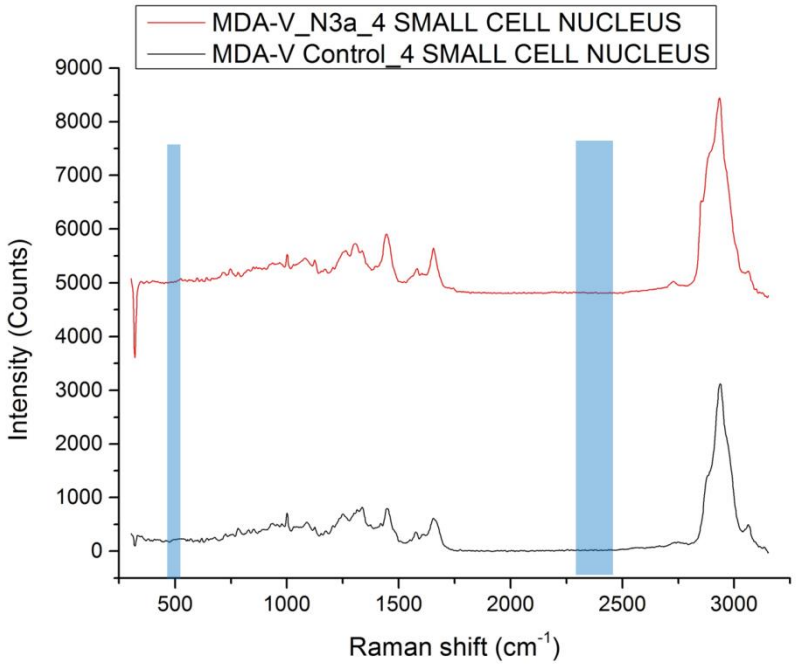


**Figure 5.1.4.** BR4 experiment. Nucleus comparison between MDA-V/HL treated (red curve) and no treated (black curve) cells. Shaded areas are where N3a's strong peaks would be detected. N3a's strong peaks are not present.

## **Chapter 6:** References


1. Oda R Shiramizu B, Kamada N, Garcia MA , Shieh T , Maeda TA , Choi SY, Lim E and Misra A, *"Unique Raman Spectroscopic Fingerprints of B-Cell Non-Hodgkin Lymphoma: Implications for Diagnosis, Prognosis and New Therapies".* J Biol Med Sci 2018.
2. Brandon J. Aubrey Liz J. Valente, Marco J. Herold, Gemma L. Kelly, Lina Happo, Clare L. Scott, Andrea Newbold,Ricky W. Johnstone, David C.S. Huang, Lyubomir T. Vassilev,and Andreas Strasser, *"Therapeutic Response to Non-genotoxic Activation of p53 by Nutlin3a Is Driven by PUMA-Mediated Apoptosis in Lymphoma Cells".* Cell Reports 2016: p. 1858-1866.
3. Ricardo E Perez Lei Duan, Ling Chen, Lothar A Blatter Carl, G Maki, *"p53 promotes AKT and SP1-dependent metabolism through the pentose phosphate pathway that inhibits apoptosis in response to Nutlin-3a".* J Mol Cell Biol, 2017: p. 1-11.
4. Leanne Marie Fullwood, *Thesis for the degree of Doctor of Philosophy in Physics, "Raman spectroscopy for rapid diagnosis of lymphomas and metastatic lesions found in lymph nodes".* University of Exeter, 2017.
5. Lauralee Sherwood, *"Human Physiology: From Cells to Systems"*. 9 ed. 2015, Boston: Cengage Learning, Inc
6. The American Cancer Society medical and editorial content team, *"What Causes Non-Hodgkin Lymphoma?"* The American Cancer Society, 2018.
7. Cancer Therapy Advisor editorial team, *"Coping With Non-Hodgkin Lymphoma".* Cancer Therapy Advisor, 2016.
8. John & Lenski Cairns, Richard, E. Mittler, John., *Lymphoma Directed Mutation.* Science, 1993: p. 1221-1224.
9. *Reed-Sternberg cell.* National Cancer Institute, 2008.
10. HiromitsuTakaba Shah Md. Abdur Rauf, Carlos A. Del Carpio, Akira Miyamot, *"How Nutlin-3 disrupts the MDM2–p53 interaction: a theoretical investigation"* Med Chem Res, 2014: p. 1998-2006.
11. Daria S. Novikovaa Tatyana A. Grigorevaa, Alexey V. Petukhova, Maxim A. Gureeva,b, Alexander V. Garabadzhiua, Gerry Melinoc, Nickolai A. Barlevd and Vyacheslav G. Tribulovicha, *"Proapoptotic modification of substituted isoindolinones as MDM2-p53 inhibitors".* Bioorg Med Chem Lett, 2017: p. 5197-5202.
12. Jeffrey H Miller Anthony JF Griffiths, David T Suzuki, Richard C Lewontin, and William M Gelbart., *An Introduction to Genetic Analysis*. 7 ed. 2000, New York: W. H. Freeman.
13. Michael Tagen Sfan Zhang, Stacy Throm, Jeremy Mallari, Laura Miller, R. Kiplin Guy, Michael A. Dyer, Richard T. Williams, Martine F. Roussel, Katie Nemeth, Fangyi Zhu, Jiakun Zhang, Min Lu, John C. Panetta, NidalBoulos, and Clinton F. Stewart,, *"Whole-Body Physiologically Based Pharmacokinetic Model for Nutlin-3a in Mice after Intravenous and Oral Administration".* Drug Metab Dispos, 2010: p. 15-21.
14. Fan Zhang, *"Preclinical Pharmacology of the MDM2 Antagonist Nutlin-3a"* Dissertation, University of Tennessee Health Science Center, 2011.
15. Natalia D. Marchenko and Ute M. Moll Angelina V. Vaseva, *"The transcription-independent mitochondrial p53 program is a major contributor to nutlin-induced apoptosis in tumor cells".* Cell Cycle, 2009: p. 1711-1719.

16. Thomaides A Drakos E, Medeiros LJ, Li J, Leventaki V, et al., *"Inhibition of p53-Murine double minute 2 interaction by Nutlin-3A stabilizes p53 and induces cell cycle arrest and apoptosis in Hodgkin lymphoma".* Clin Cancer Res, 2007: p. 3380-3387.
17. Alberto Gandolfi Krzysztof Puszynski, Alberto d'Onofrio, *"The Pharmacodynamics of the p53-Mdm2 Targeting Drug Nutlin: The Role of Gene-Switching Noise".* PLOS Comput Biol, 2015: p. 1-15.
18. Jakub Faktor Luke Way, Petra Dvorakova, Judith Nicholson, Borek Vojtesek, Duncan Graham, Kathryn L. Ball, Ted Hupp,, *"Rearrangement of mitochondrial pyruvate dehydrogenase subunit dihydrolipoamide dehydrogenase protein–protein interactions by the MDM2 ligand nutlin-3"* Proteomics, 2016: p. 2327-2344.
19. Jeffrey S. Nye, *Quick guide "The Notch proteins".* Curr Biol, 1999.
20. Sun-Young Lee Yun-Jeong Choe, Kyung Won Ko, Seok Joon Shin And Ho-Shik Kim, *"Nutlin-3 induces $HO^{-1}$ expression by activating JNK in a transcription-independent manner of p53".* Int J Oncol, 2014: p. 761-768.
21. Jan Ruger Mohamed Hassoun, Tatiana Kirchberger-Tolstik, Iwan W. Schie, Thomas Henkel, Karina Weber, Dana Cialla-May, Christoph Krafft, Jurgen Popp, *"A droplet-based microfluidic chip as a platform for leukemia cell lysate identification using surface-enhanced Raman scattering"* Anal Bioanal Chem, 2017: p. 999-1006.
22. Stephanie C. Tucker Rachel E. Kast, Kevin Killian , Micaela Trexler , Kenneth V. Honn, Gregory W. Auner, *"Emerging technology: applications of Raman spectroscopy for prostate cancer"* Cancer Metastasis Rev, 2014: p. 673-93.
23. B. Cornell, *Protein Structure.* Bioninja, 2016.
24. Alison Malkin Ines Raquel Martins Ramos, Fiona Mary Lyng, *"Current Advances in the Application of Raman Spectroscopy for Molecular Diagnosis of Cervical Cancer".* Biomed Res Int, 2015: p. 1-9
25. Lorna Ashton Holly J Butler, Benjamin Bird, Gianfelice Cinque, Kelly Curtis, Jennifer Dorney, Karen Esmonde-White, Nigel J Fullwood, Benjamin Gardner, Pierre L Martin-Hirsch, Michael J Walsh, Martin R McAinsh, Nicholas Stone, Francis L Martin, *"Using Raman spectroscopy to characterize biological materials".* Nat Protoc, 2016: p. 664-687.
26. Y.K. Agrawal Ruchita S. Das, *"Raman spectroscopy: Recent advancements, techniques and applications".* Vib Spectrosc, 2011: p. 163- 176.
27. Kratky O Glatter O., *"Small Angle X-Ray Scattering"* 1982, London: Academic Press.
28. Stellarnet, *Exploring Chemical Bonding Using Raman Spectroscopy.* StellarNet, Inc.
29. Juqiang Lina Duo Lina, Yanan Wub, Shangyuan Fenga, Yongzeng Lia, Yun Yua, Gangqin Xia, Haishan Zengc and Rong Chena, *"Investigation on the interactions of lymphoma cells with paclitaxel by Raman spectroscopy"* Spectroscopy, 2011: p. 23-32.
30. Josef Stepanek Daniel Nemecek, and George J. Thomas, Jr,, *"Raman Spectroscopy of Proteins and Nucleoproteins".* Curr Protoc Protein Sci, 2013.
31. Marco Marangoni Giulio Cerullo, Dario Polli, *Laboratory for coherent Raman spectroscopy and microscopy.* Politecnico Milano.

32. Joanne V. Volponi Huawen Wu, Ann E. Oliver, Atul N. Parikh, Blake A. Simmons, and Seema Singh, *"In vivo lipidomics using single-cell Raman spectroscopy"* PNAS, 2011: p. 3809-3814.
33. Deepak Bhanot, *What are the differences between Raman and IR Spectroscopy?* . Lab Training/Spectroscopy, 2015.
34. Auner AW and Thomas JC, *"Double-Stranded DNA Damage Assessed with Raman Spectroscopy".* Biochem Anal Biochem, 2016.
35. Benjaman A. Bryan Khalief E. Hamdena, Patrick W. Ford , Changan Xie ,Yong-Qing Li , Shaw M. Akula *"Spectroscopic analysis of Kaposi's sarcoma-associated herpesvirus infected cells by Raman tweezers".* J Virol Methods, 2005: p. 145-151.
36. Jorge Cadima Ian T. Jolliffe, *"Principal component analysis: a review and recent developments".* Philos Trans A Math Phys Eng Sci, 2016.
37. Psatha K, *Ph.D. thesis, "Genomic and proteomic analysis of the activated p53 tumor suppressor gene in Hodgkin and Non-Hodgkin lymphomas".* Faculty of Medicine, National and Kapodistrian University of Athens, 2015.
38. Hiroyoshi Matsuoka Shojl Shima, Toshiro Iwamoto, Heiichi Sakai, *"Antimicrobial action of ε-poly-l-lysine"* Jpn J Antibiot, 1984: p. 1449-1455.
39. Shoji Shima and Heiichi Sakai, *"Polylysine Produced by Streptomyces".* Agr Biol Chem Tokyo, 1977: p. 1807-1809.
40. George Sitterley, *Poly-lysine.* BioFiles, 2008: p. 12.
41. Medicago AB, *Phosphate buffered saline specification sheet.* 2010.
42. Ronald M. Atlas James W. Snyder, *"Handbook of Media for Clinical Microbiology".* 2 ed. 2006, Boca Raton: CRC Press
43. C.Gobinet F.Draux, J.Sule-Suso, A.Trussardi, M.Manfait, P.Jeannesson, G.D.Sockalingum, *"Raman spectral imaging of single cancer cells: probing the impact of sample fixation methods".* Anal Bioanal Chem, 2010: p. 2727-2737.
44. Nicholas I. Smith Alison J. Hobro, *"An evaluation of fixation methods: Spatial and compositional cellular changes observed by Raman imaging".* Vib Spectrosc, 2016: p. 1-15.
45. Zanyar Movasaghi Abdullah Chandra Sekhar Talari, Shazza Rehman, Ihtesham U Rehman, *"Raman Spectroscopy of Biological Tissues".* Appl Spectrosc Rev, 2015: p. 46-111.
46. Yoshifumi Nishimura Tadayuki Uno, Ryu Makino, TeteutaroIizukas, yuzuruIshimura, and MasamichiTsuboi, *"The Resonance Raman Frequencies of the Fe-CO Stretching and Bending Modes in the CO Complex of Cytochrome P-450cam".* J Biol Chem, 1985: p. 2023-2026.
47. Norman B. Colthup Daimay Lin-Vien, William G.Fateley, Jeanette G. Grasseli, *"The Handbook of Infrared and Raman Characteristic Frequencies of Organic Molecules".* 1991, Boston: Academic Press.
48. K.K. Innes J. D. Simmons, *"Infrared and Raman Spectra of Pyrazine-h4 and –d4".* J Mol Spectrosc, 1964: p. 190-197.
49. *Raman Band Correlation Table* University of Toronto Scarborough.
50. Koichi Itoh Ikuo Ashikawa, *"Raman Spectra of Polypeptides Containing L-Histidine Residues and Tautomerism of Imidazole Side Chain".* Biopolymers, 1979: p. 1859-1876.
51. Michael Ludwig Craig R. Johnson, and Sanford A. Ashe, *"Ultraviolet Resonance Raman Characterization of Photochemical Transients of Phenol, Tyrosine, and Tryptophan".* J Am Chem Soc, 1986: p. 905-912.

52. John T. Edsall David Garfinkel, *"Raman Spectra of Amino Acids and Related Compounds. VIII. Raman and Infrared Spectra of Imidazole, 4-Methylimidazole and Histidine"* J Am Chem Soc, 1958: p. 3808-3812.
53. Frank S. Parker, *"Applications of Infrared, Raman, and Resonance Raman Spectroscopy in Biochemistry"*. 1983, New York Plenum Press.
54. Kosuke Dodo Hiroyuki Yamakoshi, Masaya Okada, Jun Ando, Almar Palonpon, Katsumasa Fujita, Satoshi Kawata, Mikiko Sodeoka, *"Imaging of EdU, an Alkyne-Tagged Cell Proliferation Probe, by Raman Microscopy".* J Am Chem Soc, 2011: p. 6102-6105.
55. Michael Ludwig Sanford A. Asher, and Craig R. Johnson, *"UV Resonance Raman Excitation Profiles of the Aromatic Amino Acids".* J Am Chem Soc, 1986: p. 3186-3197.
56. K. Majzner K. Czamara, M. Z. Pacia, K. Kochan, A. Kaczora, M. Baranskaa, *"Raman spectroscopy of lipids: a review".* J Raman Spectrosc, 2015: p. 4-20.
57. Ion Notingher and Larry Hench, *"Raman microscopy: a noninvasive tool for studies of individual living cells in vitro".* Expert Rev Med Devices, 2006: p. 215-234.